NOTE TO USERS

This reproduction is the best copy available.

UMI®

UNIVERSITY OF CINCINNATI

May 17 19 72

I hereby recommend that the thesis prepared under my supervision by Stephen P. Reidel

entitled The Geology of the Serpent Mound Cryptoexplosion Structure

be accepted as fulfilling this part of the requirements for the degree of Master of Science

Approved by:

Frank L. Koucky Jr., Chairman

Harvey G. Sunderman

W. H. Gruner

Form 668—Grad. School—1M—12-69

GEOLOGY OF THE SERPENT MOUND CRYPTOEXPLOSION STRUCTURE

A thesis submitted to the

Division of Graduate Studies
of the University of Cincinnati

in partial fulfillment of the
requirements for the degree of

MASTER OF SCIENCE

in the Department of Geology
of the Graduate School of Arts and Sciences

1972

BY

Stephen P. Reidel

B.S. University of Cincinnati, 1970

UNIVERSITY OF CINCINNATI LIBRARY

UMI Number: EP26299

INFORMATION TO USERS

The quality of this reproduction is dependent upon the quality of the copy submitted. Broken or indistinct print, colored or poor quality illustrations and photographs, print bleed-through, substandard margins, and improper alignment can adversely affect reproduction.

In the unlikely event that the author did not send a complete manuscript and there are missing pages, these will be noted. Also, if unauthorized copyright material had to be removed, a note will indicate the deletion.

UMI®

UMI Microform EP26299
Copyright 2009 by ProQuest LLC
All rights reserved. This microform edition is protected against unauthorized copying under Title 17, United States Code.

ProQuest LLC
789 East Eisenhower Parkway
P.O. Box 1346
Ann Arbor, MI 48106-1346

ABSTRACT

The purpose of this study was to map the structure of the Serpent Mound Cryptoexplosion Structure and to study the related mineralization.

Detailed mapping has shown that the Serpent Mound Cryptoexplosion Structure can be divided into three structural units: 1) A central, elevated area of radiating anticlines cut by high angle faults, 2) A peripheral, depressed outer ring of synclines cut by high angle faults, and 3) an intermediate ring area of folded and faulted, vertical, tectonic displacements less than the central elevated area or outer depressed area. In the central area faults formed in the north area between the radial anticlines while in the south and east sides, grabens formed.

Regional geophysical evidence indicates a specialized site for the cryptoexplosion structure while on a local scale, gravity anomalies are shown to be related to surface structures.

The mineralization is typically of a Mississippi Valley type. Sphalerite is the main mineral present but a color variation is found in the samples. Paragenesis of the mineralization indicates at least two deformations occurred within the cryptoexplosion structure. Two generations were deposited after the first deformation and before the second deformation. A third generation was deposited after the second deformation.

SEP 21 72

Both a meteorite and a gas explosion can easily supply the needed energy to create a crater this size.

A gas explosion hypothesis best explains the phenomena at the Serpent Mound Cryptoexplosion Structure.

TABLE OF CONTENTS

LIST OF PHOTOGRAPHS

ACKNOWLEDGEMENTS

Sincere thanks goes to Dr. F. L. Koucky, Jr. under whom this study was carried out. Without his guidance, encouragement, and enthusiasm, this study could not have been completed.

Many thanks also goes to Dr. H. Sunderman and Dr. I. A. Kilinc. Dr. Sunderman read the manuscript and offered many valuable and helpful suggestions. Dr. Kilinc assisted in calculating the energy releaced by a gas explosion during resurgent boiling and offered many valuable suggestions envolving the application of Barnes's ideas on ore transport to this study.

This research was supported by a grant from Cominco American. This grant paid for part of the Atomic Absorption unit belonging to the Geology Department.

INTRODUCTION

In 1838 John Locke made a mention of deformed rocks near Locust Grove, Ohio. "As we descended into the channel of Crooked Creek, I did not find as I has expected, the great marl stratum. Its place seems to be occupied by thin layers of limestone. Although we travelled on that level which should have presented us with the cliff limestone, yet we were surprised with its total disappearance as we approached the spring, and in its place was found the sandstone in large upturned and broken masses. In short, it became evident that a region of no small extent had sunk down several hundred feet, producing faults, dislocations and upturning of the layers of the rocks" (Page 266). Locke's traverse into the Serpent Mound Structure, the structure considered in this paper, was from the southeast. He entered the map area just north of Locust Grove. Locke noted that the structure near the border of the thesis area was synclinal (Figures 1 and 2); however he made no attempt to determine the nature and extent of the structure, but proceeded north to the Fort Hill Indian works.

In 1920 W. H. Bucher, then on the faculty of the University of Cincinnati, mapped the above mentioned deformed rocks in southwestern Ohio near the corners of Adams, Highland, and Pike Counties in the vicinity of the towns of Louden, Sinking Springs and Locust Grove (Figure 1). Bucher (1921) compared this to the Steinheim

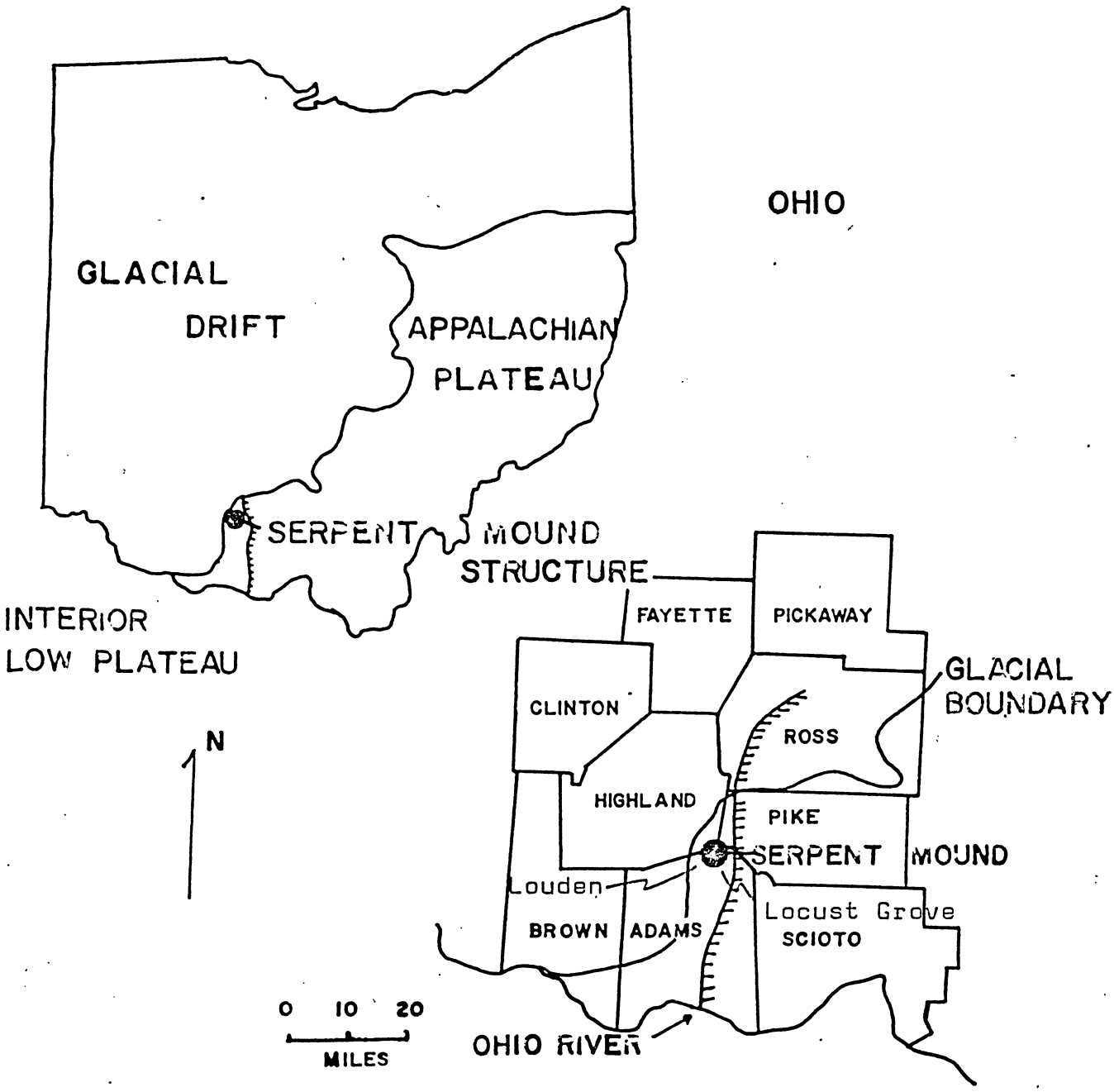

FIGURE 1 LOCATION MAP

GEOLOGIC MAP OF THE SERPENT MOUND STRUCTURE, OHIO

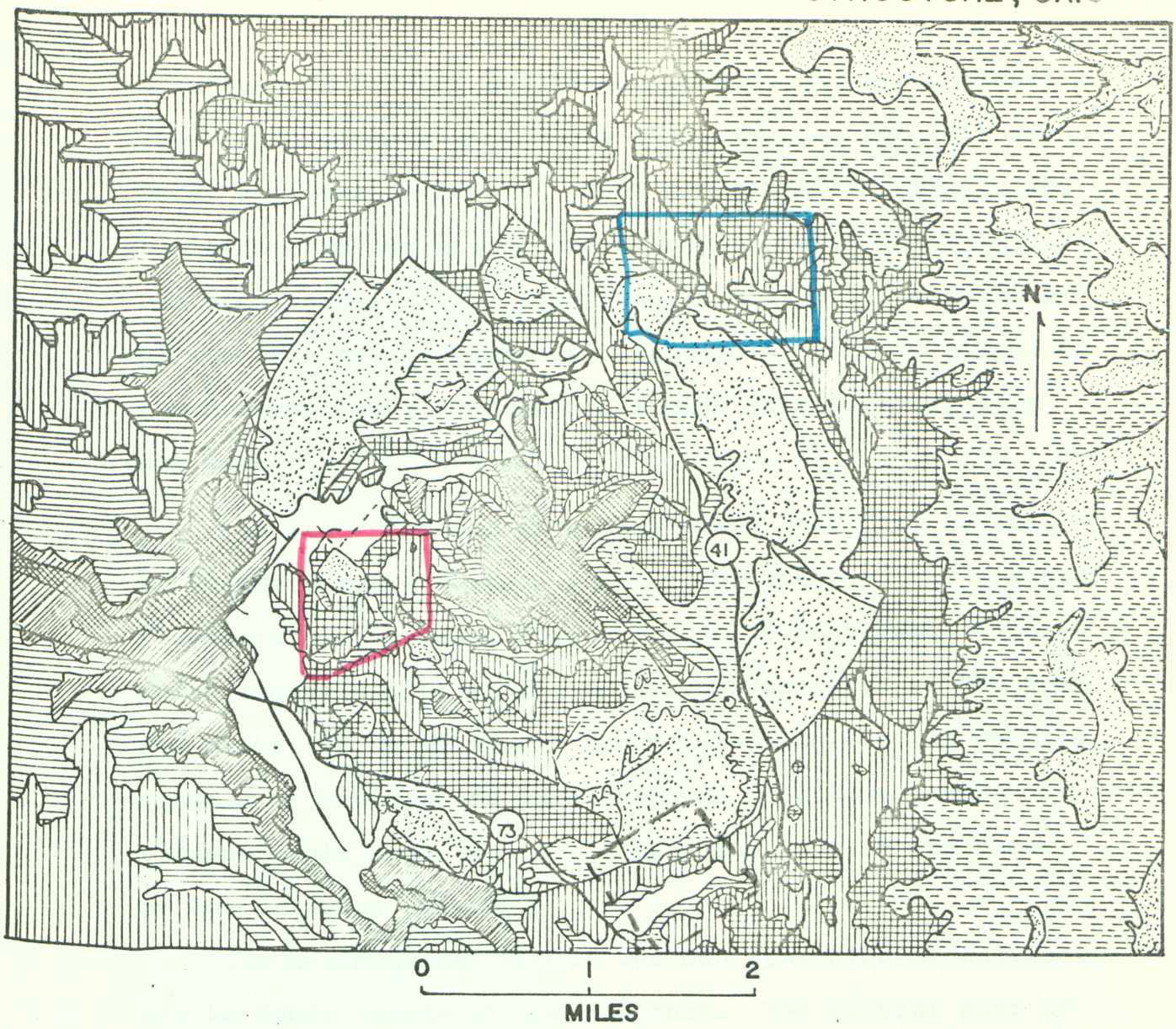

RECENT — ALLUVIUM

MISSISSIPPIAN — SANDSTONES AND SHALE

DEVONIAN — OHIO BLACK SHALE

SILURIAN
- GREENFIELD PEEBLES DOLOMITE
- LILLEY BISHER DOLOMITE
- CRAB ORCHARD SHALE
- BRASSFIELD LIMESTONE

ORDOVICIAN — ORDOVICIAN UNDIFFERENTIATED

FIGURE 2

1936
AFTER BUCHER

BOUNDARY OF :
- REIDEL 1970
- STRYKER 1971
- WACHTER 1971

PHOTO 1 THE SERPENT MOUND CRYPTOEXPLOSION STRUCTURE FROM HIGHWAY 770

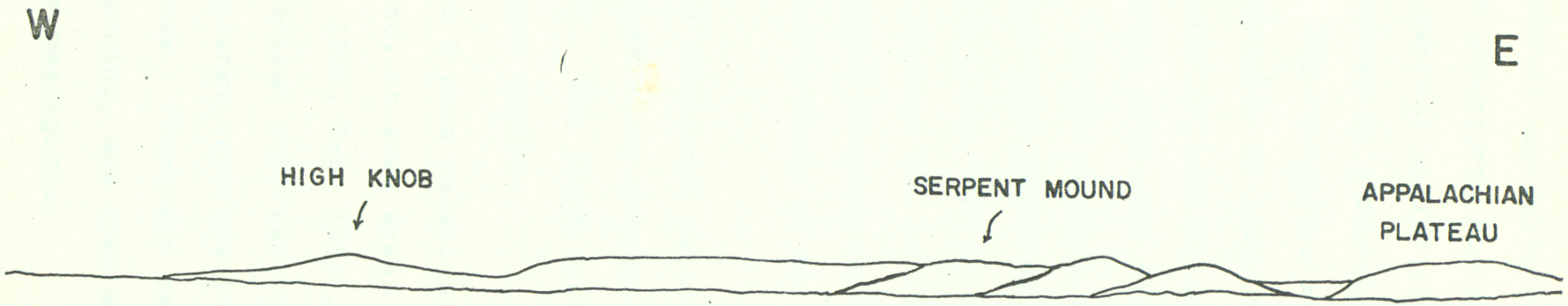

nearly circular outline with a diameter approximately four miles. It is typical of many such structures now known (Freeburg, 1966) in that it has a central uplift with intense structural deformation surrounded by a downward displaced ring shaped belt of rocks. The formations mapped by Bucher range from the upper Ordovician to lower Mississippian. The structural map by Bucher (Figure 3) indicates intense deformation in a small central area with intensity decreasing concentrically outward. In the central area the Ordovician shales and limestones have been uplifted at least 350 feet above their normal position, and in one instance, Bucher found evidence of perhaps 900 to 950 feet of uplift. He interpreted the vertical displacement to "suggest that the cause was the driving force of an explosion" (1936, Page 1062).

The central area has an angular polygonal pattern (Figure 3) as though "it had developed along preexisting joint planes" (o.c. 1936, Page 1062). The joint system in the area has a northeast and northwest strike.

The folds represented in Figure 3 have relatively small amplitudes and as Bucher stated, in some areas represent a "sort of wrinkling" (o.c. 1936, Page 1062). Steep dips and folds surround the central uplifted block. Normal faults with nearly vertical planes separate the uplifted block from the surrounding area. There are several low displacement faults, some overturning, and some minor overthrusting but they are local and negligible.

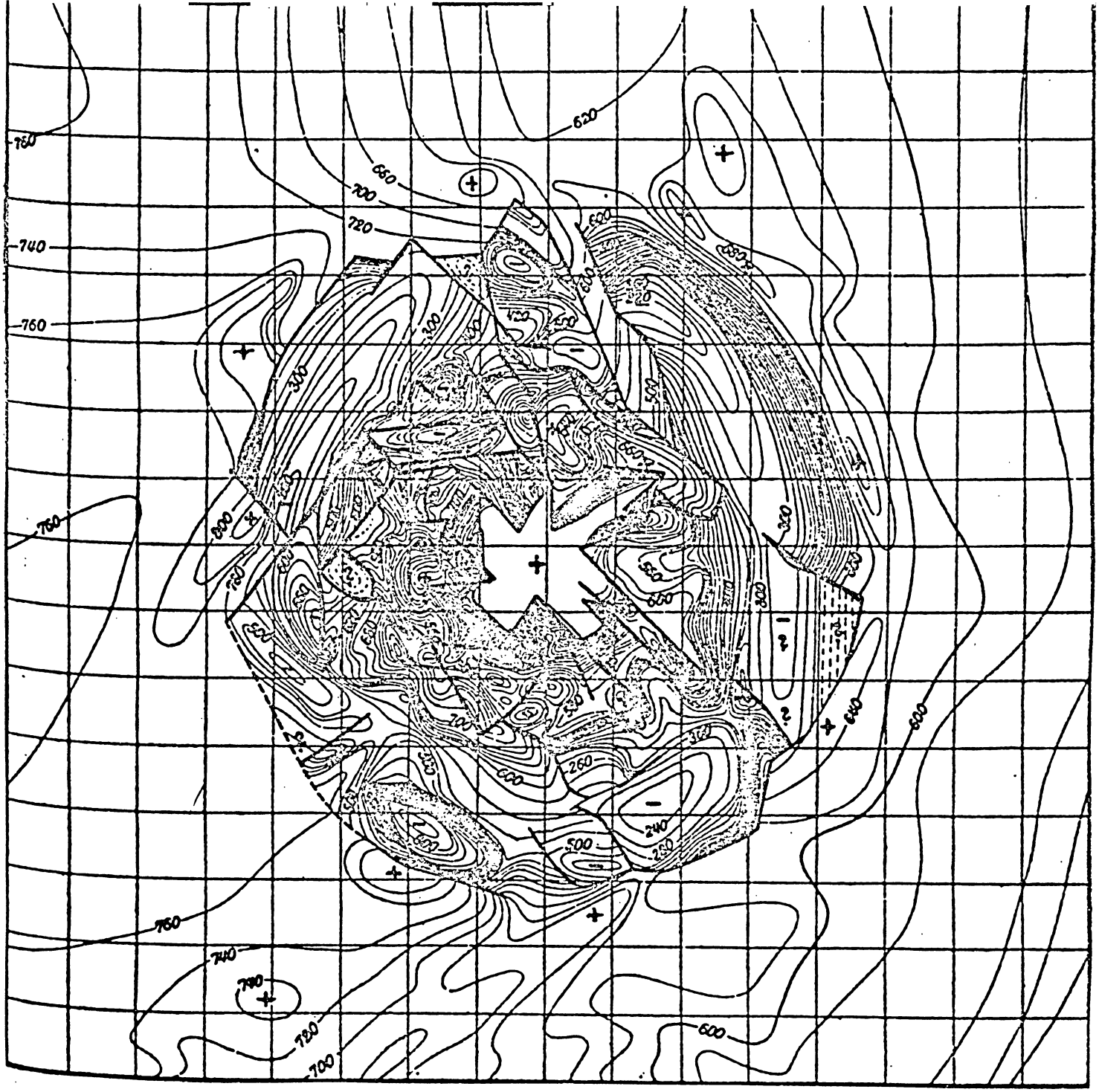

FIGURE 3

Structure Contour Map of the Serpent Mound Cryptoexplosion Structure (after Bucher,1933).

Contours are on the top of the Brassfield limestone
+ is anticline, - is syncline, contour interval = 20'

As indicated by Bucher, the large peripheral blocks surrounding the central area dip inward and form a ring depression. Faults generally define the boundaries of the large blocks except on the northeast side where there is a sharp flexure. Several marginal anticlines lie outside the peripheral area; the largest is on the northeast side.

According to Bucher (1933), over 60 percent of the surface of the cryptoexplosion structure exposes strata that are more than 100 feet below their original positions; less than 30 percent lie within 100 feet of their original positions; and less than 10 percent lie more than 100 feet higher than they did originally.

The absolute age of the Serpent Mound deformation cannot be determined because there is no igneous material present. The relative age of the structure lies somewhere between early Mississippian time and middle Pleistocene, since undisturbed Illinoian glacial deposits lie upon the northwest portion of the structure and early Mississippian formations have been included in the deformation.

The cryptovolcanic origin has not been completely accepted for there is no real proof of an internal explosion. Boon and Albritton (1936) first suggested this resembled a meteoritic impact crater. According to Dietz (1963) shatter cones that have been found in the central

area indicate an intense shock loading far in excess of any known volcanic forces. Their concentration in this bull's eye of a cryptoexplosion structure indicates "a highly localized ground zero" (Dietz, 1963, Page 661).

Coesite has been described by Cohen, Bunch, and Reid (1961) from the central uplifted area of the Serpent Mound Cryptoexplosion Structure. The material was concentrated from the residue of a "shatter cone that weighed over two pounds and was disolved in hydrochloric acid" (o.c. Page 1624). However this occurance has not been verified (Jenks, 1965).

Sappenfield (1950) found a pronounced broad linear positive vertical magnetic anomaly trending N 25°W through the structure (Figure 4). He explained this anomaly as perhaps being caused by the intrusion of a basic magma into the upper part of the siliceous basement.

A gravity survey of Ohio by Heishanen & Uotila (1956) also shows a zone in N.E. Adams County with a N. W. trend and a somewhat smaller negative Bouger anomaly than that in the surrounding area (Figure 5). Zahn (1965) conducted a gravity survey over the disturbance but found little direct relationship between his survey and the boundary marked by Bucher. Zahn's survey did show an increasing negative anomaly toward the southwest (Figure 6) and his contour lines are remarkably similar in direction to those of Sappenfield's.

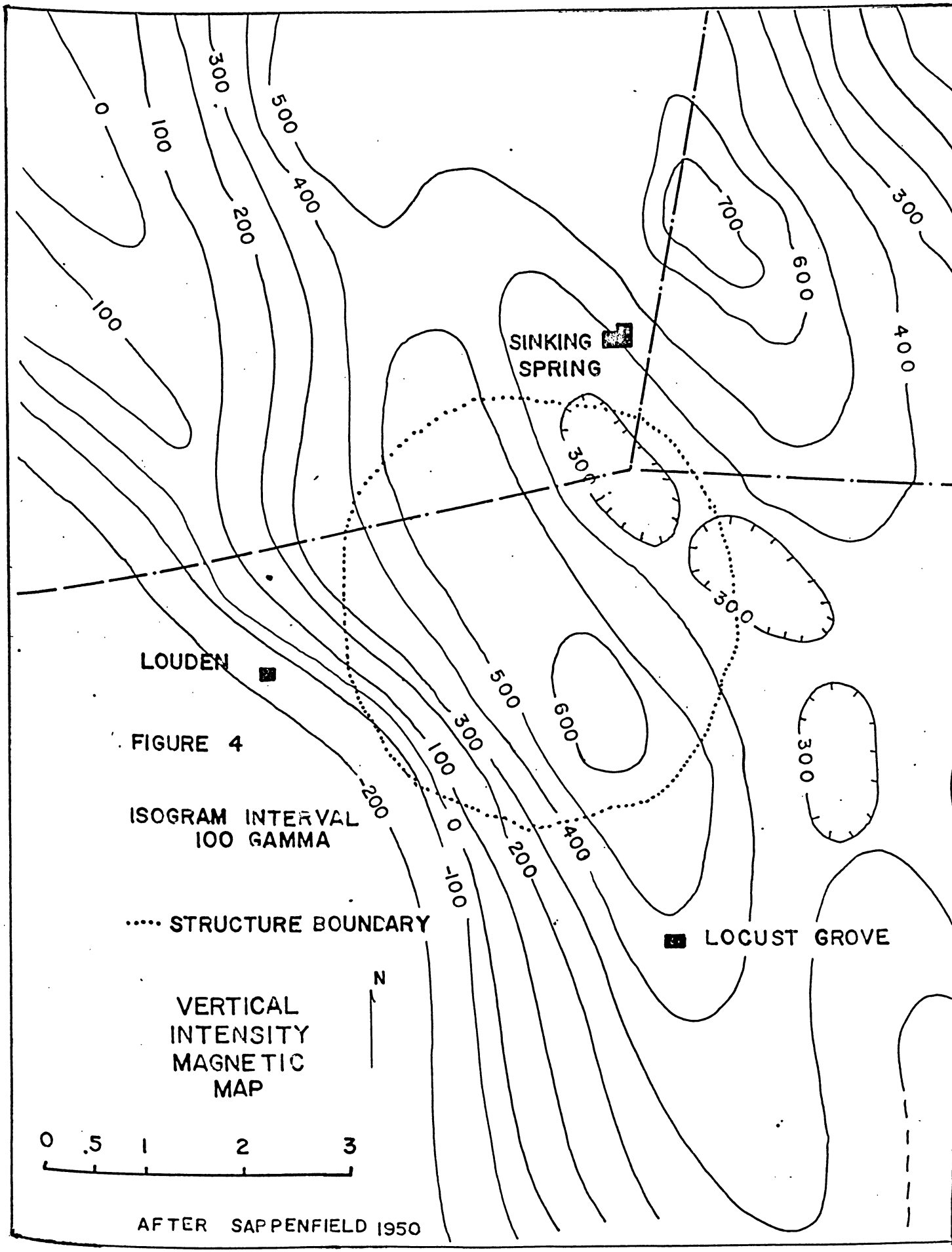
0
100
300
500
400
200
100
700
600
300
400
SINKING
SPRING
300
300
LOUDEN
500
600
300
100
0
-200
-100
200
400
300
LOCUST GROVE
FIGURE 4
ISOGRAM INTERVAL
100 GAMMA
STRUCTURE BOUNDARY
N
VERTICAL
INTENSITY
MAGNETIC
MAP
0 .5 1 2 3
AFTER SAPPENFIELD 1950

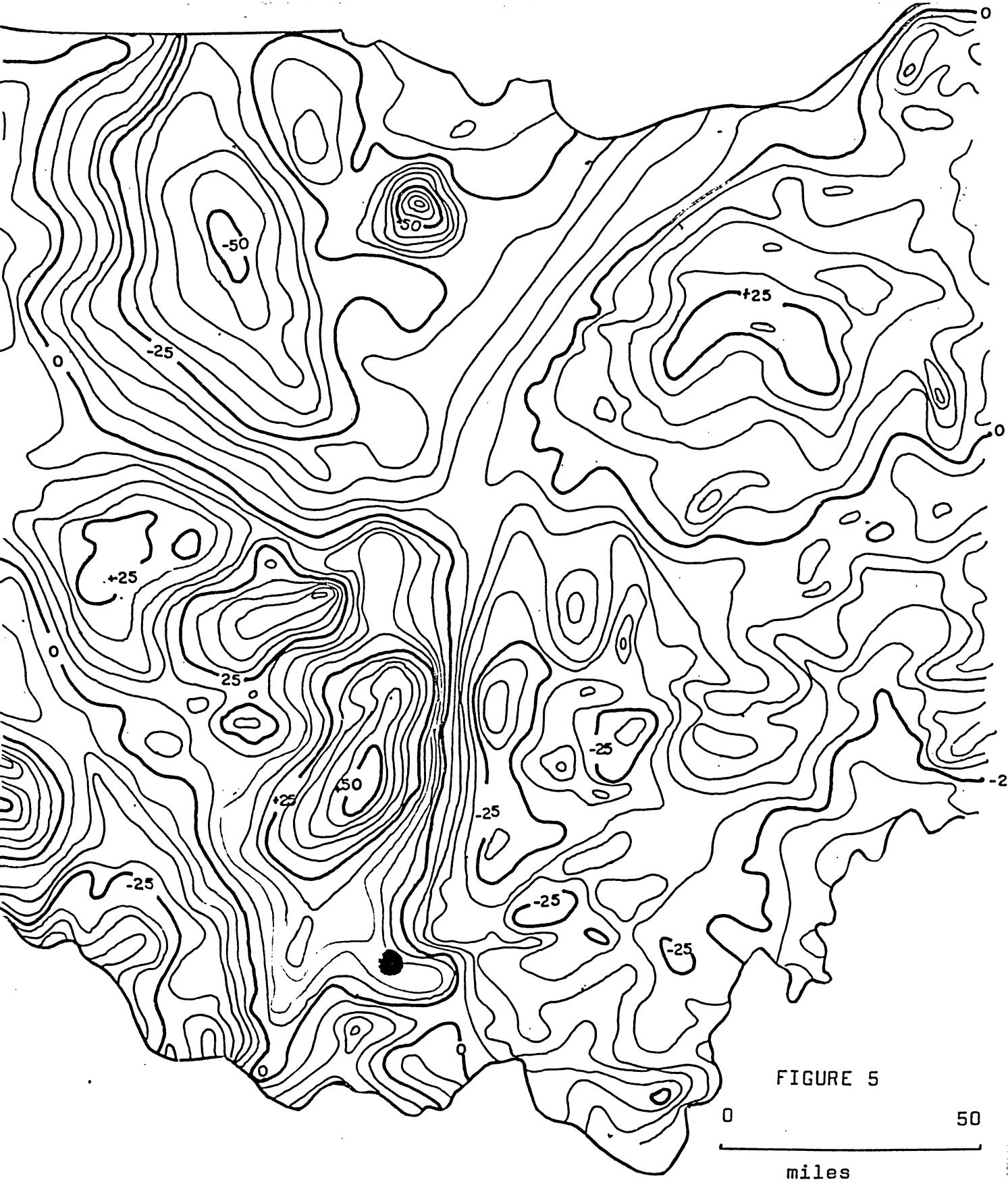

Free Air Anomaly Map of Central and West Ohio

Gravity Map after Heiskanen and Uotila, 1956

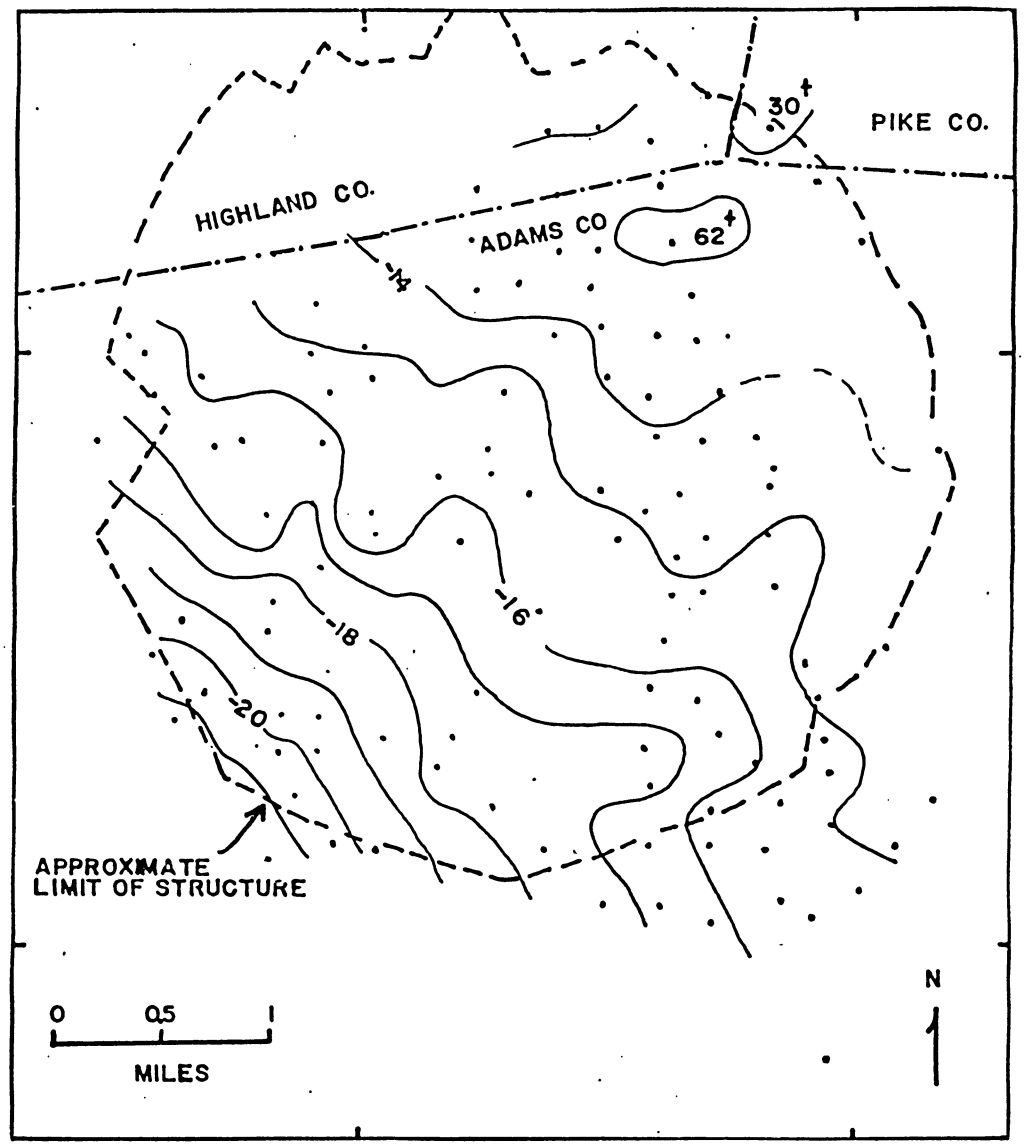

FIGURE 6

Bouguer Gravity Map of the Serpent Mound Cryptoexplosion Structure, Adams Co. Ohio

Gravity Anomaly interval
1 Milligal

Gravity Station

after Zahn, 1969

Outside the structure Bowman (1961) a geologist from the Plum Run Stone Division of Davon, Inc., has found N.W. trending normal faults which strike in the direction of the cryptoexplosion structure.

Galbraith (1968) mapped a northeast trending monocline extending from near the southern border of Ohio (near the West Hickman fault) through the Serpent Mound Cryptoexplosion Structure. The Serpent Mound structure was found to lie near the east side (Figures 7 & 8) of the monocline. Faulting was found outside the boundary of the cryptoexplosion structure to the northeast and southwest.

Heyl and Brock (1962) described an occurence of sphalerite, hydrozincite, and smithsonite in the Greenfield Peebles dolomite within the structure. The mineralization occurs on a low western trending hill just off a township road due west and about halfway out from the central area. They reported that the sphalerite is emplaced in a grey dolomite shatter breccia which was formed by the same explosion that formed the structure. Recrystallization of the dolomite grains along the brecciated fragments cemented the breccia. The breccia was then fractured a second time forming small shear zones and open fractures. The latter were filled with dolomite and hydrocarbons. Supergene alteration followed. They believe the sphalerite to be the result of hypogene

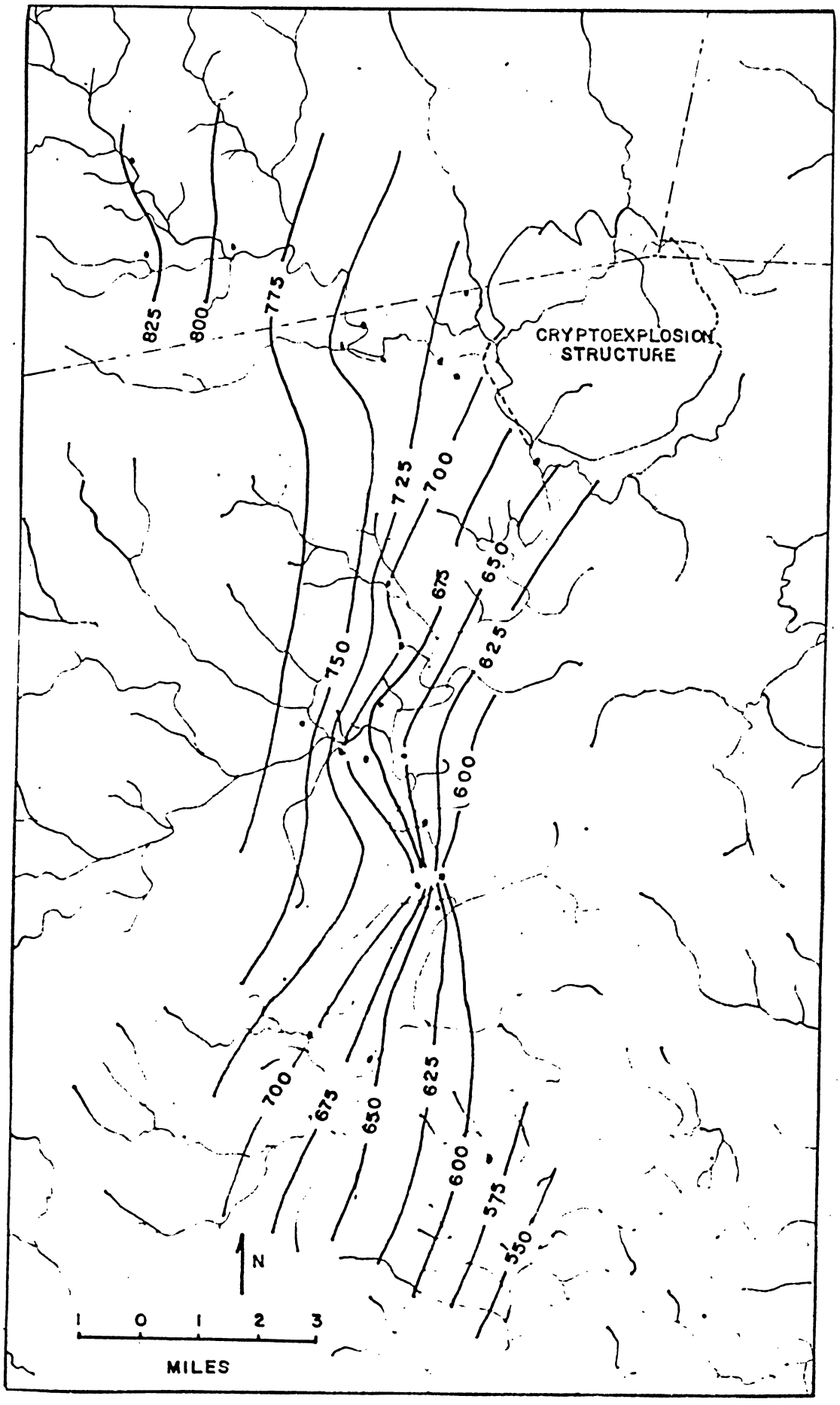

FIGURE 7 Structure Contour Map on the Base of Brassfield Limestone

contour interval = 25' after Galbraith, 1968

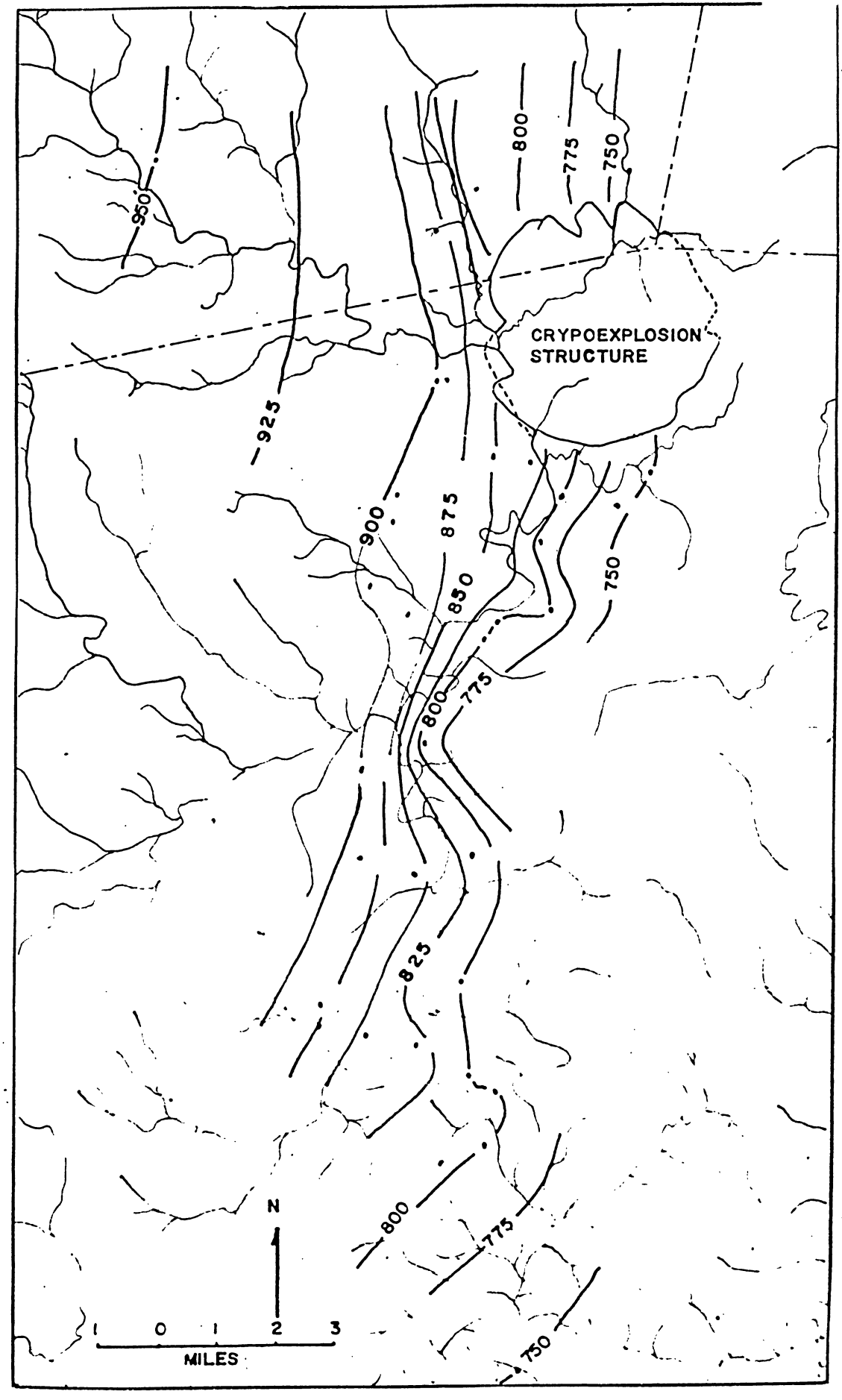

FIGURE 8 Structure Contour Map on the Base of the Bisher Dolomite

contour interval = 25' after Galbraith, 1968

mineralization. The sphalerite itself is red to reddish brown at the crystal's core surrounded by an orange colored zone and a pale yellow rim.

More recently Reidel (1970) remapped the western portion of the cryptoexplosion structure (Figures 2 & 9) and attempted to determine, geochemically, the pattern of heavy metal distribution in the soils in this area (Heyl and Brock's occurence). He concluded that faulting within the cryptoexplosion structure is responsible for the localizing of the sphalerite and that the Greenfield, Peebles, and Tymochtee dolomites are the most favorable host rocks.

Stryker (1971) remapped a portion of the northern boundary of the Serpent Mound Structure, (Figures 2 & 10). He attempted to determine the northern extent of mineralization by the same method as Reidel. Stryker also concluded that the mineralization in this northern portion of the structure was controlled by faulting and that the same rock units Reidel had found favorable, were also the most favorable host rocks here.

Wachter (1971) (Figure 2) working on the southeast border attempted to trace the mineralization just outside the structure. He found an extension of the mineralization; however, he did not reach any conclusions as to the controlling factors.

GEOLOGIC AND HEAVY METAL ISOPLETH MAP OF THE WESTERN PART OF THE STRUCTURE

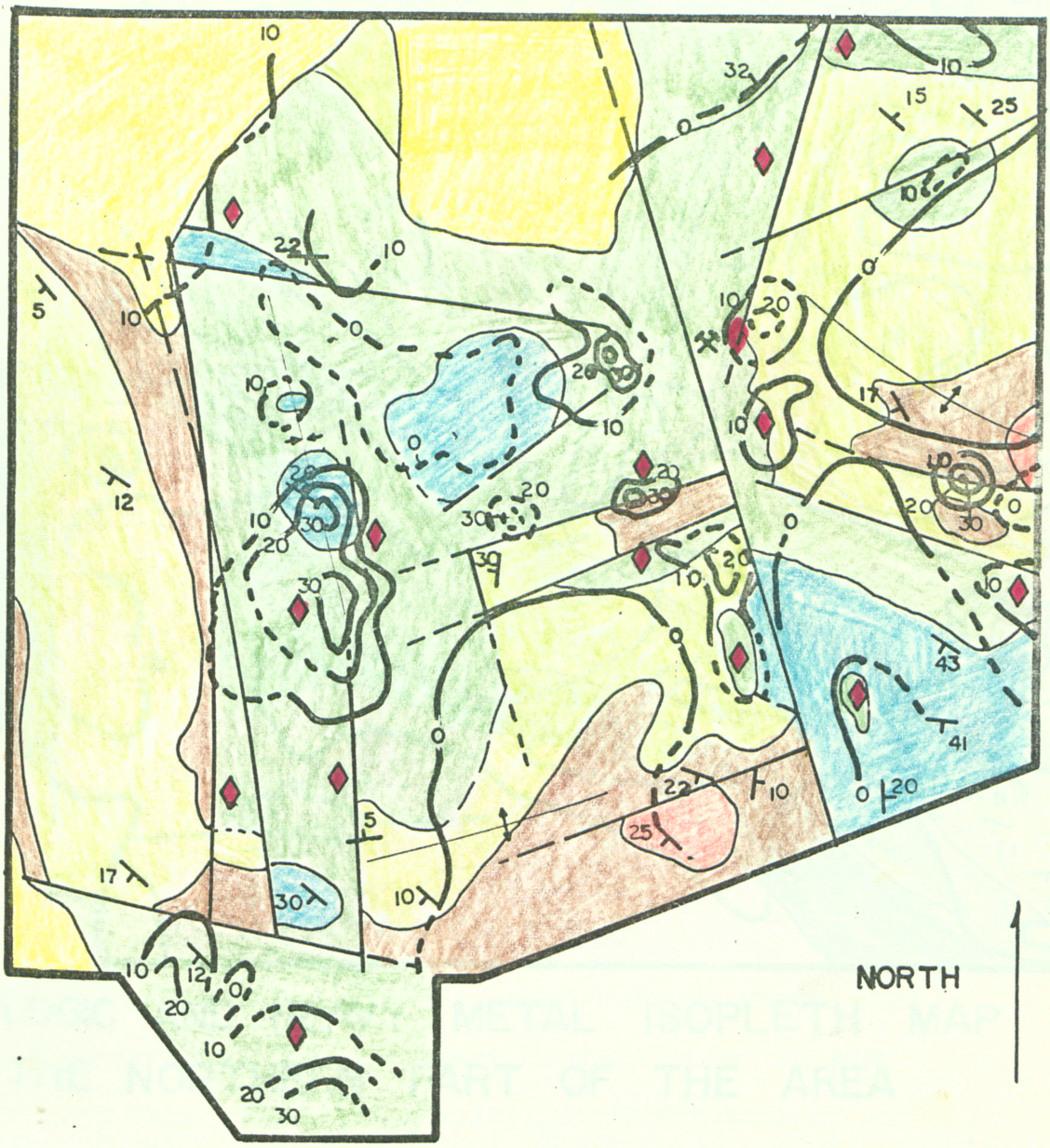

HEAVY METAL ISOPLETH IN PPM

FAULT

CONTACT

SCALE

0 1000 2000

FEET

FIGURE 9

AFTER REIDEL 1970

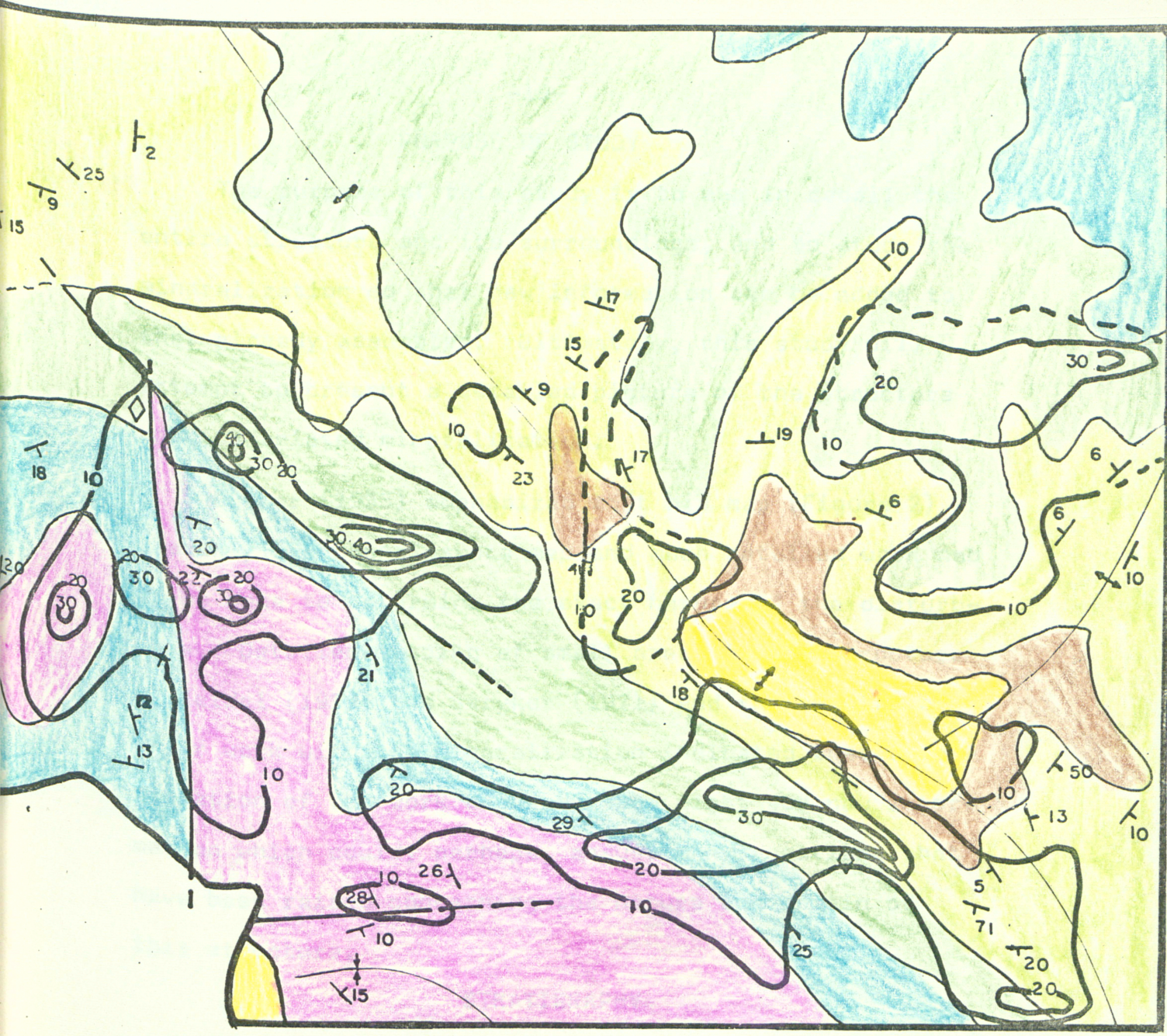

GEOLOGIC AND HEAVY METAL ISOPLETH MAP OF THE NORTHERN PART OF THE AREA

HEAVY METAL ISOPLETH IN PPM

FAULT

CONTACT

NORTH

SCALE

0 1000 2000

FEET

FIGURE 10

AFTER STRYKER 1971

PURPOSE OF STUDY

The purpose of this study is to map in detail the entire structure and its surroundings, and to study the mineralization so that new information can be added to that already assembled. Ultimately, this study will attempt to present a detailed picture of the structure and its related mineralization.

Bucher (1933) emphasized that his map (Figure 2) was only a reconnaissance map and much detailed work had to be done to determine the exact nature of the disturbance. Detailed mapping of small areas in the structure by Reidel (1970) and Stryker (1971) and the results of their work with the mineralization indicated that a continuation of the work begun by them might add new information which could, perhaps, answer many questions that have been raised concerning the nature and origin of this structure.

STRATIGRAPHY

The formations exposed in this study area range from Ordovician through lower Mississippian in age (Figure 11). The rocks consist of a sequence of carbonates, shales, and sandstones. There are no metamorphic or igneous rocks exposed in the area.

In this section field and literature descriptions of the stratigraphy are combined. Because of the poor exposures and the highly disturbed nature of the rocks a detailed study of the stratigraphy within the study area

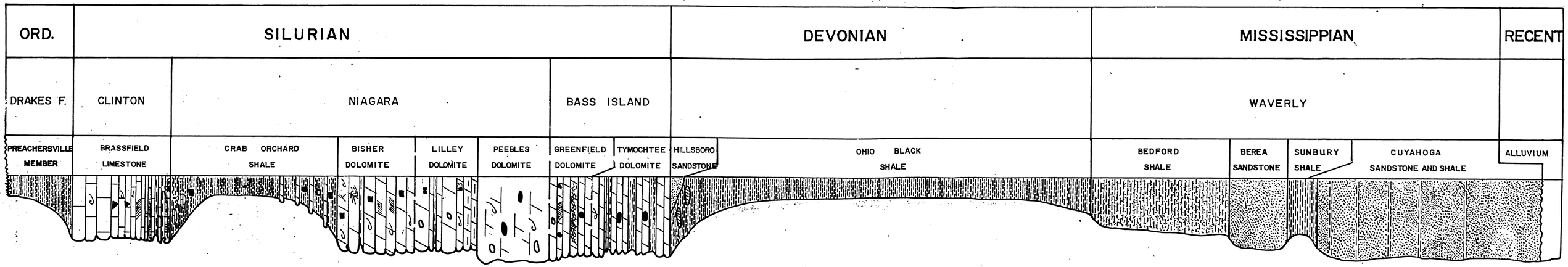

KEY: VUGS o , ASPHALT ● , FOSSILS , CROSSBEDDING , CARBONACEOUS BANDING , PYRITE ■ , MARCASITE □ , CHERT ▲ , GLAUCONITE , HEMATITE , SIDERITE NODULE , CONTORTED PRIMARY STRUCTURE

SCALE

0 20 40 60 80 100 FEET

GENERALIZED STRATIGRAPHIC SECTION OF THE SERPENT MOUND AREA

FIG. 11

is impossible. The only new stratigraphic information, which will be considered later in the text, was derived from drill cores which extended from the Greenfield Peebles dolomite to the upper Brassfield.

The upper Ordovician, Cincinnati Series rocks are perhaps the oldest exposed in the area. Figure 12 shows the most recent stratigraphic nomenclature used in the Cincinnati area (Peck, 1966). The unit most commonly seen in the cryptoexplosion structure is the Preachersville member of the Drake formation. This consists of a greyish green, thin bedded, limy to dolomitic mudstone that becomes purple near the top (older name - Elkhorn) (Photo 2). Thin lenses and irregular beds of dolomitic limestone occur throughout the fossiliferous unit. One of the more interesting fossils reported is an Eucypterid zone occuring not far below the contact with the Brassfield limestone. Because of the poor exposures of the Ordovician beds in this area, the Ordovician rocks have been undifferentiated when mapped.

The Brassfield limestone of early Silurian age lies above the Ordovician. The contact (Photo 2) appears to be conformable throughout the area. Galbraith (1966) divided the Brassfield limestone into three parts. The lower most part is a massive grey limestone. The middle unit is a thin, white irregularly bedded limestone with thin green shale or clay partings. The third part is a thinly bedded, coarse, granular, bioclastic limestone

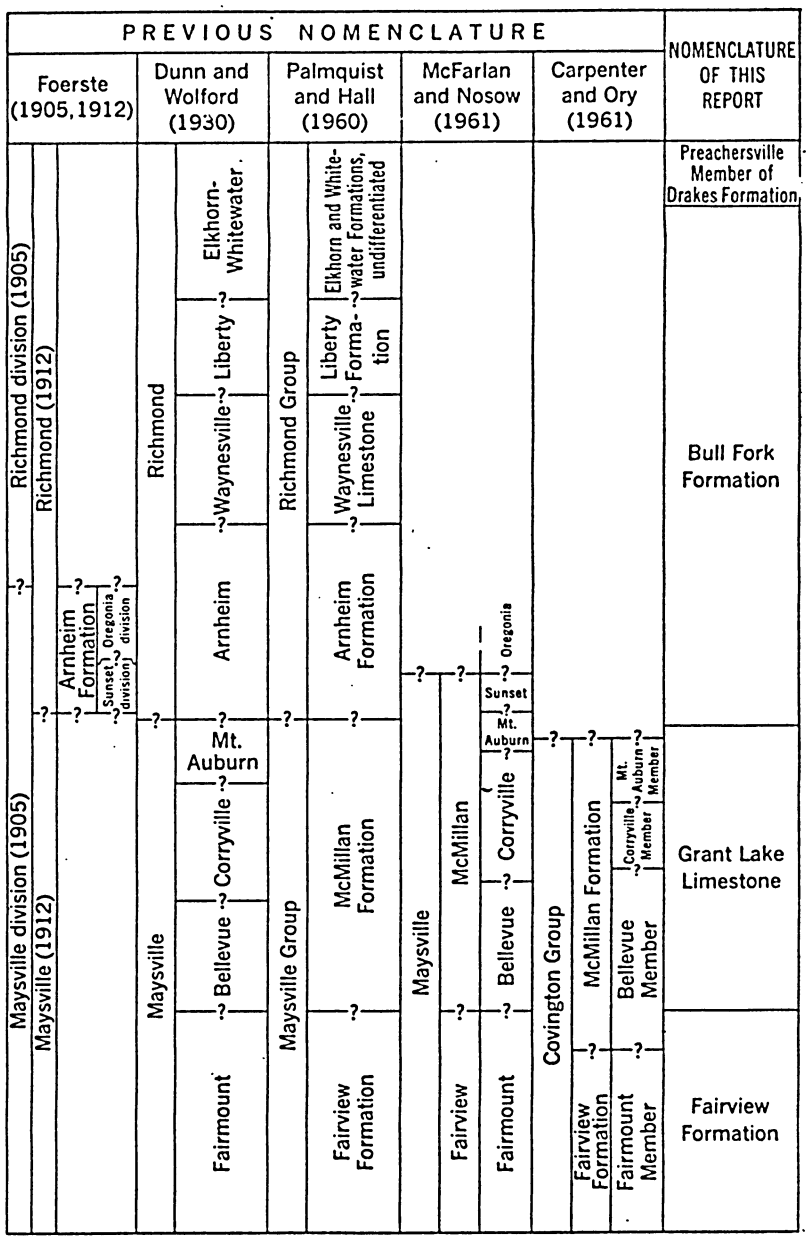

Figure 12

Nomenclature of Upper Ordovician rocks above the Kope Formation in the Maysville area of Kentucky (after John H. Peck, 1966).

PHOTO 2

Contact between the Preachersville member of the Drakes formation(Ordovician) and the Brassfield limestone(Silurian). West of study area on highway 73.

with varying amount of hematite.

Three core drill holes were completed by Cominco American in the cryptoexplosion structure during the summer of 1971. The cores are described in Figure 13 and their locations can be found on the north central part of Plate 1. The shallow wells averaged approximately 300 feet in depth and only penetrated down to the middle and upper parts of the Brassfield limestone.

In the cores the beds of the middle and upper Brassfield contain a considerable amount of glauconite. The glauconite occurs as small pellets resembling the glauconitic fecal pellets described by Van Wie (1971) and becomes more concentrated near the contact with the overlying Crab Orchard shale. The glauconite appears to be oxidized in places and it is this oxidized glauconite that could possibly have formed some of the hematite which is so very common in the upper part of the Brassfield. The green shale beds of the Brassfield vary in thickness from one core to another, as can be seen in cores C.A. 110 and C.A. 59, where the shale is more plentiful than limestone. Although the full section is not present in the cores, the thickness is estimated to be 60 feet from exposures outside the structure.

The Crab Orchard shale conformably overlies the Brassfield limestone and consists of 112 feet of alternating green and red shale. Beds of finely laminated dolomite several inches thick occur near the top while lenses

and thin beds of limestone and limy dolomite occur near the base. A great amount of glauconite, similar to that described above, is found near the contact with the Brassfield limestone. Near the Brassfield contact, the alternating red-green lower shale changes to a pistachio green, yellow and yellow-red at the contact (Photo 3). Pyrite and marcasite are common throughout, but fossils are extremely rare.

The Bisher dolomite overlies the Crab Orchard shale with a sharp contact (Photo 4) and is a silty, fine-grained, grey to blue-grey dolomite that weathers to a characteristic reddish-brown color. Glauconite and pyrite are found near the base. Pyrite usually occurs as cubic crystals modified by octrahedrons. In core C.A. 59, pyrite can be found along fractures near the base. Vugs are uncommon but those that did exist are now filled with calcite that often fluoresces blue or yellow under ultraviolet light. Within the calcite, doubly terminated, euhedral crystals of quartz are quite common (Photo 5). Fossils are abundant throughout the dolomite but are especially common in the thin white porous limestone bands. The brachiopod, Cryptothyrella cylindrica, is a prominent marker several feet above the Crab Orchard contact. Individual beds vary in thickness from 2 to 8 feet. The Bisher dolomite is approximately 45 feet thick in the study area.

PHOTO 3

The comtact between the Brassfield limestone and the Crab Orchard shale.(from well core CA 59)

PHOTO 4

The contact between the Crab Orchard shale and the Lilley Bisher dolomite.(south of location 39,Appendix IV)

PHOTO 5

A vug in the Bisher dolomite that has been filled by calcite.The calcite has a core of euhedral crystals of quartz.(near 43)

PHOTO 6

A quarry of Greenfield Peebles dolomite.(north of 23)

The Lilley dolomite is a grey, fossilliferous, weakly bedded dolomite that makes a gradational contact with the Bisher dolomite. The Lilley becomes increasingly silty and argillaceous as the top is neared.

In the field, the Lilley and Bisher dolomites are extremely difficult to differentiate so they have been mapped in this study as one unit. To the south, the U.S. G.S. maps them as only the Bisher formation. The total measured thickness in the study area is 87 feet.

The Peebles formation is transitional with the Lilley. Interfingering of the two units can be seen south of the area, in the Plum Run quarry (Bowman et al., 1961). In the study area a distinct break from an argillaceous, extremely silty, dark grey dolomite to a relatively pure, white to tan dolomite marks the contact. This is easily recognized in the field because the argillaceous silty dolomite of the Lilley erodes more rapidly than the Peebles dolomite. The Peebles dolomite is a massive, medium to coarse grained, white to tan reef dolomite (Photo 6). It is a very pure dolomite that contains numerous vugs and pores which are commonly filled with asphalt. The dolomite is so porous that euhedral, rombic crystals of dolomite are quite common throughout the rock, and when a section of dolomite core is immersed in water, it will absorb the water like a sponge. Asphalt is common in the pores as well as vugs. Calcite, quartz, pyrite, marcasite and sphalerite are seen throughout the formation. Fossils are common,

but their preservation is quite poor. The Peebles formation is 50 to 60 feet thick but can reach a thickness of 100 feet. Bedding in this unit can rarely be seen in the field.

The Greenfield dolomite unconformably overlies the Peebles dolomite with pockets of clayey material marking this unconformity. The Greenfield dolomite is a tan, well bedded dolomite. The bedding is of medium thickness and exhibits small scale crossbedding. Megaripples are seen in the formation within the study area. Vugs are common, but the dolomite is not as coarse grained as the Peebles formation.

The Tymochtee formation conformably overlies the Greenfield formation. The Tymochtee-Greenfield contact is an arbitrary one set at the top of the Greenfield dolomite where a thick bed displays contorted primary structure (Bowman et al., 1961). The Tymochtee formation is a thin bedded, blue-grey dolomite with a fine grain, dense texture. Bedding is distinct with argillaceous partings and carbonaceous laminee.

The Greenfield and Tymochtee formations comprise the Bass Island Group. The thickness of each formation is unknown in southern Ohio, due to the erosion of the Silurian before the advance of the Devonian sea, however, the approximate thickness of the Bass Island Group in southern Ohio is 45 feet.

The Peebles, Greenfield, and Tymochtee formations are difficult to differentiate in the field; consequently they have been mapped as one unit in this study. Their total thickness is estimated to be between 110 feet and 150 feet.

The Devonian, Ohio Black shale lies unconformably above the Silurian, Tymochtee formation. The contact is everywhere uneven and an irregularly occuring sandstone called the Hillsboro sandstone, occasionally outcrops near the contact. One to five feet of Olentangy shale may be present at the base of the Ohio Black Shale; siderite nodules (Photo 7) occur ranging in size from 6 inches to 2 feet in diameter, some having a core of calcite and pyrite. There is a "lag" deposit that contains abundant fish fragments and sulfide minerals at the contact. The thickness is almost 260 feet in the study area.

A sharp color break marks the contact between the Devonian Ohio Black shale and the Mississippian Bedford shale. The change is from the uniform texture and black color of the Ohio Black shale to the non uniform texture and blue to blue-green color of the Bedford shale. The Bedford shale is an argillaceous shale with increasing amounts of thin ripple marked sandstones toward the top. Its thickness is from 90 to 95 feet and is rarely exposed in the area.

PHOTO 7

The Ohio Black shale with siderite nodules at the base.(north of structure on rt. 41)

The Berea sandstone overlies the Bedford shale and makes a distinct contact in the study area. The Berea sandstone is a moderately coarse grey sandstone with occasional thin shale partings and ripple marks. Beds are of medium thickness and show crossbedding.

The Berea sandstone is conformably overlain by the Sunbury shale making a distinct contact in the area. The Sunbury shale is a fissile, black shale, and on close examination it resembles the Ohio Black shale. The Sunbury shale is very carbonaceous and is 12 feet thick in the map area. The upper part is frequently more argillaceous than the lower part.

The Cuyahoga formation is the youngest Paleozoic formation exposed in the area. It consists of a series of sandstones and shales but because of their poor exposure, only the Henely shale and Buena Vista sandstone will be briefly described.

The Henely shale member overlies the Sunbury shale and is apparently separated from the Sunbury on the basis of color and textural change. The Henely is an alternating red and grey shale near the top, while at the base, it is an argillaceous, slightly gritty shale. Its thickness is about 12 feet.

The Henely shale is overlain by the Buena Vista sandstone member and makes a distinct contact. The Buena Vista sandstone is approximately 70 feet thick. It is a moderately coarse, buff, massive sandstone and is exposed in the map area as a single bed or as two beds.

DESCRIPTION OF THE STRUCTURE

(a) Procedure

Prior to commencing field work, a preliminary topographic base map of the cryptoexplosion structure was prepared from three United States Geological Survey topographic quadrangles; the Bainbridge, Seaman and Peebles 7½ minute sheets. Mapping was carried out on weekends, vacations and during the summers of 1969, 1970, and 1971. An estimated time of over six months was spent in the field collecting data to prepare the geologic map, Plate I. Because of the reduced scale of the base map 1.5 inches to 1000 feet, several minor structures do not appear on Plate I. The major structures of the mapped area which are considered in the remainder of the text, can easily be found on Plate I, the geologic map, by referring to the numbered index map for Plate I. The numbered index map is in Appendix IV.

(b) General

The Serpent Mound Cryptoexplosion Structure is nearly circular in plan view with a diameter that varies between 4½ and 5 miles in length. The structure is elongated in a north-south direction and has an area of approximately 16 square miles. As Photo I shows, it stands topographically above the surrounding countryside.

The Serpent Mound disturbance can be divided into three structural units (Plate I) as follows: 1) a central, circular elevated area of radiating anticlines but by high-angled faults,

2) a peripheral, depressed outer ring of synclines cut by high-angled faults, and 3) an intermediate ring area of folded and faulted, vertical tectonic displacements less than the central elevated area or the outer depressed area.

c) The Central Area

The central area is characterized by uplifted and faulted Silurian and Ordovician rocks that have been folded into seven centrally radiating anticlines. The seven radiating anticlines are the predominate structural features and make the map pattern of the central area appear similar in outline to a starfish with seven arms (Plate I).

The northernmost anticline of the seven radial anticlines (Appendix IV, Location 1) is asymetric and overturned to the east (Plate 2, Section EE'). The western limb of this anticline has comparatively gentle dips, 25° to 50° to the west, while the eastern limb is overturned, and in some cases, dips 50° to the west. The most intense overturning is in the southernmost part of the fold. Toward the north from this locale, the overturning becomes progressively less until the altitudes approach horizonal at the extreme northern limit of the fold.

The second of the centrally radiating anticlines is the most open fold of the group. It can be located on Plate I by proceeding counterclockwise from Location 1 to Location 2 on the index map (Appendix IV, Location 2). This fold, like the first of the seven anticlines, is

asymmetric with the steepest dips on the east limb (Plate 2, Section EE'); however, this second anticline is not overturned.

Continuing counterclockwise around the seven centrally radiating anticlines, that is from the second to the third anticline (Appendix IV, Location 3), the third, or western radiating anticline, has an undulating axial line that is clearly delineated along the trace as small domes, basins, and a plunging nose (Plate 2, Section AA) (Photos 8 and 9). As in the northern anticline (Appendix IV, Location 1), the steepest dips of the western radiating anticline are near the central part of the cryptoexplosion structure area, while dips become more gentle toward the periphery of the major structure. The trace of the axial surface is straight near the center of the central area and then curves to the northwest away from this center.

Continuing counterclockwise around the central area, the fourth of the seven radiating anticlines, the southwest anticline (Appendix IV, Location 4), is folded in such a way that it is actually two anticlines separated by a minor, intermediate syncline (Figure 14). The limbs are Brassfield limestone while in the center, the upper

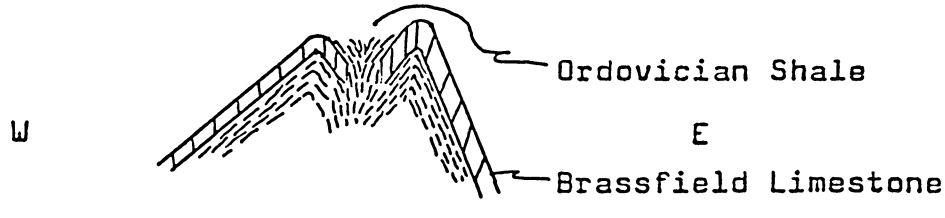

Figure 14 Southwest radial anticline (Appendix IV, Location 4)

PHOTO 8
Oblique air photograph of the west side of the Serpent Mound Cryptoexplosion showing the west radial anticline and middle ring fault

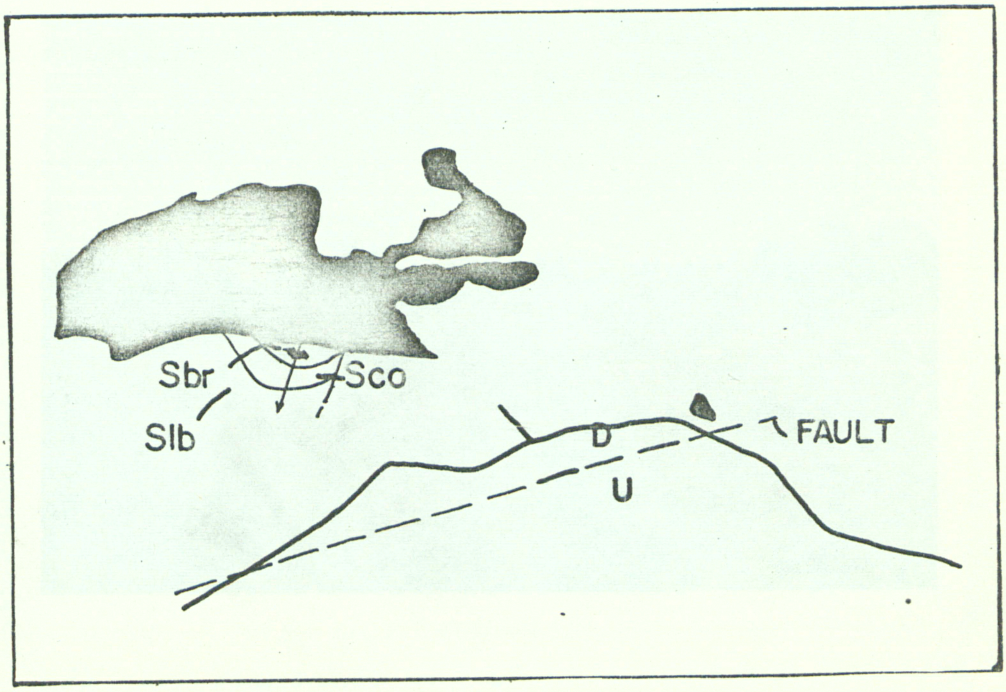

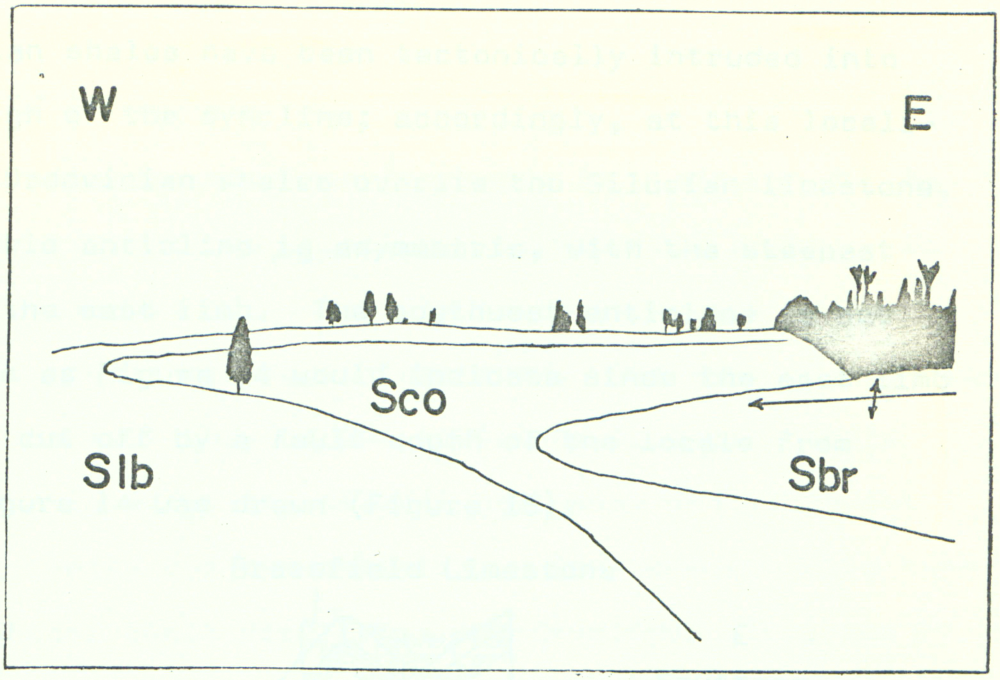

PHOTO 9

Morphologic expression of the west radial anticline (looking north)

Ordovician shales have been tectonically intruded into the trough of the syncline; accordingly, at this locality, the Ordovician shales overlie the Silurian limestone. This double anticline is asymmetric, with the steepest dips on the east limb. The southwest anticline is not as simple as Figure 14 would indicate since the east limb has been cut off by a fault south of the locale from which Figure 14 was drawn (Figure 15).

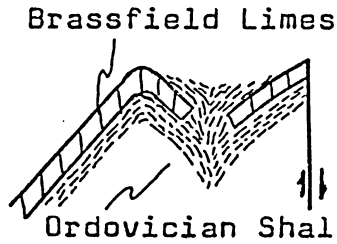

Figure 15 South of Figure 14

The fifth, and southernmost of the seven radiating anticlines of the central area (Appendix IV, Location 5) is very small. This structure has a large part of both limbs cut off by high angled faults, giving the anticline the appearance of a horst block.

The sixth and largest of the radiating anticlines (Appendix IV, Location 6) has a length of over 1½ miles. This fold is characterized by a vertically undulating axial line. The trend of the axial line also changes significantly from the southeast, to east, and then to the southeast again. The dips of the limbs of this anticline, like the dips of several of the other radiating anticlines, are highest toward the center of the central area and decrease

toward the periphery.

The seventh anticline (Appendix IV, Location 7), has a northeast trend and relatively symmetrical limbs. The structure becomes a dome at its farthest extension towards the center of the central area. The dome is separated from the main body of the anticline by a high angle fault, and in addition, several northeast and southwest striking faults cut the anticline. The dome is quite complex and many small drag folds are developed along and near the faulted borders (see Photo 10).

High angle faults and grabens are the dominant structures that separate the seven radiating anticlines of the central area. The faults are located primarily on the western and northern parts of the central area while there are six grabens on the east and south parts of the central area.

The simplest graben is on the northwest side of the central area (Appendix IV, Location 8) between the northwest radial anticline (Appendix IV, Location 2) and the northern radial anticline (Appendix IV, Location 1) (see Section EE'). A slice of Greenfield Peebles dolomites has been caught between the anticlines during their upward movement. This actually is a faulted limb of the north radial anticline.

Due south of the central area is an intensely folded

minor syncline just south

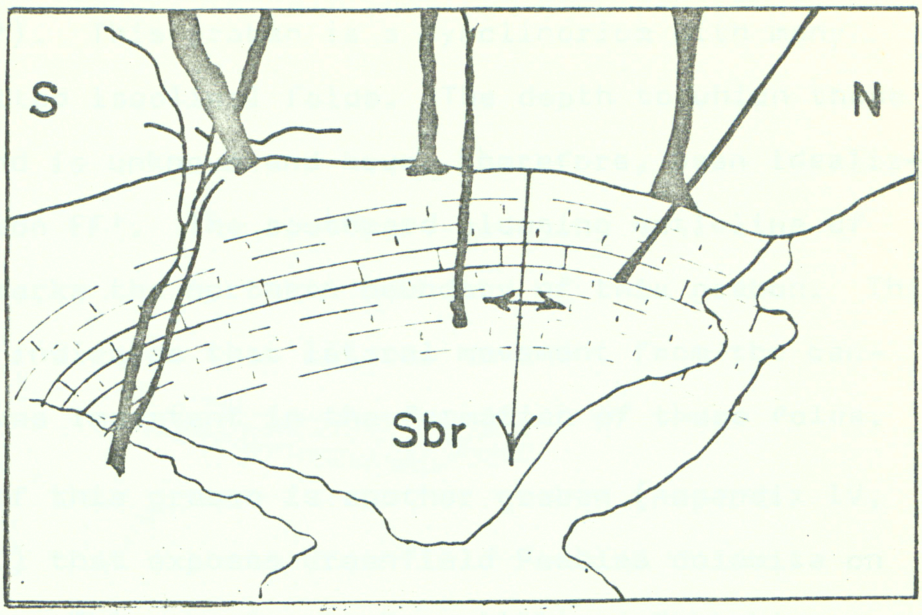

PHOTO 10

Drag fold on the northeast radial anticline. To the south the bedding is vertical. Adjacent to this on the south is a minor syncline.

and faulted graben (Appendix IV, Location 9) (see Plate 2, Section FF'). This graben is a synclinorium with many small, faulted isoclinal folds. The depth to which these folds extend is unknown and have, therefore, been idealized in Section FF'. The southward plunging anticline of Figure 14 marks the northern boundary of this graben. This apparently indicates that lateral movement from the central area was important in the formation of these folds.

East of this graben is another graben (Appendix IV, Location 10) that exposes Greenfield Peebles dolomite on the surface. This appears to have little deformation. The rocks dip to the northeast, however, the exposed stratagraphic section is too thick and therefore the graben is interpreted to have several unexposed faults.

The fourth graben (Appendix IV, Location 11) is southeast of the central area. The beds have been overturned near the center of the central uplift. The overturning is apparently the result of underthrusting from the central area causing those formations above the Crab Orchard shale to slide over those below, using the shale as a slide plane. The dashed lines show an idealized profile of the resulting structure.

The graben with the most intense deformation is located east of the central area (Appendix IV, Location 12), (Plate 2, Sections AA' and CC'). The structure sections are a generalization of a more complex structure. The

graben is an overturned fold that has been faulted by normal and reverse faults. (see Figure 16).

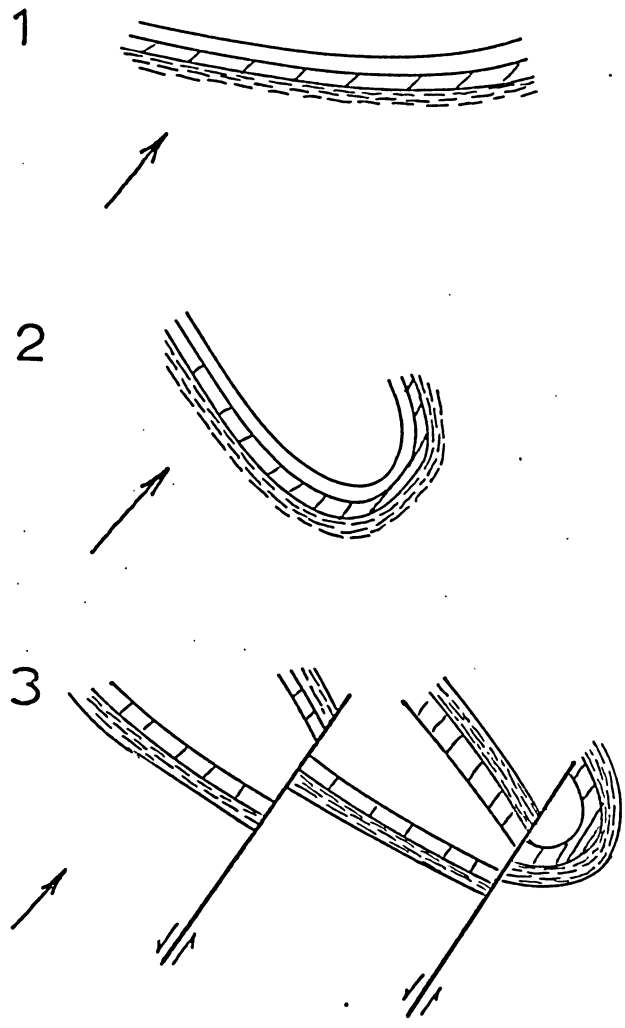

Figure 16 Generalized reconstruction of the formation of the east central graben.

This fold is similar to the folds of the south central graben (Appendix IV, Location 9) except major high angle faulting has completely broken the east one while the south one is more intact and there is no overturning. On the northernmost part of this graben (Appendix IV, Location 12) is another of Greenfield Peebles dolomite (Appendix IV, Location 13). This is small and most likely represents a splinter of dolomite caught up in the folding and faulting.

The central uplift area, in summary, is characterized by seven radial anticlines with grabens between them on the south, southeast, and east, and faults on the west and north sides. The one exception is the small graben on the northwest side. There is a definite pattern of overturning to the east and south. This overturning is clearly delineated by the grabens and the major radial anticlines. When overturning is not present, there may only be asymmetry in a fold with the steepest limb on the east side.

The starfish shaped pattern of the central uplift is similar to the pattern obtained by pulling a piece of cloth through a small hole, in other words, a pattern of compression and shorting. The deformation of the central area was asymmetrical with grabens forming where deformation was greatest and simple faulting where deformation was least.

The greatest amount of uplift described by Bucher (1936, Page 1062) is 950 feet. This was based on some "typically Eden fossils" from the southwest anticline

(Appendix IV, Location 4, but these were not in place. They were found in a rock pile (1933, Page 76). A specimen of the fossile Merocrinus was collected in the central area by Mr. Tom Weaver (personal communication). Merocrinus is found within a 20 feet range in the Point Pleasant formation of upper middle Ordovician, consequently the uplift may be at least 1000 feet.

(d) Outer Downdropped Ring

The outer downdropped ring is characterized by a series of curved synclines and basins that rim the peripheral boundary of the cryptoexplosion structure. Mississippian rocks, the youngest lithified rocks in the area, are exposed in these synclines. The synclines on the east side are more continuous than those on the west side.

The largest and most continuous syncline is on the east side (Appendix IV, Location 14 and 15). This structure is bisected by a small anticline in the locality due east (Appendix IV, Locality 16) of the central area (Plate 2, Section AA' and OO'). Here folding has brought up Greenfield Peebles dolomite in the core of a minor asymmetrical anticline (Plate 2, Section OO') whose east side has the steepest dips.

There are two small basins in the outer downdropped ring, one is north northwest of the central area (Appendix IV, Location 17) and one is southeast of the central area (Appendix IV, Location 18). The deepest of these is the southeast basin (Appendix IV, Location 18) and has

a stratigraphic throw of more than 800 feet. The largest syncline west of the central area is on the northwest side (Appendix IV, Location 19). This structure is somewhat similar to the large syncline on the east; however faulting and minor folding is much more common. Just as on the east side, there is a very prominent anticline (Appendix IV, Location 20) with a core of Greenfield Peebles dolomite.

The similarity with the east ends on the southwest rim. The southwest sector of the outer peripheral area has not been downdropped as much as that on the east, however it is structurally much more complex. The southwest area is also synclinal, but there is more faulting, especially due west of the central area. Serpent Mound State Park lies in this most unusual area. The syncline is not continuous but broken into two separate parts (Appendix IV, Locations 21 and 22). The south one (Location 21) is exposed along the cliff at Serpent Mound Park. This is a low amplitude fold and dies out to the east. The north-south trending one (Location 22) is similar but exposures are poor and it dies out to the south.

On the southern border of the cryptoexplosion structure is a small, asymmetrical syncline (Appendix IV, Location 23) with faulted ends. It is similar to those on the northwest (Location 19) and east (Locations 14 and 15) sides.

Two areas of little tectonic movement are located on

the north border of the peripheral area (Appendix IV, Location 24) and on the south border (Appendix IV, Location 25). Bucher (1936) described the southern locality (Location 25) as continuous with the undeformed rocks outside of the cryptoexplosion structure and also as a significant interruption in the peripheral ring graben. Detailed field mapping has revealed that this interpretation should be modified. There is no interruption in the peripheral ring graben at this locality. The outer ring is separated from the country rock outside the cryptoexplosion structure by a well defined fault (Appendix IV, Locality 25).

Due north of the central area is the second uninterrupted area described by Bucher (1936) (Appendix IV, Location 24). This area has been faulted on both east and west sides, forming a horst, however, the south end of the horst is folded downward, and in this sense, it is continuous with the undisturbed rock outside the cryptoexplosion structure.

The peripheral outer downdropped ring, in essence, consists of a series of curved synclines that have been separated to the north and south by basins. The east side of the peripheral ring is rather homogeneous while the west side consists of two distinct parts: a northwest side similar to the east side and a southwest side that has a comparatively low stratigraphic throw. The west side of the peripheral ring is faulted and folded more complexly

than the east side.

(c) The Middle Ring Area

The middle ring area is generally a transitional area between the central uplifted area and the outer downdropped ring graben. It is an area of folds and faults with concentric and radial patterns. To the south, southwest and west of the central area is a long curving fault (Appendix IV, Location 26a and 26b) which marks the boundary between the central uplifted area and the downdropped ring area in this sector. The east and north sides are downdropped while the south and west sides are uplifted, the reverse of what would be expected from comparison with other middle area boundary faults from similar structures like Crooked Creek, Missouri (Snyder et al., 1965) (Page 36). This fault could possibly link with a poorly exposed fault (Appendix IV, Location 27) along the north boundary of the central uplifted area. The northern faults (Location 27) south side is uplifted and north downdropped, the opposite of the western fault's (Locations 26a and 26b) pattern. Northwest of the central area and cut by this northern fault is a dome (Appendix IV, Location 28) (Section BB') with Ordovician rocks brought up almost as high as in the central area. This dome is a dominent structural feature with an effective diameter of a mile. Northeast of this dome and on the northeast side of the north radial anticline (1) is another dome (Section FF') (AppendixIV, Location 29) that has been faulted on the

south and east sides. South of the central area there are also some domes. The most noticable dome is on the southwest side (Appendix IV, Location 30) south of the southwest radial anticline (Location 4). The Crab Orchard shale marks the core. Between this dome and the southwest radial anticline is a fold (Appendix IV, Location 31) whose axial plane has been folded possibly showing two periods of deformation. The middle ring area (Appendix IV, Location 40) to the northeast has undergone minor deformation. This area appears to be a southward extension of the undeformed horst (Location 24). Its width is much larger and spans from the east fault of the undeformed horst to a major north-south fault (Appendix IV, Location 32) on the east side of the north dome. The north basin (Location 17) lies within these boundaries. A few minor folds and some northwest faults mark the disturbance in this section.

In summary, the middle ring area is characterized by folds and faults with concentric and radial patterns that probably signify a damping of the central area folds. There is a major fault rimming the western half of the central area, possibly related to the same process that caused eastward movement in the central area. The rest of the middle ring area is relatively undisturbed except for three domes and some minor folding and faulting.

(f) The Area Outside the Cryptoexplosion Structure

For the most part the area outside the cryptoexplosion

structure is relatively undisturbed. Galbraith (1968) mapped some northwest trending faults near the southeast corner (Appendix IV, Location 33) of the structure (Plate 1). Bucher (1933) also mapped some northwest trending faults on the northwest side of the structure which were confirmed by this study. There is a small flexture (Appendix IV, Location 34) 1000 feet west of the western border resulting from the downdropping of the outer ring. This flexture is continuous along this border for quite some distance, however to the north it becomes arched into an anticline (Plate 2, Section CC').

(g) Boundary of the Cryptoexplosion Structure

The boundary of the cryptoexplosion structure is marked by faults except in four places. Along the northeast side, there is an anticline (Appendix IV, Location 35) mapped by Bucher (1933), over one-half mile long dying out to the north and faulted off to the south. The northernmost interuption is the dolomite horst (Location 24) discussed before. The third interruption is on the west side (36, Appendix IV). Just south of this, the normal circular character of the border is broken by a northwest trending fault (36). The fourth break in the structure is on the east opposite the western interruption (37, Appendix IV).

(h) Stratigraphic Throw

The amount of stratigraphic throw above, below, and at its normal position was determined by constructing a

PHOTO 11

Sharp vertical fault contact from a well core.The bedding is dipping 15^{o} .

PHOTO 12
Fault contact between the Bisher dolomite
and the Peebles dolomite along Purcel road

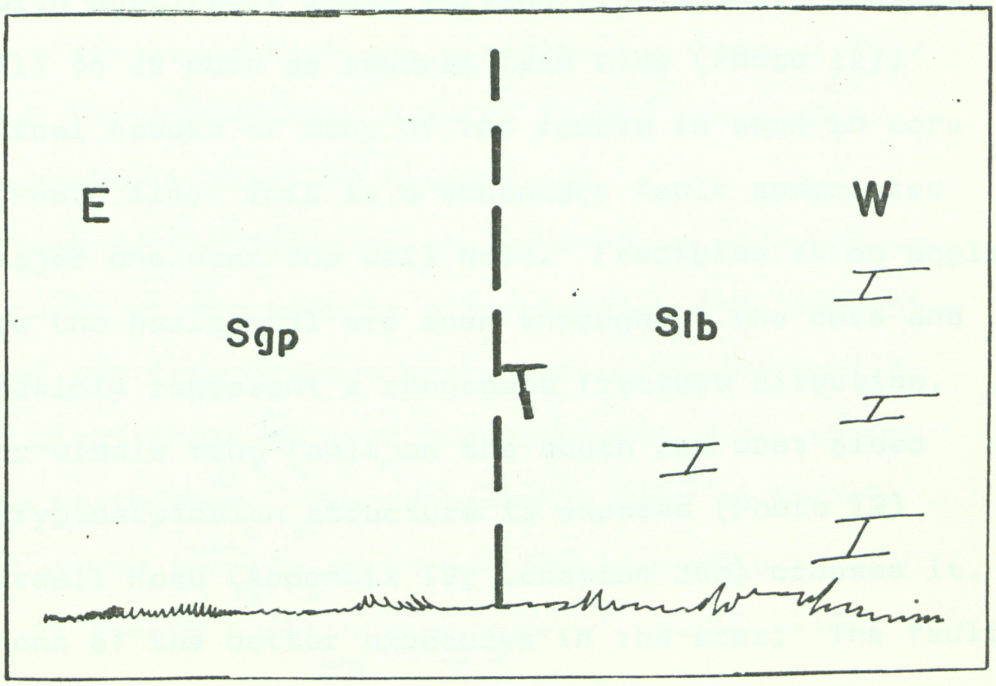

structure contour map of the Serpent Mound Cryptoexplosion Structure (Appendix III) and weighing the parts. Percentages were determined from the weights. The surface area of the Brassfield limestone at its normal position is 19.5% while 71.4% is below and 9.1% is above. No volume measurements were made for obvious reasons but it can be reasonably estimated that more material is below its normal position than above. These measurements compare favorably to Bucher's (1933).

(i) Character of the Faulting

Practically all the faults that occur in the structure are normal faults with vertical or near vertical fault planes. Exposures are poor throughout the area so the exact attitudes of the fault planes were impossible to measure. The contact between most fault blocks is easily marked with most fault zones varying from a sharp contact (Photo 11) to as much as several feet wide (Photo 12). The vertical nature of many of the faults is seen in core Ca 111 (Photo 11). This is a secondary fault associated with a major one near the well hole. Fractures at an angle of 30^{o} to the horizontal are seen throughout the core and could possibly represent a congugate fracture direction. The major middle ring fault on the south and west sides of the cryptoexplosion structure is exposed (Photo 12) where Purcell Road (Appendix IV, Location 26b) crosses it. This is one of the better exposures in the area. The fault zone at this point is only several feet with a vertical

component of net slip over 100 feet. This fault zone is typical of the structure. The widest and most unusual fault zone was described by Reidel (1970) along the same fault but northwest (Appendix IV, Location 26a) of the previous exposure. The width of this fault zone is marked by two isolated outcrops of Greenfield Peebles dolomite west (Appendix IV, Location 38)) of the central area and on either side of the fault. Here the fault zone is over 600 feet wide with a vertical displacement of only 400 ft. These highly brecciated exposures are the result of drag along the fault. North along this fault (Location 26a) is the same wide zone of intense brecciation. Not all the faults are vertical however, as Sections AA' and CC' point out. These nonvertical faults are in the east central graben (12) where some of the most intense deformation occured. These fault planes dip about 60^{o} to the west. They are a series of high angle reverse and normal faults that break the graben into several horsts and grabens in a manner already described (Figure 16).

Because of the lithologies involved, a very common type of fault is the bedding plane fault. The incompetent natures of the Crab Orchard shale and the lower part of the Ohio black shale allowed the carbonate units to use them as glide planes. The disharmonic fold of Section CC' is an excellent example of this. The bedding plane faults are very difficult to detect because of crossfaulting and poor exposures.

(j) Fault Direction

The fault pattern of this structure would normally be expected to be radial and concentric with respect to the central area. The faults were measured and plotted as length percentage frequency versus 10^{o} interval directions. This is represented in Figure 17. An examination shows a tendency for more faults to be west of north rather than east of north with the greatest single class frequency (11.5%) occuring N 30^{o}-20^{o}W. The Tucky Chi Square Test for Preferred Orientation, however, shows this is not significant. Since the boundary faults obviously make a considerable part of this, another plot was made excluding the boundary faults (Figure 18). The direction N 30^{o}-20^{o}W becomes even more pronounced (14%) but still tests insignificant. Another direction N 60^{o}-50^{o}W, becomes prominent (11.5%). Although these directions test nonsignificant, the dominance of these northwest directions of faulting cannot be disputed.

(k) Cataclastic Rocks

Tectonic brecciation is almost always developed along all fault surfaces in the map area. The type of breccia is a function of the physical properties of the lithologic units and the intensity of faulting. Two types of breccias are present: a monolithologic breccia of shattered rocks of a single lithology and polylithologic breccia of several rock types together. Many of the fault zones, especially in the carbonate rocks, have been mylonized (Photos 13 and 14). Photo 13 is a mylonite (according

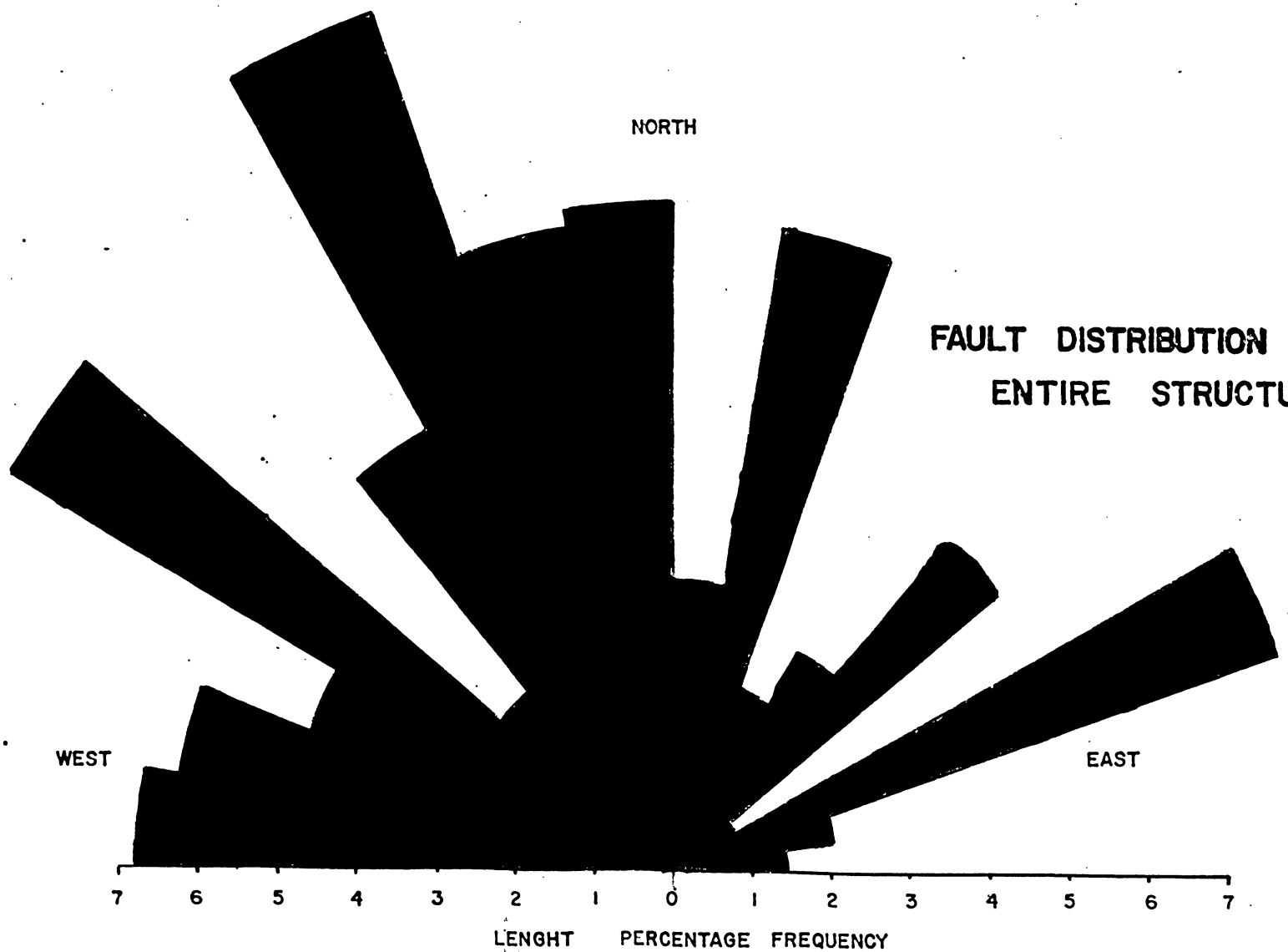

FAULT DISTRIBUTION FOR
ENTIRE STRUCTURE

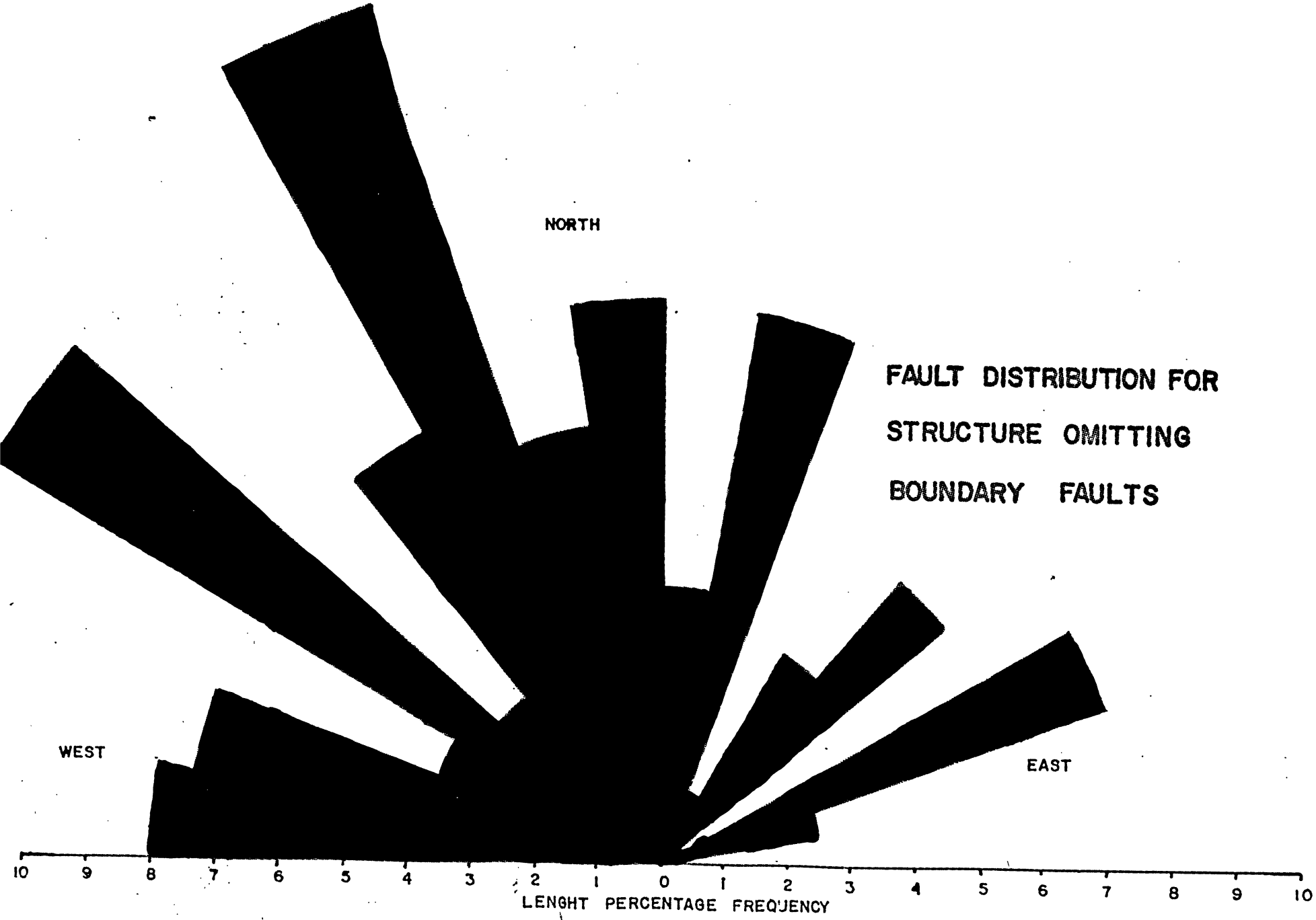

FAULT DISTRIBUTION FOR STRUCTURE OMITTING BOUNDARY FAULTS

FIGURE 18

to Higgins, 1972, Appendix V) that shows the linear fluxion structure and angular fragments. This is from the quarry just east of the north part of the middle area fault (Appendix IV, Location 26a). In this quarry not all the cataclastic rock is mylonite, some shows less mechanical effect and grades into protomylonite (See Appendix V). The fluxion structure of the mylonite in this quarry has a 45° dip to the northeast. Bucher (1933) used this as criteria for his "zigzaged fault"; however, the writer interpreted this to be a local effect of the large fault zone. This is based on the lenticular nature and limited extent. It probably represents rotation in the fault zone. Rotation is seen in other mylonites (Photo 14) from this fault zone. Ultramylonites are present where faulting occurs in the shales.

Coarser cataclastic rocks occur in fault zones away from the center. A fault zone of microbrecciated Mississippian sandstones from the northwest syncline (Appendix IV, Location 39) has many angular fragments (Photo 15) with limonite coating the grains of the matric. Photo 16 shows a microbreccia composed of Hillsboro sandstone from a hillside exposure (Appendix IV, Location 40) just south of the north central patch of alluvium at the contact of the Greenfield Peebles dolomite and the Ohio black shale. The light colored parts are fragments of the original rock, while the red matrix (Photo 17) is ground up sandstone coated with limonite. Dark veinlets and pockets

PHOTO 13

Mylonite from a road quarry on the west side of the structure (near 26)

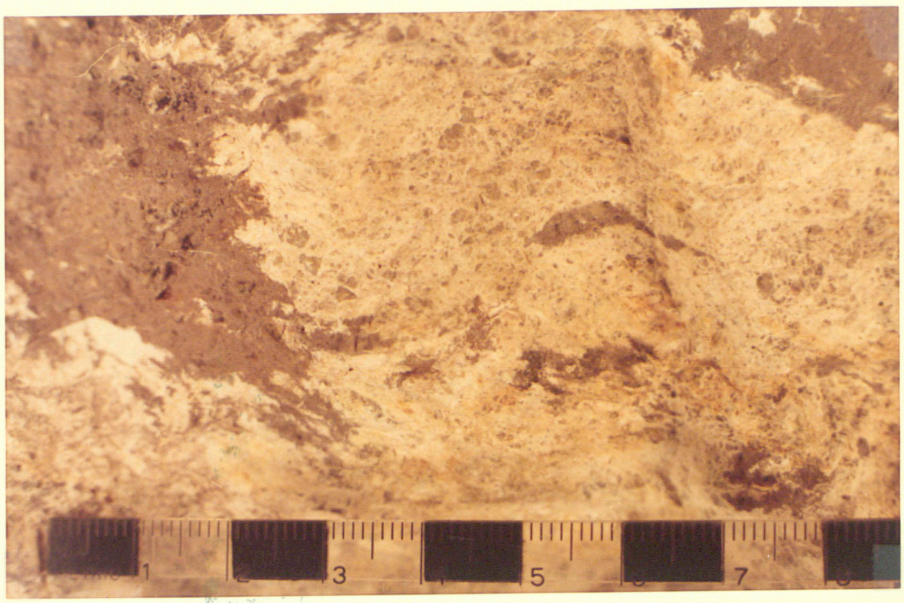

PHOTO 14

Mylonite showing rotation of fluxion structure (near 38 west)

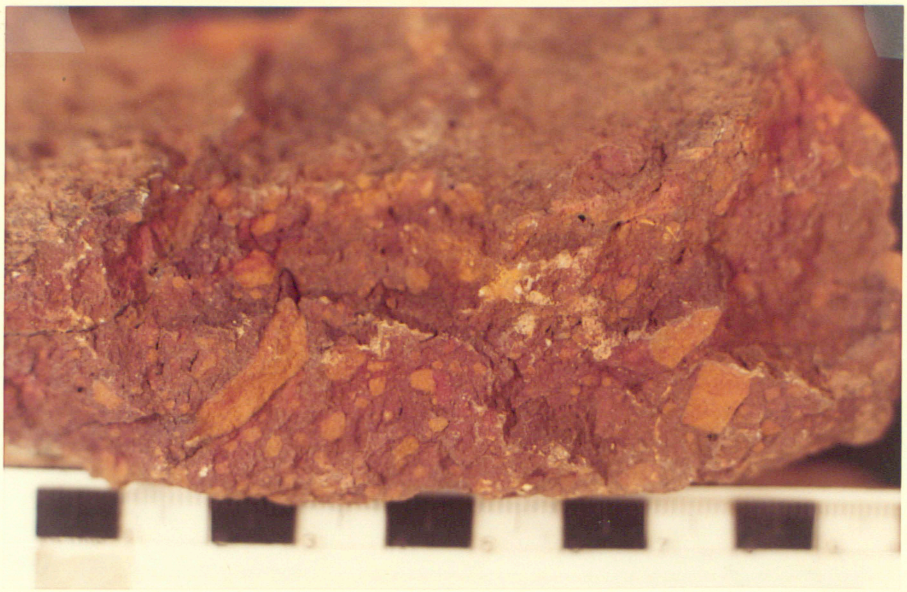

PHOTO 15

Microbreccia of Berea sandstone from the northwest ring graben (39) location

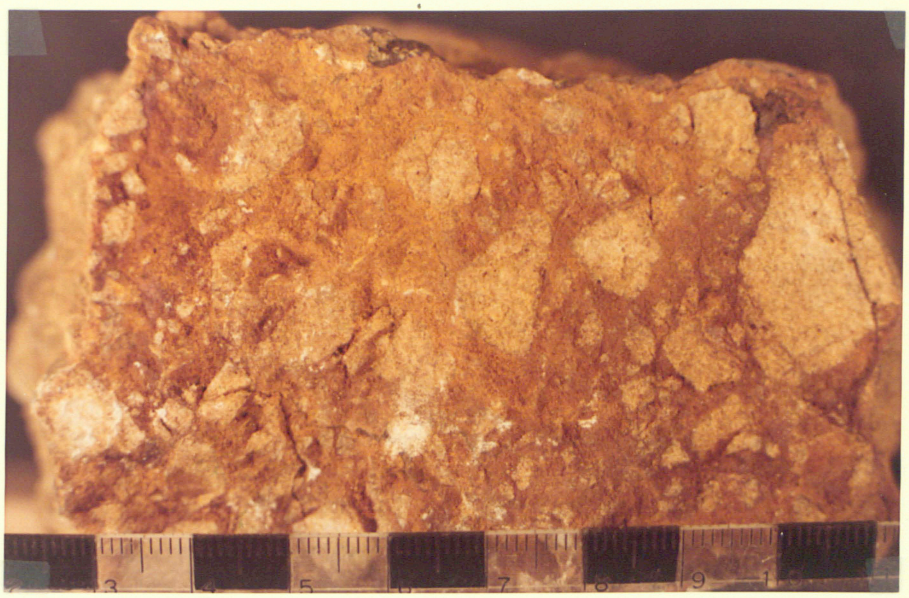

PHOTO 16

Microbreccia of the Hillsburo sandstone (40) location

of clay cut the rock everywhere. Along several faults there are microbreccias composed of Ohio black shale (Photo 18).

Mixed breccias are rare in this structure. The best exposure is located on the northwest part (Appendix IV, Location 41) of the outer ring between the north central basin (Location 17) and the northwest syncline (Location 19) (Photos 19 and 20). This is a microbreccia of dolomite which has been simultaneously intruded by a sandy shale. The width of the exposure is about 10 feet and its length is unknown. It parallels the boundary fault and resembles a dike. The sandy shale has slicken sides and small fragments of dolomite are suspended in the shale (Photo 20). The sandy shale was probably derived from the sandy shale contact of the Peebles and Lilley dolomites.

(1) Folding

The types of folds are dependent upon the lithology and the intensity and rate of deformation. As would be expected, in the more brittle carbonates and sandstones, plastic deformation never occurs and fracturing is more important. In the simplest case of folding, there is a shear fold with flexure slip (Photo 21) just outside the structure on the northwest side (Appendix IV, Location 34). The rocks are horizonal west of this and then suddenly at this point the rocks dip 55^{o} to the east. The shear fold here is actually a series of fractures giving the rock its inclination. There is no brecciation of the rock. This

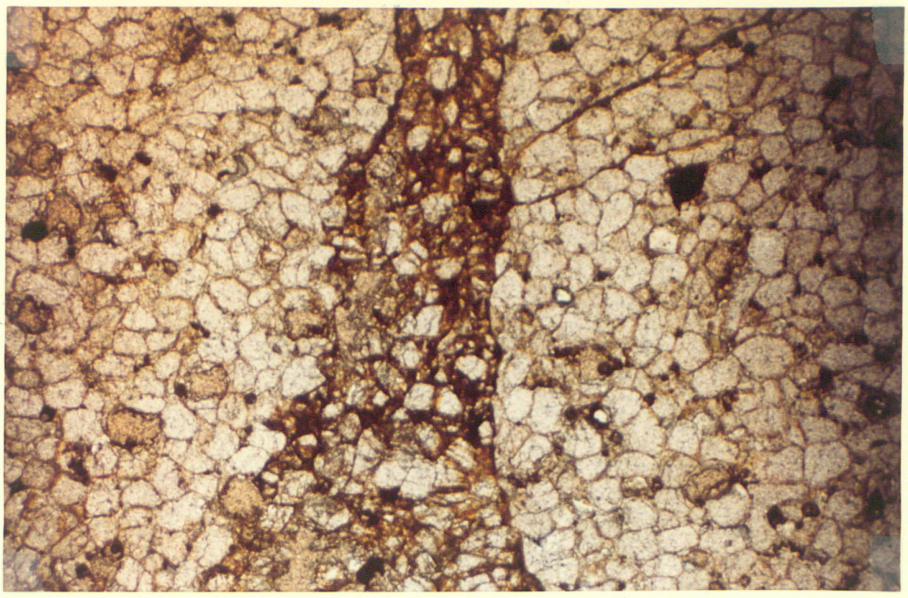

PHOTO 17

Microphotograph of the contact between the porphyroclasts of a sandstone breccia

(location 40)

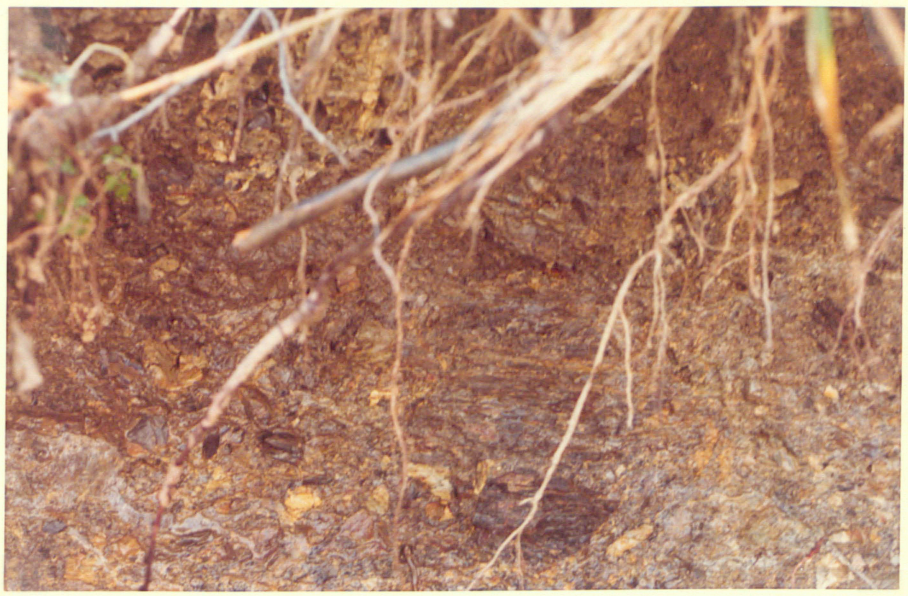

PHOTO 18

Microbreccia of Ohio Black shale

(east of location 12)

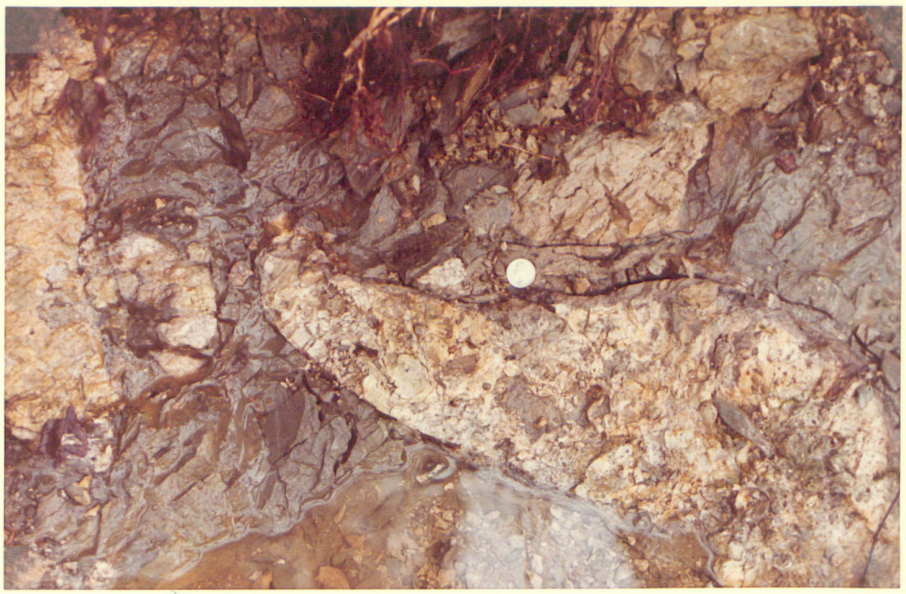

PHOTO 19

Mixed breccia in the Greenfield Peebles dolomite (location 41)

PHOTO 20

SAME

shear fold is the result of drag caused by the down dropping of the outer ring. Inside the structure this type of folding has progressed to greater degrees. Just north of the east central graben is a small plunging anticline (Appendix IV, near Location 13) with an adjacent syncline on the south (Photo 10). This is a shear fold in the Brassfield limestone between the graben (Appendix IV, Location 12) and the northeast radial anticline (Location 7). It is no more than 20 feet across and asymmetrical with the southern limb near vertical. The plunge of this anticline can be traced down the creek to the east for some distance. Upon cursory examination this fold appears to be plastically folded but close scrutiny shows that small healed fractures are responsible for the folding. This is a shear fold with geometric rotation of the limbs. Where greater deformation has occured, there is the same pattern. On the southern limb of the west radial anticline (Appendix IV, Location 42) (Photo 22 and 23, and Section EE') is an example. Photo 22 is farthest away from the axial plane of the radial anticline and shows a small fold similar to the one described above. Photo 23 is adjacent to this fold only closer to the axial plane of the radial anticline. This deformation becomes more intense and fracturing plays a greater importance in the folding. Virtually every radial anticline near the central area carries this to the extreme. The limbs of the radial anticline are a series of slip or shear folds that result from minute displacements, that resemble

PHOTO 21

Simple flexture on the west border

(location 34)

PHOTO 22
Drag fold on the south limb of the west radial anticline. See PHOTO 23 which is the northern extension of this.

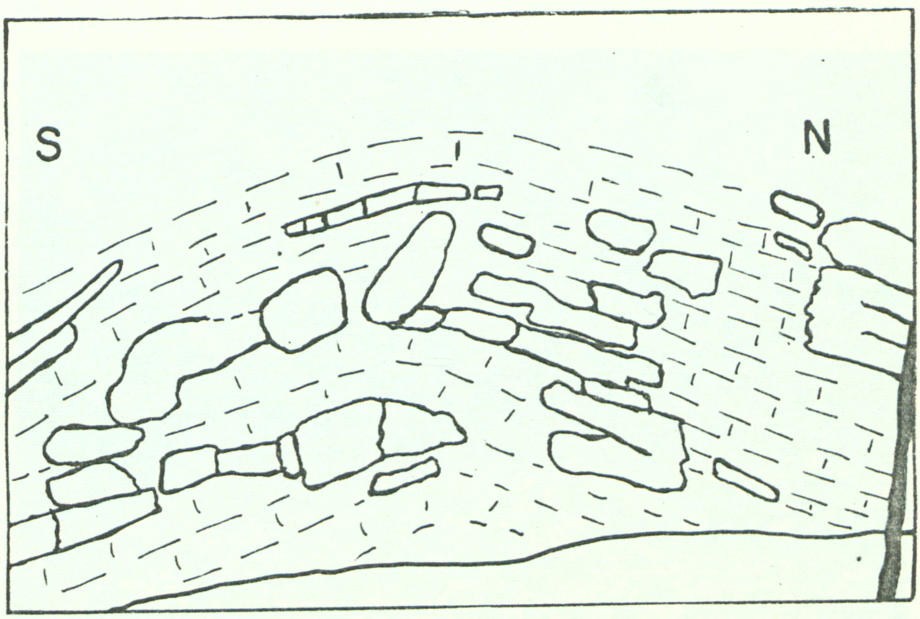

S

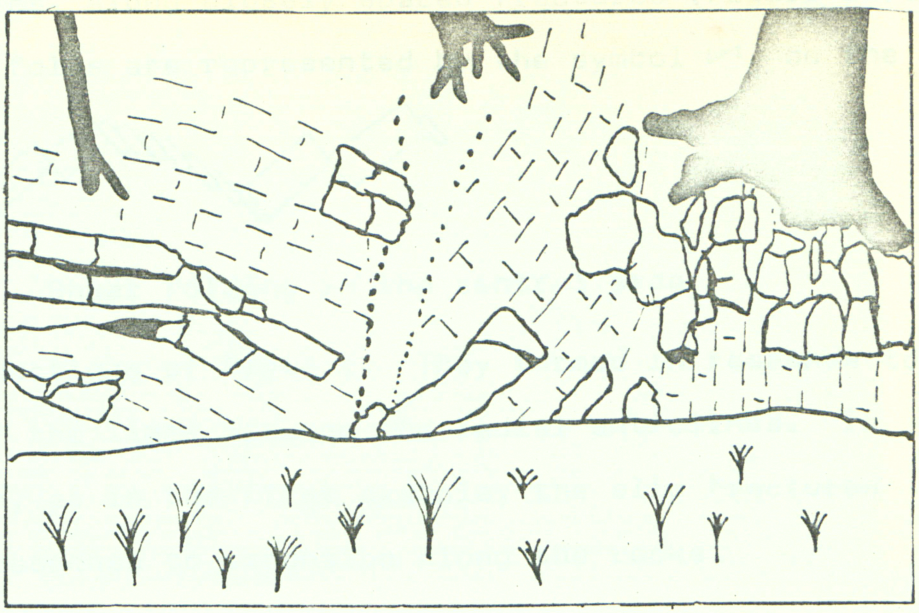

N

PHOTO 23

Northern extension of PHOTO 22.The drag fold to the south grades into more deformed rocks as the axial plane of the west radial anticline is approached

chevron folds, along closely spaced fractures (Figure 19). These slip folds are represented by the symbol ⌐ on the

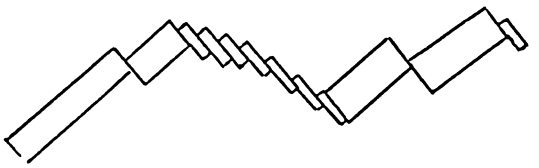

Figure 19 Shear folding in the central area

structure sections of Plate 2. They formed in response to shorting of the limbs between the radial anticlines. In other cases, as in the first example, the slip fractures formed in response to extension along the rocks.

Folding takes a more plastic form in the incompetent shales. The clayshales are so mobile that they will thicken at the crest and thin on the limbs of a fold so that the thickness of the Crab Orchard shale varies throughout the structure. The clay shale part of the Ohio black shale acts like the Crab Orchard. This makes absolute measurements impossible for the structure contour maps (Appendix III).

Because of the different lithologies, disharmonic folds are found in certain instances. Section CC' shows the best example in the area.

(a) Minor Structures

Where some of the more competent units have been fractured and are in contact with incompetent units, the fractures have been tectonically intruded by incompetent material. This was pointed out on a large scale in one of the breccias

PHOTO 24
A pelite dike of Ohio Black shale in the Tymochtee dolomite. This is located east of the central uplift.

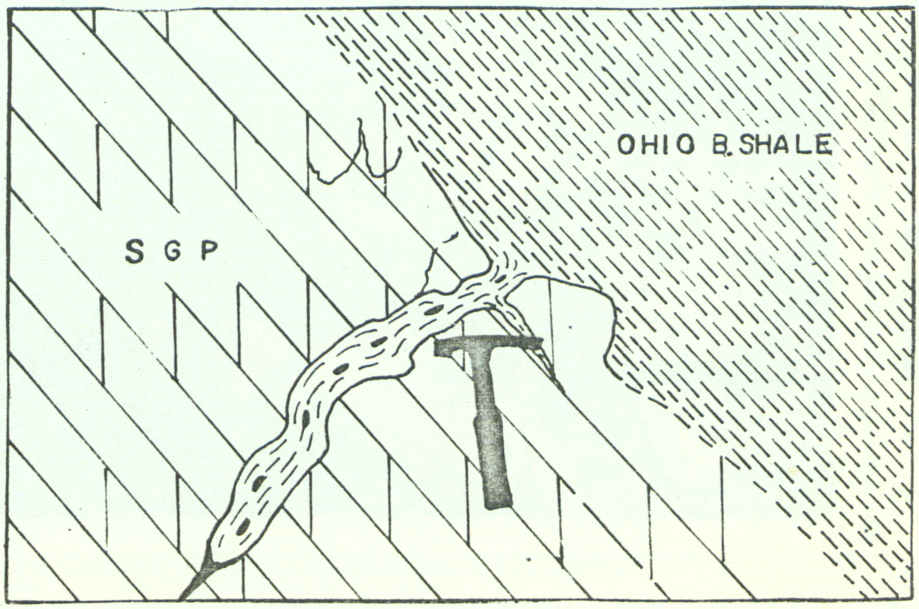

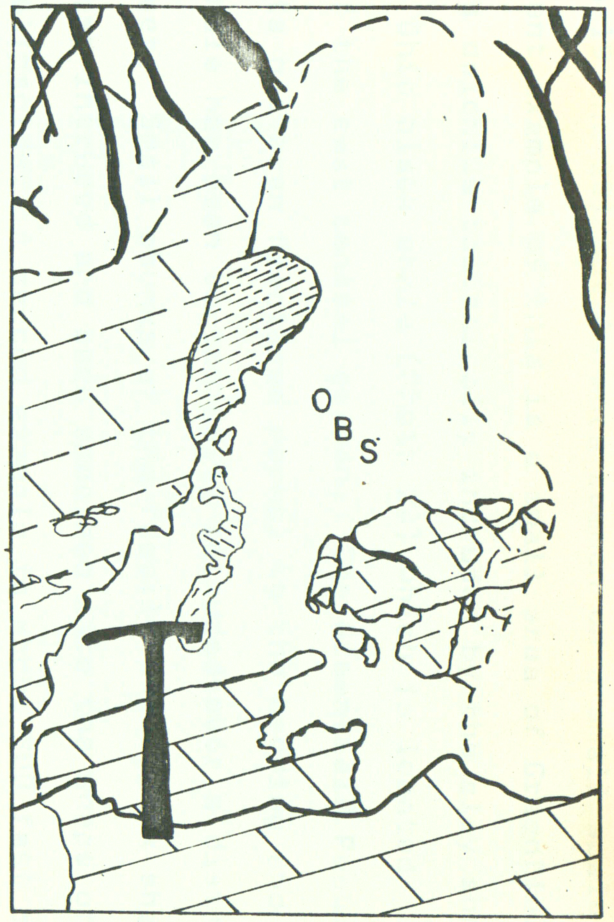

PHOTO 25 A pelite dike of Ohio Black shale in a fractured Tymochtee dolomite. Fissile bedding of the shale is preserved.

(location - east of 12)

(Photo 19 and 20) but is more common on a small scale. An excellent example of this is a small area of Greenfield Peebles dolomite tectonically intruded by the clay shale of the Ohio black shale (Photo 24) which is located just east of the east central graben. The Greenfield Peebles dolomite has been fractured normal to the bedding and the clay shale has been tectonically intruded over a distance of 3 feet. Small chunks of the fissile Ohio black shale have been intruded and been smoothed into the shape of tri-axial elipsoids. A second example is about 200 feet down the creek (Photo 25). This is more complex with a larger fracture intruded from the lower left. Much larger chunks of the fissile Ohio black shale are found with good bedding preserved but still showing smoothing.

(n) Shatter Cones

Shatter cones are present at several locations in the structure, most are found in the central uplift but several have been found in the peripheral ring graben. This location is Location 43. These shatter cones occur in the Greenfield Peebles dolomite (Photo 26).

Several different styles of shatter cones are present in the area. Photo 26 is a typical cone for the area while Photo 27 shows cones developing on other cones forming the horsetail type.

In the east central graben (Appendix IV, Location 12) shatter cones were found in place but they are so poorly developed that no reliable orientations could be obtained.

PHOTO 26
Shatter cones in the Greenfield Peebles dolomite found west of the central area.
(location 43)

PHOTO 27
Horsetailing shattercones
Location south of 1

MINERALIZATION

A small amount of sphalerite is found in the Serpent Mound structure. Mostly it is found as weathered float on the surface but occasionally good exposures can be found (Photo 28). The sphalerite locations on Plate I are related to the faults and this conclusion is consistant with the work of Reidel (1970) and Stryker (1971). The mineralization does occur in other rock formations as well as the Greenfield Peebles dolomite. Mineralization was found in the Brassfield limestone (Photo 29), the Crab Orchard shale (Photo 30) the Bisher dolomite (Photo 31), and as part of the "lag deposit" at the base of the Ohio black shale. These occurances however, are minor compared to the amount found in the Greenfield Peebles dolomite.

Sphalerite is not the only mineral present. Marcasite and pyrite are both common sulfides that weather on the surface to limonite. Several unidentified minerals are present but are rare in occurance. A green mineral (Photo 32) is found in calcite (Reidel, 1970) and occasionally along fractures (Stryker, 1971). This is similar to pyromorphite specks identified at Gratz, Kentucky (Malcolm, 1952). A red mineral occurs occasionally in calcite but the grains are so small that it can rarely be seen even under high magnification.

There are two main types of sphalerite occurrences: simple fracture filling and replacement. In many locations, where fractures once existed they are now healed by sphalerite (Photo 33). In the simplest case there has

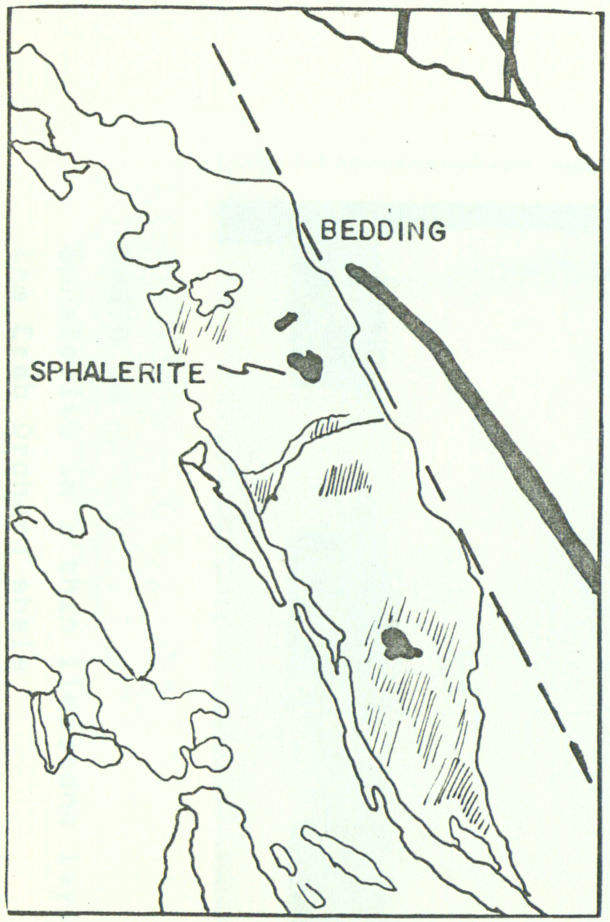

PHOTO 28 Sphalerite in Greenfield Peebles dolomite from the south graben of the central area

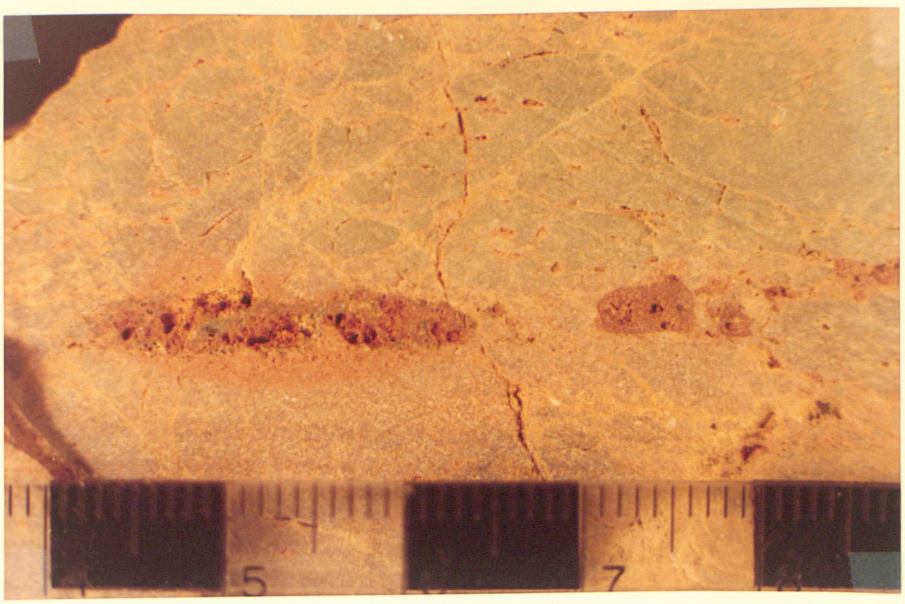

PHOTO 29
Mineralized fracture in the Brassfield limestone (location north of 4)

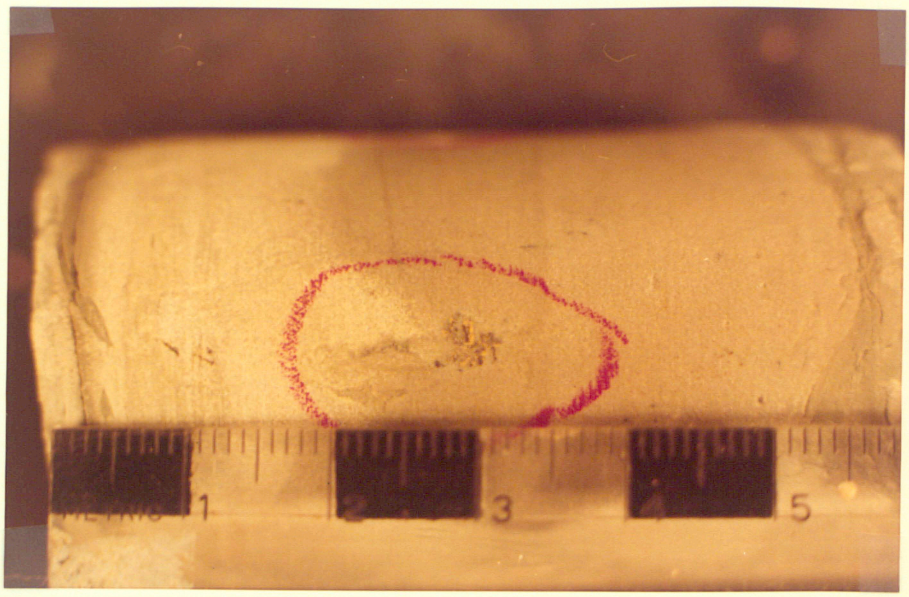

PHOTO 30
Sphalerite in a thin limestone layer from the Crab Orchard shale
(location -from core CA 110 -)

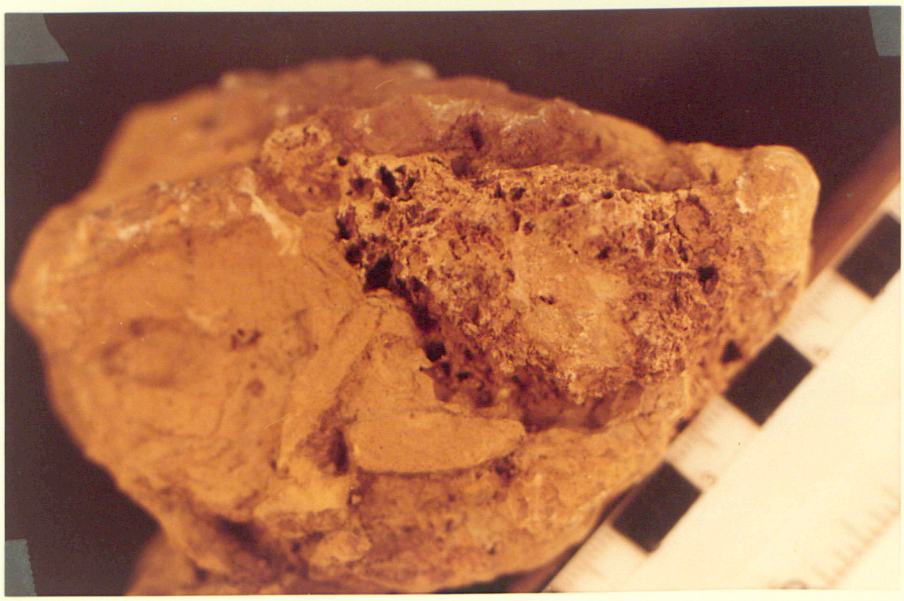

PHOTO 31
Sphalerite altered to smithsonite within a vug in the Bisher dolomite (located on the south east part of structure on Rt. 41)

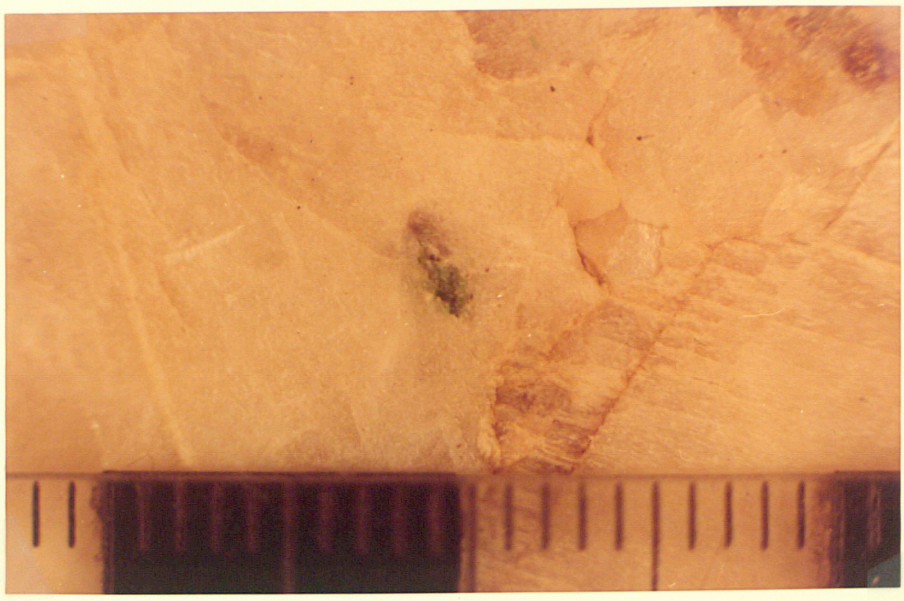

PHOTO 32
Unidentified green mineral in calcite(located north of 38)

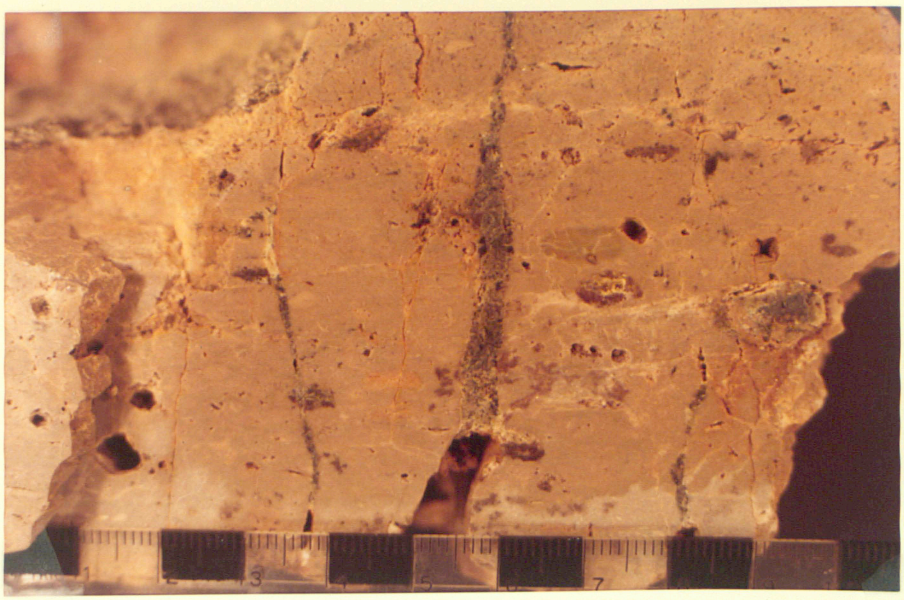

PHOTO 33
Sphalerite filling fracture
(located east of 24)

PHOTO 34
Minor replacement of dolomite by sphalerite
along a fracture
(Located east of 24)

been no movement and the sphalerite contact with most host material is sharp in hand specimen. In thin section these fracture margins do show a small amount of replacement (Photo 34). Where there is movement along the fractures, pinch and swell structures are commonly filled by sphalerite (Photo 35). Movement along fractures usually results in brecciation and sphalerite commonly cements the breccia fragments, as shown in photograph 35.

Sphalerite commonly fills the open spaces in fault breccias and replaces some of the finer matrix (Photo 36). Where there is fluxion structure (see Appendix V) the sphalerite alines with it. Iron staining in the rock shows the same relationship with the fluxion structure as the zinc minerals. Replacement of the matrix is so complete in some samples that masses of sphalerite are as large as some of the porphyroclasts (Photo 37). This is not that common and usually the sphalerite is so fine-grained and light in color that it can hardly be differentiated from the breccia matrix. Where there is a mylonite zone within a protomylonite (Appendix V), the sphalerite will prefer the mylonite giving an appearance similar to a mineralized vein. (Photo 38).

Replacement of dolomite by sphalerite is less important than fracture filling. Quite commonly fractures have large patches of replacement sphalerite associated with them (Photo 39). Bleaching of the dolomite, where replacement occurred is not common but occasionally it is found

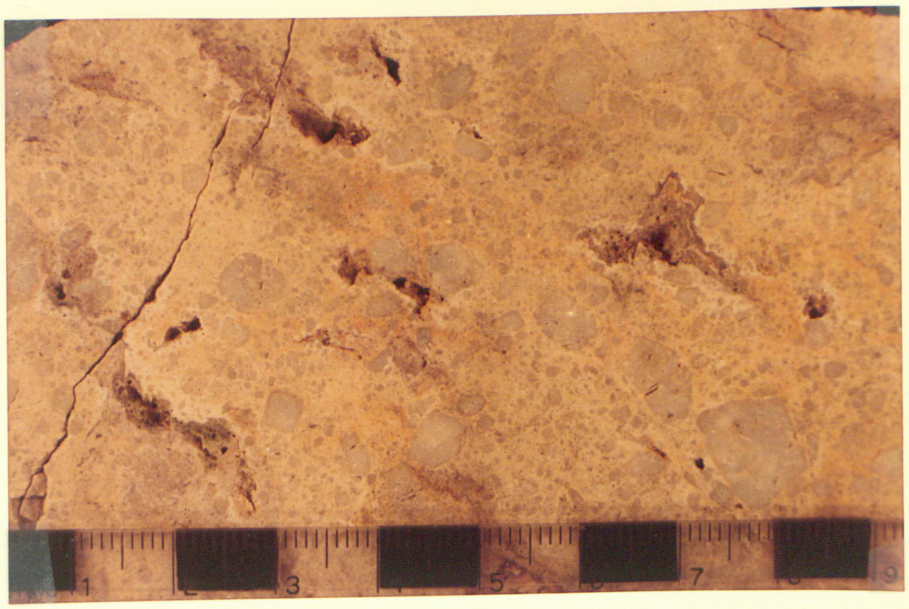

PHOTO 35
Sphalerite cementing breccia in fracture zone
(located NE of 33)

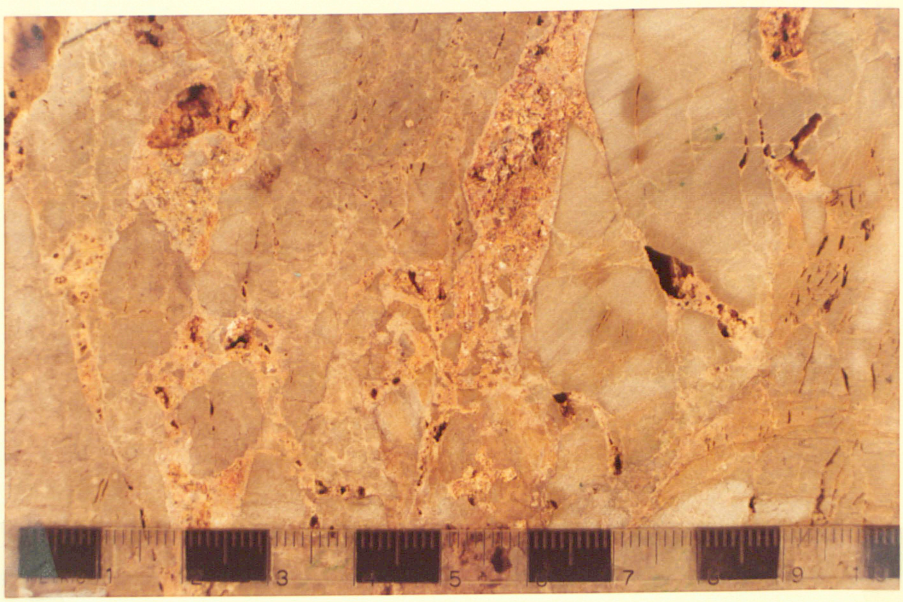

PHOTO 36
Sphalerite in mylonite following the
fluxion structure (location 38)

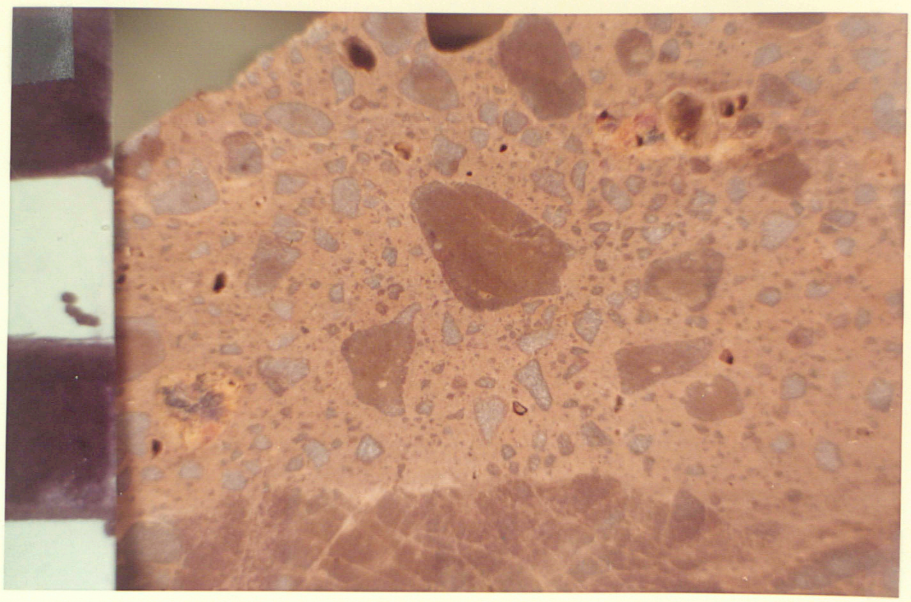

PHOTO 37
Porphyroclasts of sphalerite in a breccia
(located near 27)

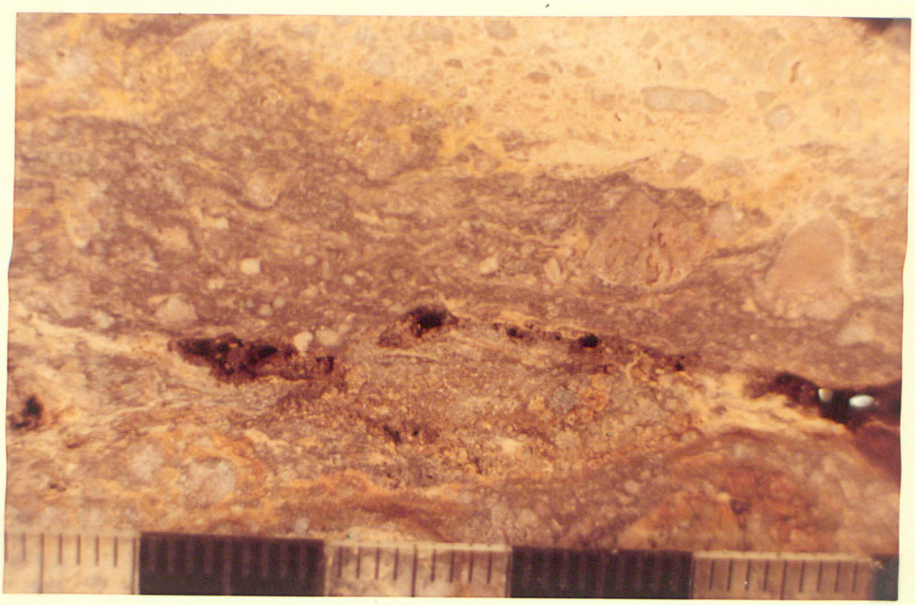

PHOTO 38
Spheralite replacing mylonite.The finest parts show the greatest amount of replacement
(located near 5)

near the dark "Black Jack" sphalerite (as in Photo 39). Replacement without visable fracturing is found in many locations (Photos 28 and 40). These specimens show contemporaneous solution of the dolomite and deposition of sphalerite.

Fossil replacement is the least important occurence. Occasionally replacement of Stromatopora is found where a mineralized fracture cuts it. Bryazoans and corals in some cases are partially replaced (Photo 41) but this is the exception rather than the rule.

Limonite is almost always found in association with sphalerite and gangue minerals. It commonly occurs as pseudomorphs after pyrite. Where sphalerite occurs, the contact with the wall rock is often marked by a thin rim or layer of limonite which can be seen both in thin section (Photo 42) and in hand specimen. Where calcite has replaced dolomite, this same limonite rim is seen (Photo 43). The limonite is usually a soft, yellowish-brown mass (Photo 44) but in fresher samples, some samples show a core of marcasite (Photo 45).

Many samples show asphalt (Photo 46) coating the mineraliztion. It usually fills fractures and open spaces in the sphalerite. The asphalt is clearly later than the main mineralization and might be expected to accumulate in anticlines and fault zones. Commonly natural springs have oil seeps and during the summer of 1971 a farmer plowing a

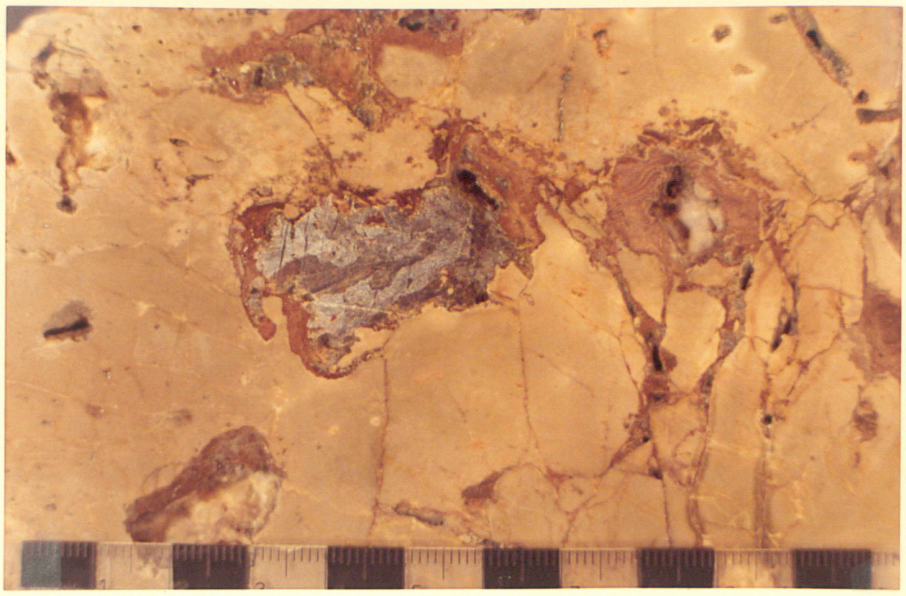

PHOTO 39
Sphalerite filling fractures and replacing the dolomite.Note the bleaching of the dolomite near the replacement sphalerite.
(located east of 24)

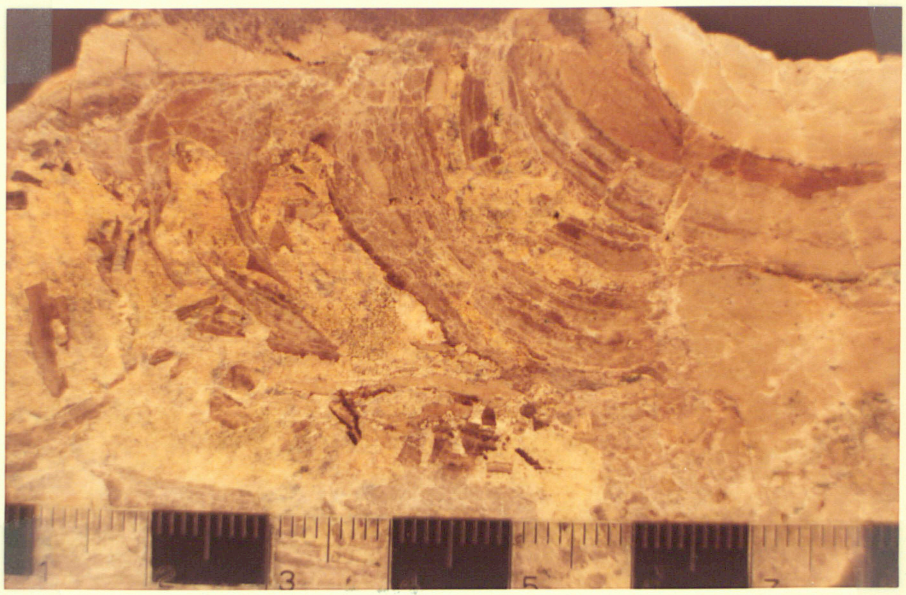

PHOTO 40
Replacement Sphalerite
(Located near 5)

PHOTO 41
Sphalerite replacing fossils
(located near 5)

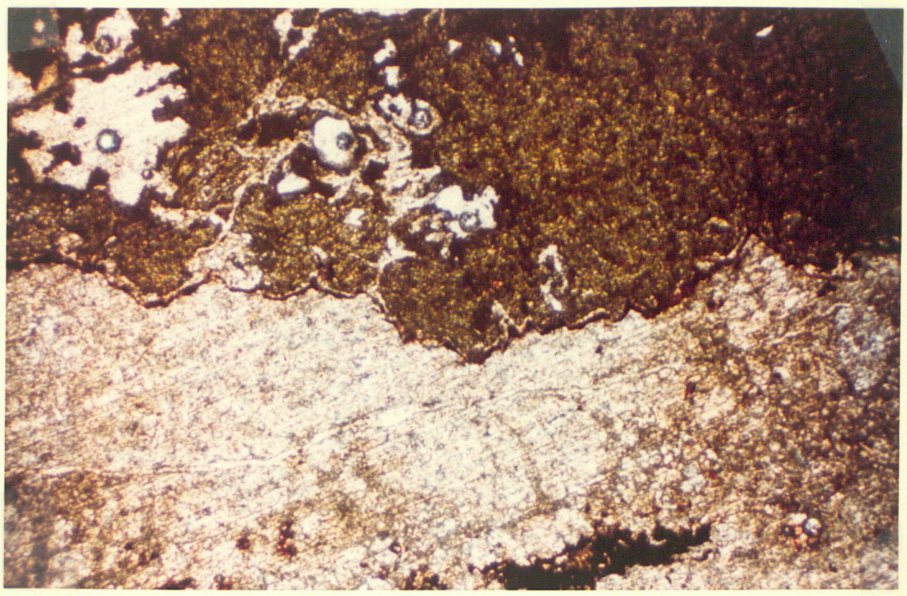

PHOTO 42
Microphotograph of a limonite border
between dolomite and replacement sphalerite
(located near 17)

PHOTO 43
Limonite border between dolomite and replacement calcite
(located near 43)

PHOTO 44
Massive
Limonite
(N of 29)

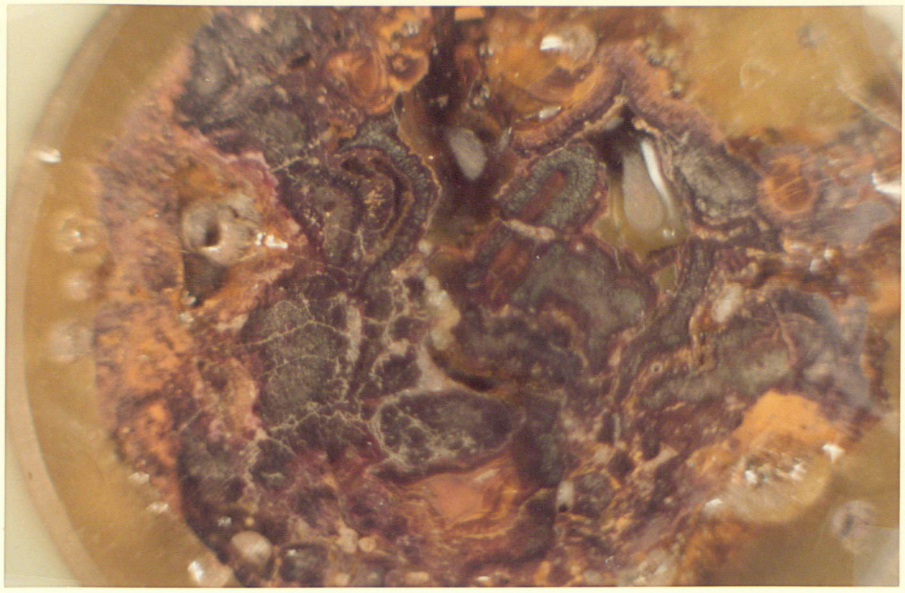

PHOTO 45
Limonite with a core of marcasite
(located SW of 35)

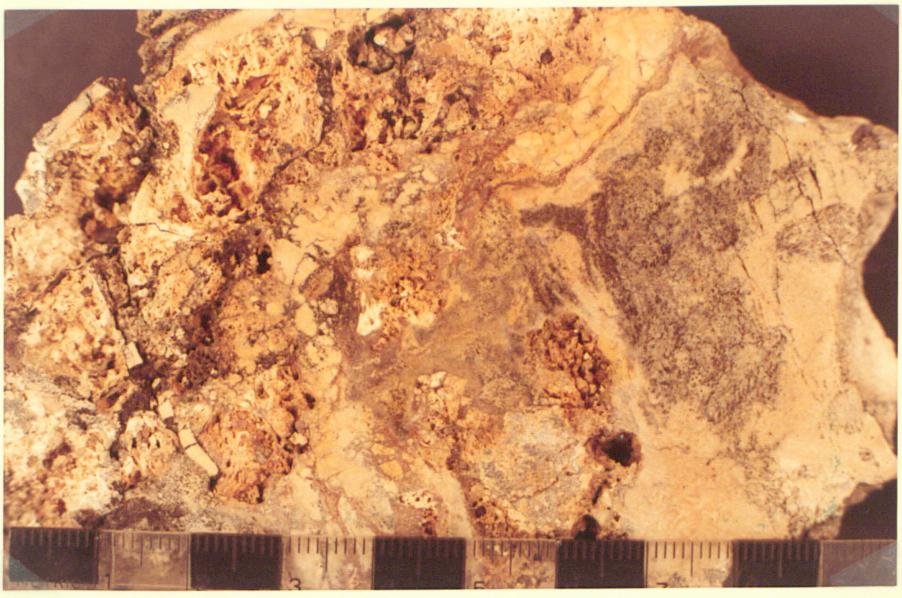

PHOTO 46
Asphalt in association with sphalerite
(located east of 24)

field uncovered a 400 square feet surface area of asphalt mixed with soil (Appendix IV, near Location 6).

Heyl (1962) described sphalerite crystals from the area as having a red to reddish-brown core surrounded by an orange zone and a pale yellow rim. This is an incomplete description since most crystals show still darker core surrounded by a red to reddish-brown zone, then an orange to pale yellow zone and finally a yellow rim (Photo 47). In hand specimens, based on color, two types of sphalerite are observed: a yellow (Photo 35) and a "Black Jack" type (Photo 33).

The "Black Jack" sphalerite, in thin section is the result of a combination of several colors of sphalerite (Photo 48): purple, brown, orange, and grey-white. The "Black Jack" color is primarily due to the purple color which is second in abundance to the grey-white sphalerite. Both are always coarse-grained and highly fractured. The fracturing results in an internal reflection of light on the fracture planes so that the sphalerite never becomes optically black under the crossed nicols of a microscope (Photo 54). The boundary between the various colors is sharp in handspecimen but on close examination shows a gradation in color across unfractured grains (Photo 49). This is not a fracture contact but simply a color change. The purple color is not uniform but has within sample variations, usually as lamellae or rods (Photos 48, 50, and 51). In a single fracture ($\frac{1}{2}$ cm. x 3 cm.), almost

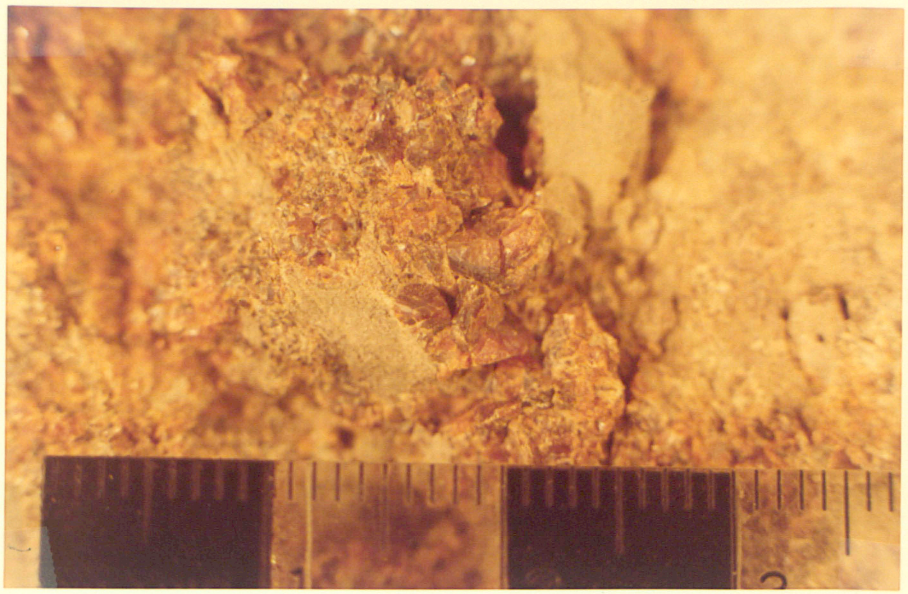

PHOTO 47
Crystalline Sphalerite
(located NE of 33)

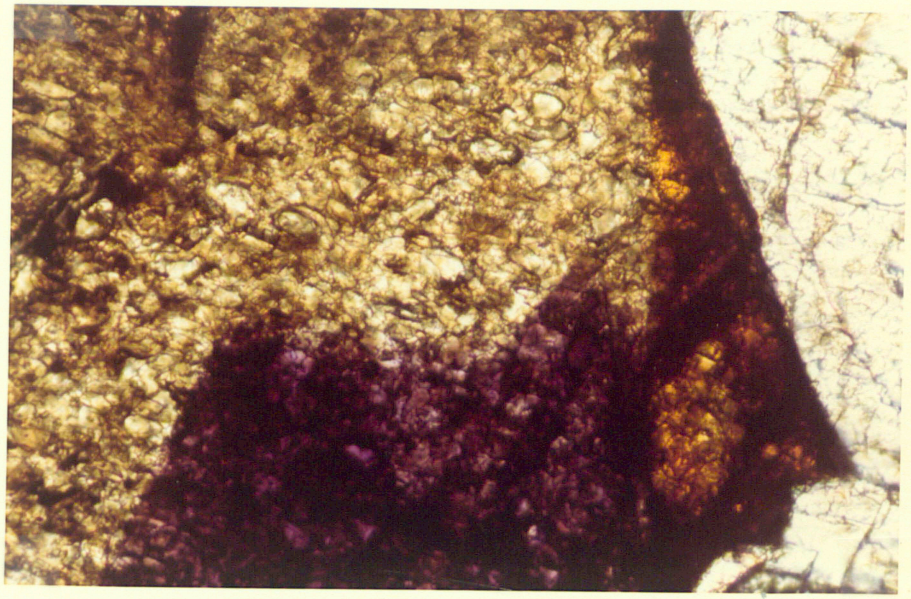

PHOTO 48
Multicolored Sphalerite
(located east of 24)

all the lamellae have the same orientation throughout the length of the thin section. The width of the lamellae is the main variation. The purple, brown, and orange shades are interpreted to be either growth lamellae or exsolution of sphalerite containing certain trace elements. The elements that are causing the coloring are unknown for reasons discussed later.

In some cases there is a gradation from one color of sphalerite to another while in others there is none. In one thin section the length of a lamella graded from purple at one end to brown and finally grey-white at the other end. The color relationships are not always this simple. In some thin sections the purple will grade into grey-white on one side while on the other side the purple is in contact with yellow sphalerite. The yellow is also in contact with the grey-white (Photo 48). In other cases there are purple and yellow sphalerite with no contact between them in a matrix of grey-white sphalerite. It is interesting to note that the limonite bears no unique relationship to any of the colored sphalerites. It is found in contact with all colors.

The purple sphalerite is not restricted to any single formation but occurs in all the mineralized units. There does appear, however, to be more purple sphalerite as fracture filling than replacement.

Examination of the field occurrences of the purple sphalerite shows a rough zonation (Figure 20). It occurs

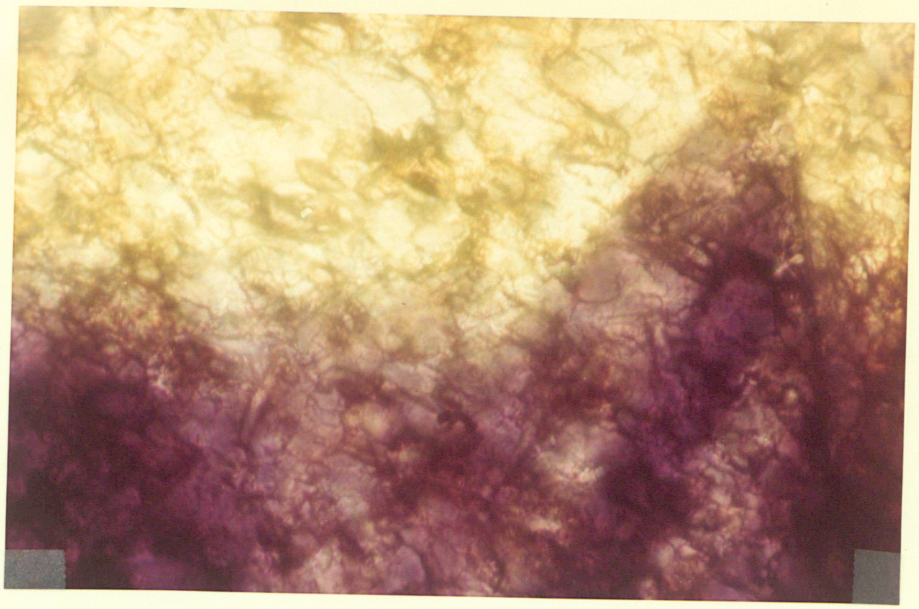

PHOTO 49

Microphotograph of purple sphalerite

(located east of 24)

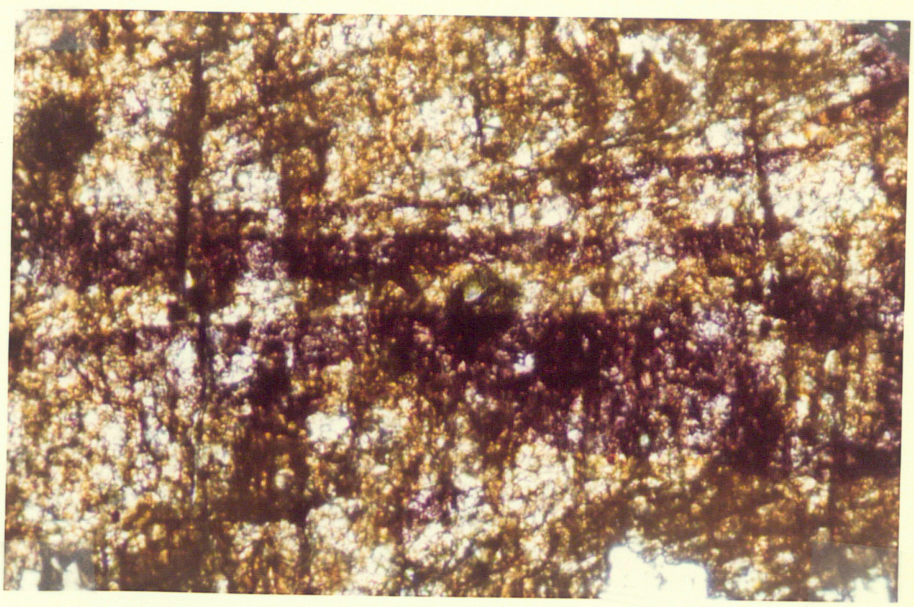

PHOTO 50

Lamellae of the purple sphalerite that has been fractured

(located east of 24)

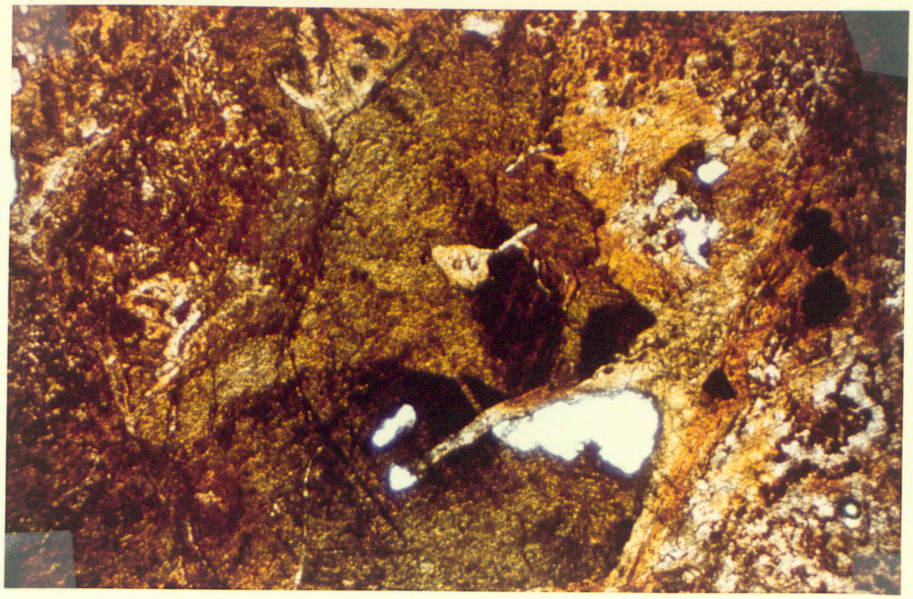

PHOTO 51

Purple lamellae in sphalerite from the Brassfield limestone

(located north of 4)

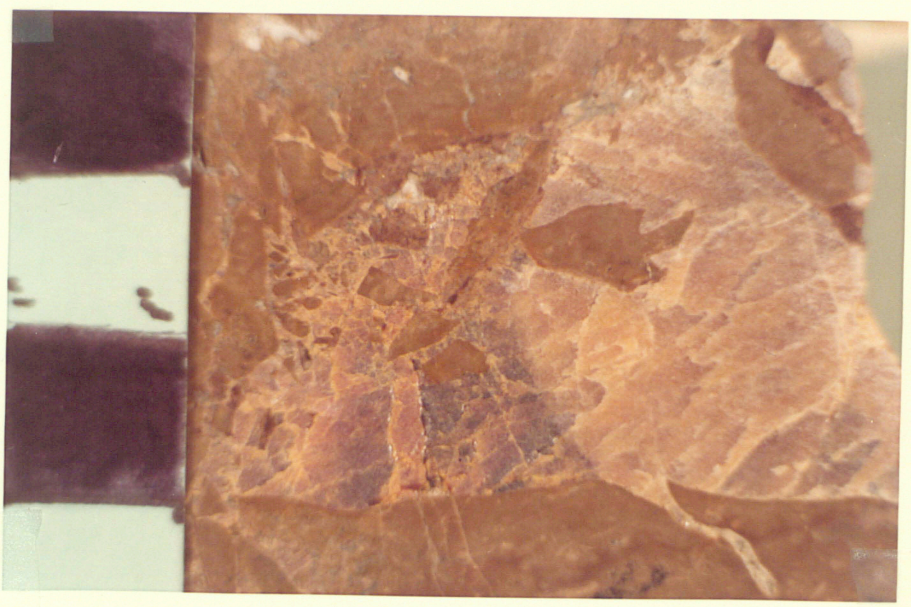

PHOTO 52

Color zoning in sphalerite

(located near 17)

in two patches that make a general northeast-southwest trend through the cryptoexplosion structure. There is no obvious structural control for these occurrences. The break between the two patches is in the area of mild deformation (Appendix IV, Location 40) but there are many sphalerite occurences (Plate I) ruling out the idea of an unfavorable area for mineralization.

The other type of sphalerite, originally described by Heyl and Brock (1962) is rarely found with the multicolored "Blsck Jack" sphalerite. As pointed out by Heyl and Brock (1962), there is a color change in handspecimens (Photo 52) but none that can be detected in thin section. For the most part these appear similar to the grey-white sphalerites in thin section mentioned earlier. This is the most common type of sphalerite and is found as both replacement and fracture filling. Just as with the "Black Jack" sphalerite, this is also fractured and displays internal reflection.

A cloudy yellow sphalerite has replaced some of the earlier sphalerites. This usually has replaced the growth or exsolution lamellae or appears as a stain on the earlier sphalerite. It is difficult to resolve in plane polarized light but it can be seen with crossed nicols. This is because of internal reflection similar to the other sphalerites mentioned.

A minor amount of unfractured yellow sphalerite was deposited along fractures in the earlier sphalerite.

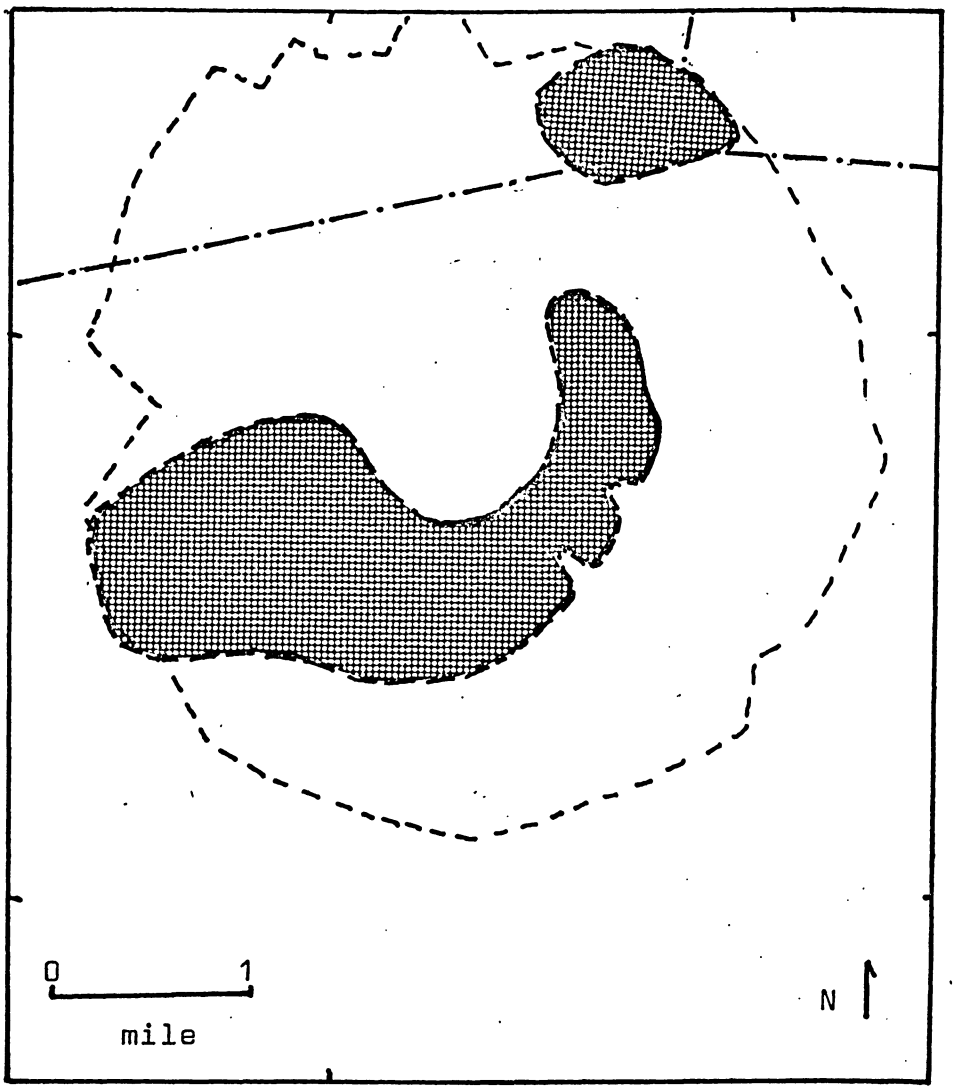

FIGURE 20

Area of multicolored sphalerite

Map of the Serpent Mound Cryptoexplosion Structure with zone of multicolored sphalerite

This later generation occurs as discreet little blebs and does not have the internal reflection that the previously mentioned sphalerites have. This unfractured sphalerite is commonly associated with asphalt.

Calcite and quartz are important minerals to consider not necessarily because of their location but because of their anomalous optical properties. Quartz commonly occurs as small doubly terminated enhedral crystals in a matrix of calcite that fills vugs and replaces dolomite (Photo 5). Occasionally these crystals have a later growth of chalcedony. An examination of these crystals shows that they are optically strained and have a small 2 V of approximately 5 degrees.

Calcite also has anomalous optical properties. It is optically strained and has a small 2 V of about 5 degrees. Optically strained calcite has replaced the early fractured sphalerite. This calcite has been cut by fractures of a later carbonate that has not been strained. Optically strained calcite was also found in "dog tooth" crystals.

Calcite frequently is found replacing siderite concretions from the Ohio black shale near the central uplifted area (Appendix IV, Location east of 12). Usually only a few small fragments of siderite remain after replacement.

Thin sections of sphalerite from the area were examined in a cathode ray for luminescence. This technique

has been used to study sphalerite from other areas (Goni and Remond, 1969). The results were disappointing for there was hardly any luminescence observed in the sphalerite. Goni and Rémond (1969) have shown that there is no luminescence when iron, nickel, and cobalt are present in large quantities. Trace element studies have shown there is no significant amount of iron (Koucky, personal communication). The only luminescence observed was a spotty yellow luminescence, rare in the sphalerite, but more common in calcite. These spots would luminesce for only a short time and stop. Upon leaving them set for a short time, they would not luminesce when examined again. Goni and Remond (1969) attribute a yellow luminescence to cadmium.

The cores drilled by Cominco were sectioned and analyzed by Xray fluoresence for iron and zinc. (Appendix I). The results indicate that the formations examined have a very low content of these elements. Iron on the average was less than $\frac{1}{2}\%$ with the greatest values occuring in the Crab Orchard shale, followed by the Bisher dolomite, then the Brassfield limestone while the Greenfield Peebles dolomite was almost iron free. The zinc content of the formations was less than the amount contained in the lowest standard (less than 50 ppm) and too low to work with quantitatively. For all practical purposes, the zinc content of the rock is negligable.

Trace element studies were conducted on sphalerites

by Koucky (Personal communication) and Farrer (1971). The trace element content as determined by Farrer (1971) is listed below:

Sphalerite, west side of study area by Reidel (1970)

ELEMENT	AMOUNT
Cd	0.11%
Fe	0.03%
Cu	0.08%
Ag	Not detected
Ba	Not detected
Sn	Not detected
Te	Not detected

$= 3.923$

$a_o = 5.4062 \pm 0.0011$ Å

Lynx sphalerite (quarry south of cryptoexplosion structure)

ELEMENT	AMOUNT
Cd	0.4%
Fe	0.04%
Cu	0.08%

$= 3.973$

$a_o = 5.4066 \pm 0.0013$ Å

Farrer (1971) also concluded that the color has no relationship to the iron content. Pure ZnS has an a_o value of approximately 5.4000 Å. As the sphalerites from the Serpent Mound Cryptoexplosion Structure and Lynx Quarry indicate by their a_o values, they are almost pure ZnS.

Additional trace element work has been done by Koucky (personal communication). In sphalerites from the Serpent Mound area, he has found as much as 0.25% cadmium. From

calcite veins (near the quarry on Fault 26a, Appendix IV) Koucky has found almost 1% lead and zinc with close to 300 ppm mercury, cadmium and copper. He has also found that cadmium in sphalerites from the "lag" deposit at the base of the Ohio black shale is below the detectable limit.

Jolly and Heyl (1968) were unable to spectrographically detect mercury. It is noted, however, that this sphalerite was weathered float.

These studies seem to indicate that the sphalerites from the study area are relatively free from trace elements. The presence of lead in the calcite, as determined byKoucky, throws more weight on the argument that the unidentified green mineral in the calcite (Photo 32) is pyromorphite. The presence of mercury also suggests a connection with the central Kentucky mineral district which has anomalous values of mercury in the sphalerite (Jolly and Heyl, 1968).

Paragenesis

The paragenesis of the mineralization was worked out from the study of over 70 thin sections and hand specimens from various localities in the cryptoexplosion structure (Plate I). It is similar to that determined by Heyl and Brock (1963) but more complex.

Reidel (1970) and Stryker (1971) have shown that the major mineralization is controlled by faults in the structure. Heyl and Brock (1962) have also described mineralization from one location of "shatter breccia" on the west

side of the cryptoexplosion structure. It was concluded from these studies that the first mineralization occured after the initial activity that formed the structure. Fluids carrying zinc ions (Possibly as zinc bisulfide or chloride complexes) and minor trace elements moved through the fault zones.

Sphalerite, rich in coloring agents, initially began to crystallize. Apparently the purple, brown, orange, yellow, and grey-white sphalerites were crystallizing simultaneously, either as growth lamellae on crystal faces, or as exsolution lamellae (Photos 48, 50, 51 and 53). As the coloring agents were used up only the grey-white sphalerite (in thin section) crystallized. As the grey-white sphalerite crystallized, it underwent a color change, in hand specimens, from dark to light. The color change cannot be detected in thin section, however.

The first sphalerite occurred as fracture fillings, but later considerable replacement of the rock by sphalerite took place. In the earliest stages bleaching (Photo 39) of the rock occured then later limonite was concentrated along replacement boundaries between the dolomite and sphalerite (Photo 42).

The earlier sphalerite then underwent partial replacement by a second generation of sphalerite (Photo 54). It is characterized, in thin section, by a cloudy yellow appearance. The second generation is minor and was selective in that only some lamallae of the previous sphalerite

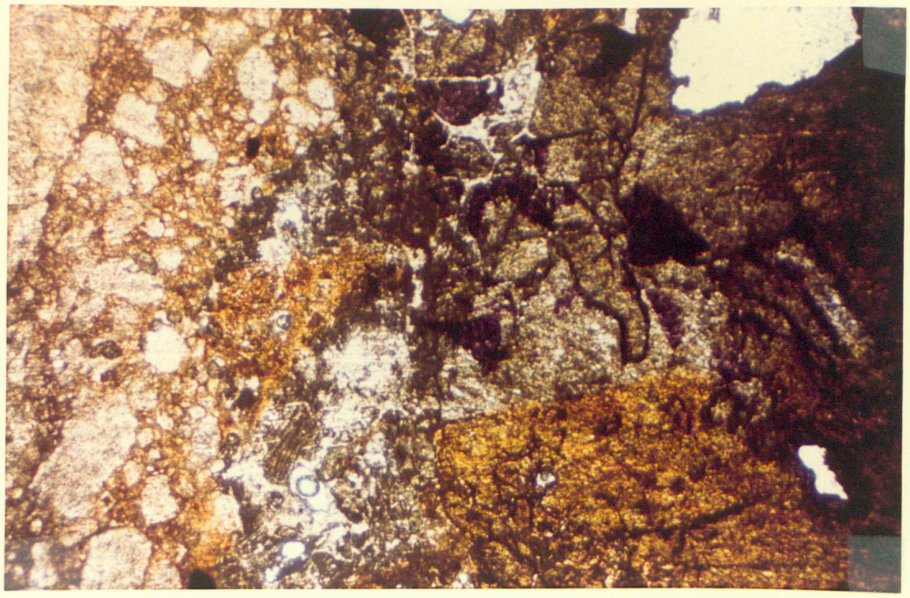

PHOTO 53
Brown,Purple,Yellow,and White-Grey Sphalerite
(located east of 22)

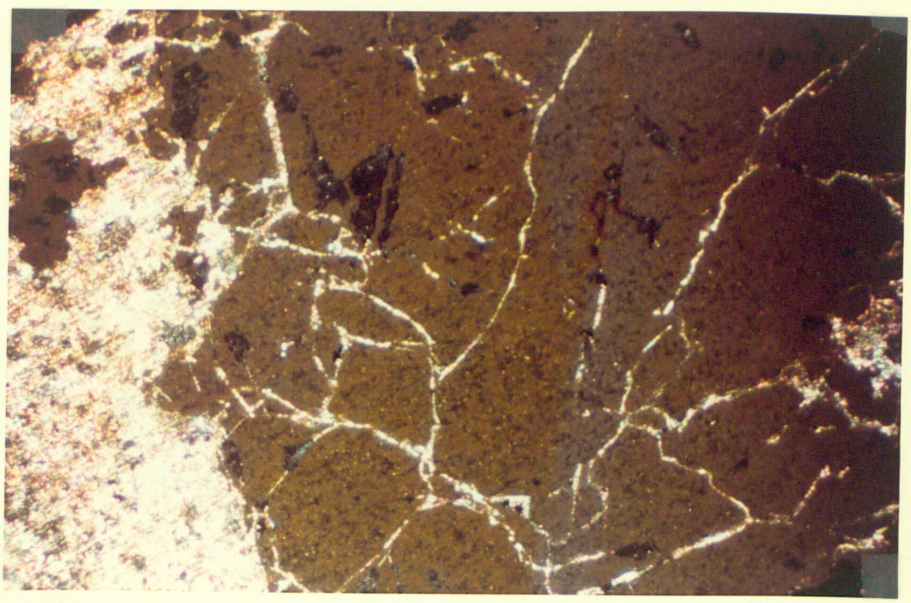

PHOTO 54
Cloudy yellow sphalerite replacing the earlier sphalerite.
(located near 27)

were replaced.

Calcite followed the second generation of sphalerite and began to replace both generations (Photo 55). This is coarse-grained and often found as large crystals in vugs.

The structure underwent a later minor shock and both sphalerite and calcite were shattered (Photos 55 and 56). The intensity of reactivation was strong enough to produce anomalous optical properties in calcite and fracture the sphalerite (Photo 55).

Carbonate deposition along fractures followed reactivation. The unstrained calcite and dolomite filled fractures in the porphyroclasts of both dolomite and sphalerite.

Asphalt was introduced before the end of the calcite deposition. In many samples of calcite, hydrocarbons cause the calcite to fluoresce under ultraviolet light.

The final mineralization in the structure is an unfractured honey yellow sphalerite (Photo 57). This follows thin fractures in the initial mineralization and commonly occurs as small blebs.

The supergene stage is characterized by the weathering of sphalerite and the development of smithsonite (Photo 58) and hydrozincite. The smithsonite has a typical "boxwork" structure and commonly occurs as the "drybone ore".

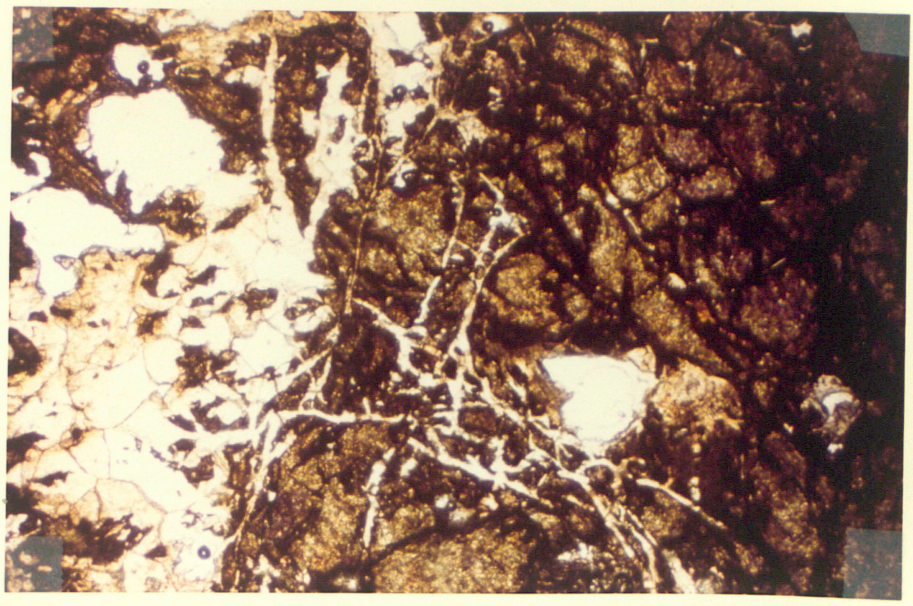

PHOTO 55
Calcite replacing sphalerite before
second deformation
(location 22)

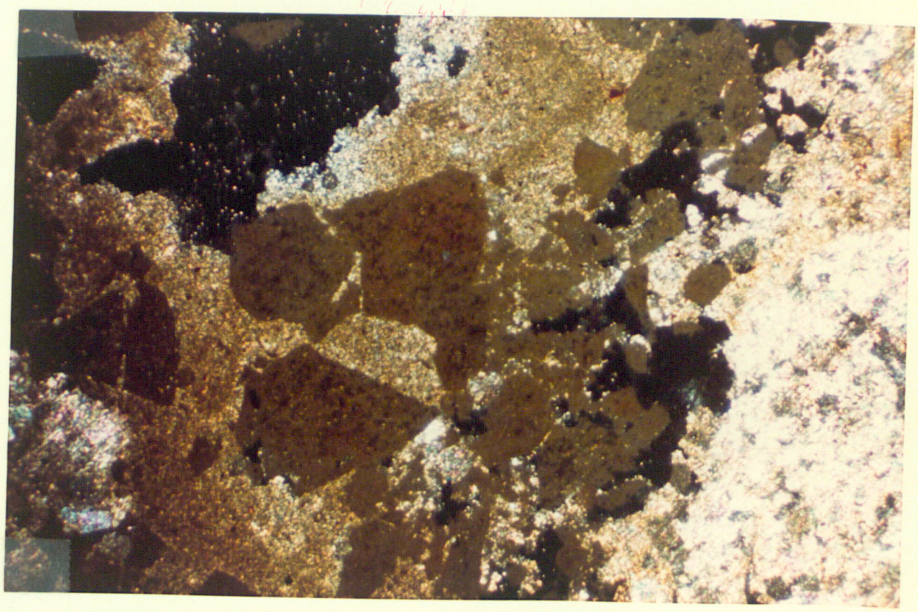

PHOTO 56
Shattered prophyroclasts of sphalerite
(located west of 25b)

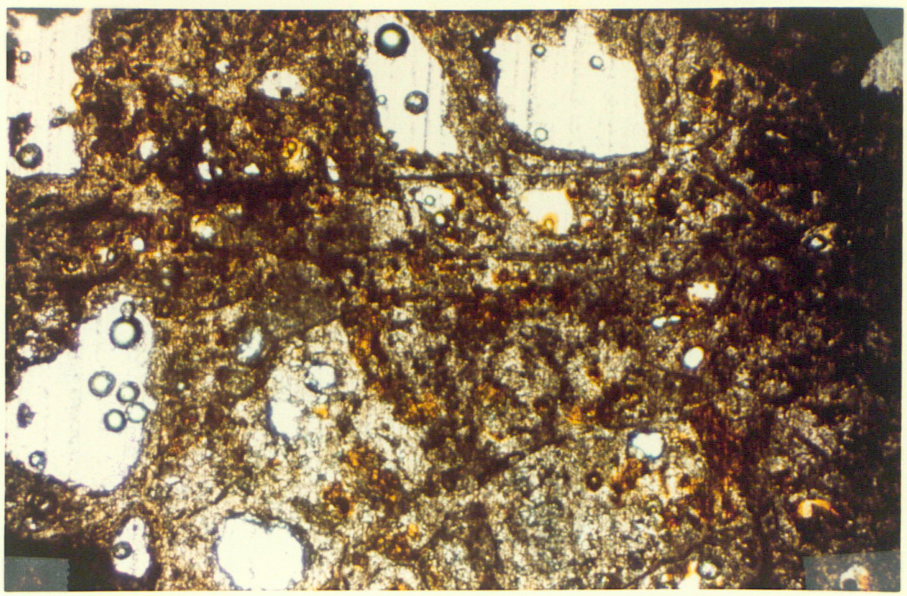

PHOTO 57
Unfractured yellow sphalerite
(located near 40)

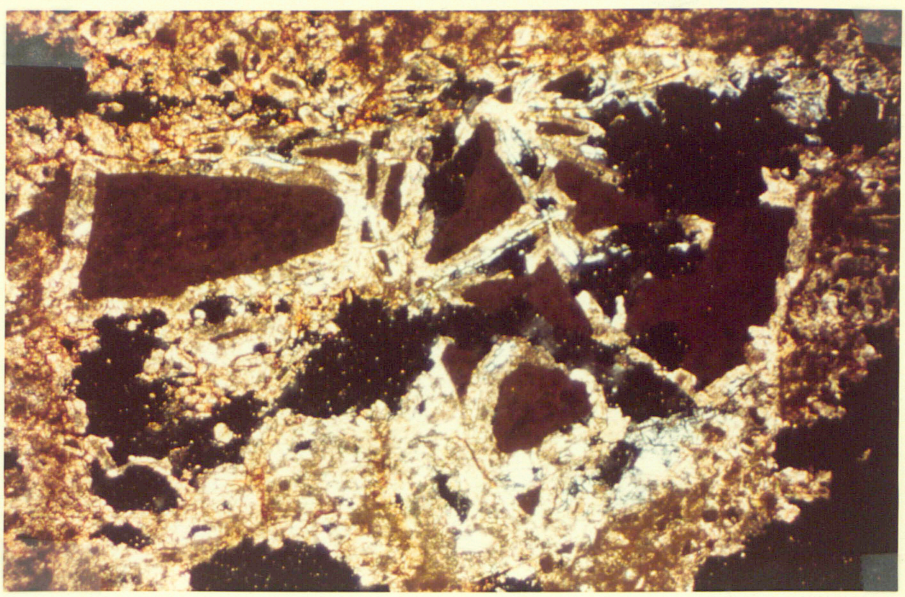

PHOTO 58
Supergene alteration of sphalerite to smithsonite
(located near 33)

DISCUSSION

Interpretation of the origin of the Serpent Mound Cryptoexplosion Structure requires a consideration of the regional geology as well as the geology of the structure itself. The purpose of this section is to summarize the regional geology and its relation to the cryptoexplosion structure, and to examine some ideas concerning the origin of the structure.

Both regional and local geophysical studies indicate a specialized site for the Serpent Mound Cryptoexplosion Structure. Rudman et al., (1965) published a regional gravity map of the midwest (Figure 21) that shows a regional positive gravity trend passing from southwest Michigan through northeast Indiana, west and southwest Ohio into Kentucky. He interpreted this to be possibly the result of Keweenawan type basalt flows in the basement rock and might be related to the "midcontinent gravity high". The "midcontinent gravity high" is a positive linear gravity anomaly that extends from Minnesota through Iowa and Nebraska (Figure 21). Rudman (1965) believes that this is the result of Keweenawan basalt flows in the basement of the Midcontinent. The interpretation of the anomaly in Ohio is based upon basement well tests that have been penetrated basalts in Ohio and Indiana resembling the Keweenawan types. A more detailed gravity map of Ohio (Figure 5) by Heiskanen and Uotila

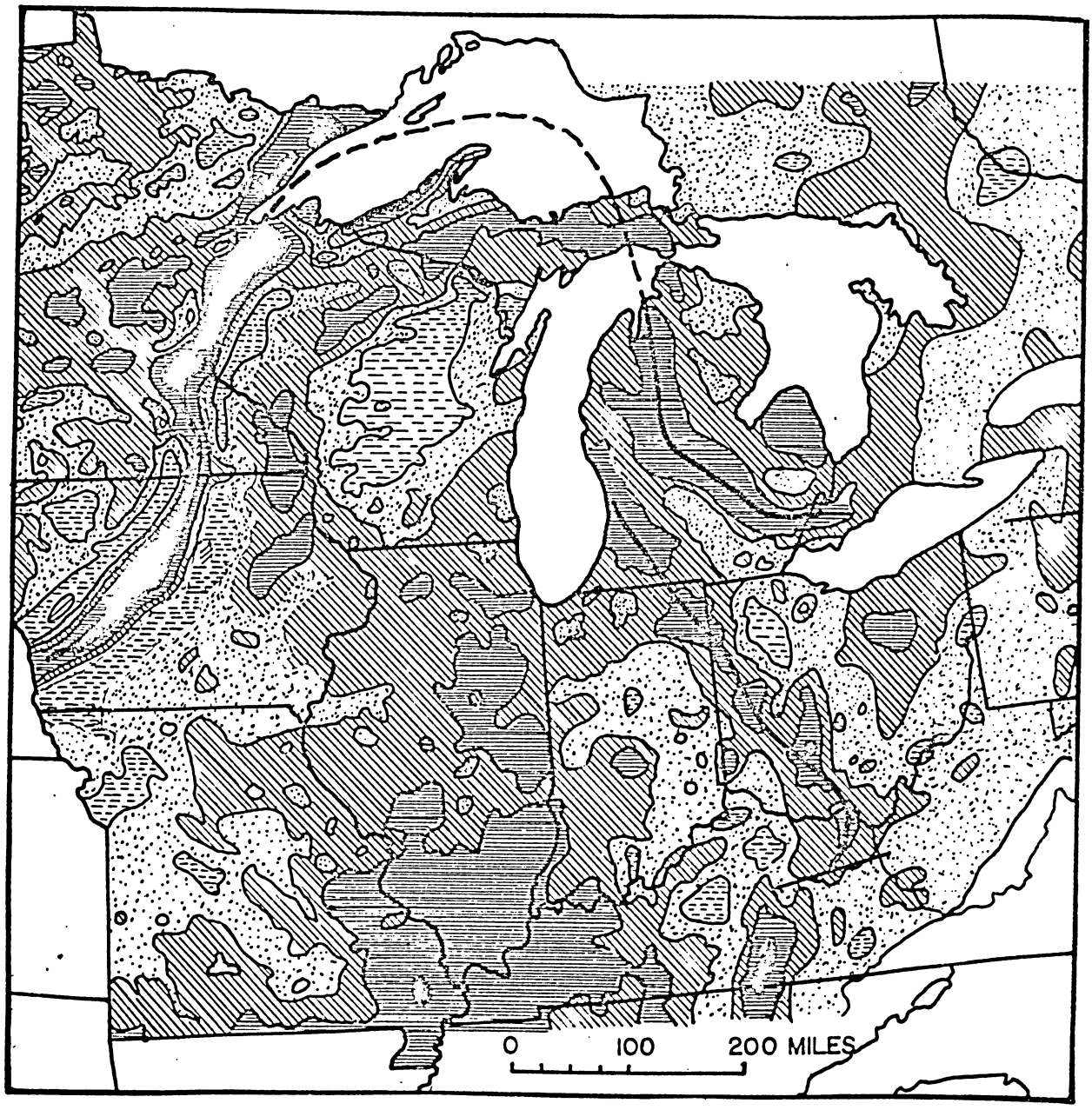

FIGURE 21

Bouguer Gravity Anomaly Map of the Midwestern U.S.A.

Bouguer Gravity Intensity in Milligals

Greater than -100

-60 to -100

-40 to -60

-20 to -40

20 to -20

Greater than 20

---Gravity Trend

Basement Scarp

(after Rudman et al ,1965)

(1956) clearly shows: a tightening of contours north of the Serpent Mound Cryptoexplosion Structure which Rudman (1965) interpreted as a basement fault and the Serpent Mound structure lies on the positive gravity high mentioned by Rudman (1965).

The results of two "great circle" magnetic surveys (Zietz, Stockard and Kerby, 1968) conducted by the Navy and the U.S.G.S. also show a special relationship for the site of the Serpent Mound structure. The two surveys overlap to the east but separate through most of Ohio. The Serpent Mound structure lies on the southern boundary of the most northern survey (Figure 22). The regional trends are east-west (Zietz, 1969) however in Ohio there are high amplitude magnetic anomalies along a belt between longitudes 82^{o} and 84^{o} west in central Ohio (Zietz, 1969). This was interpreted to represent a basement complex of schists and gneisses which might possibly be an extension of the Grenville Province of Canada (Figure 23). It should be noted that the Serpent Mound Cryptoexplosion Structure lies on a longitude of 83^{o} west, almost in the center of this belt of magnetic anomalies.

The Serpent Mound Cryptoexplosion Structure is located along the area of the northwest-southeast regional gravity high and the north-south high amplitude magnetic anomaly.

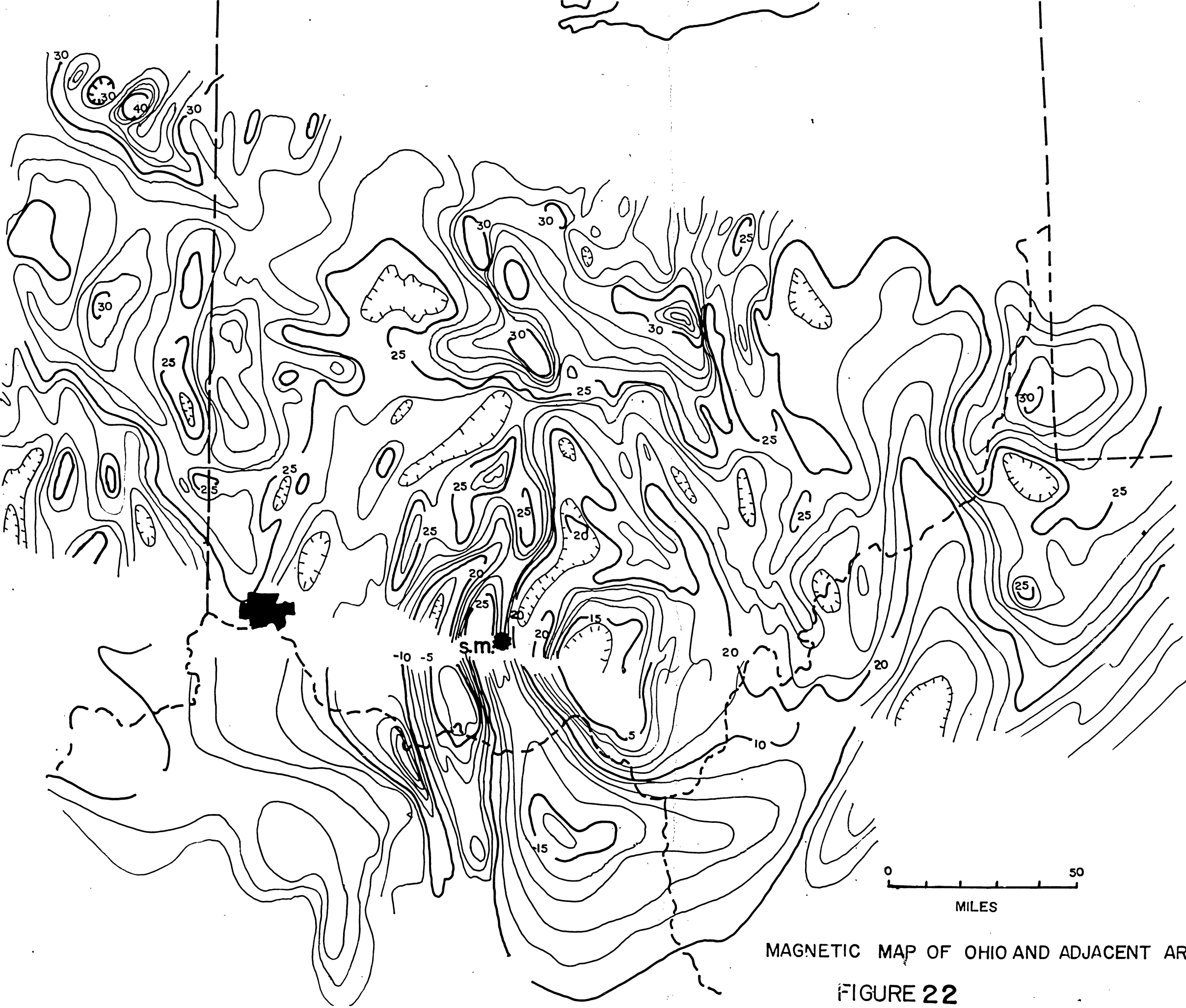

MAGNETIC MAP OF OHIO AND ADJACENT AREA

FIGURE 22

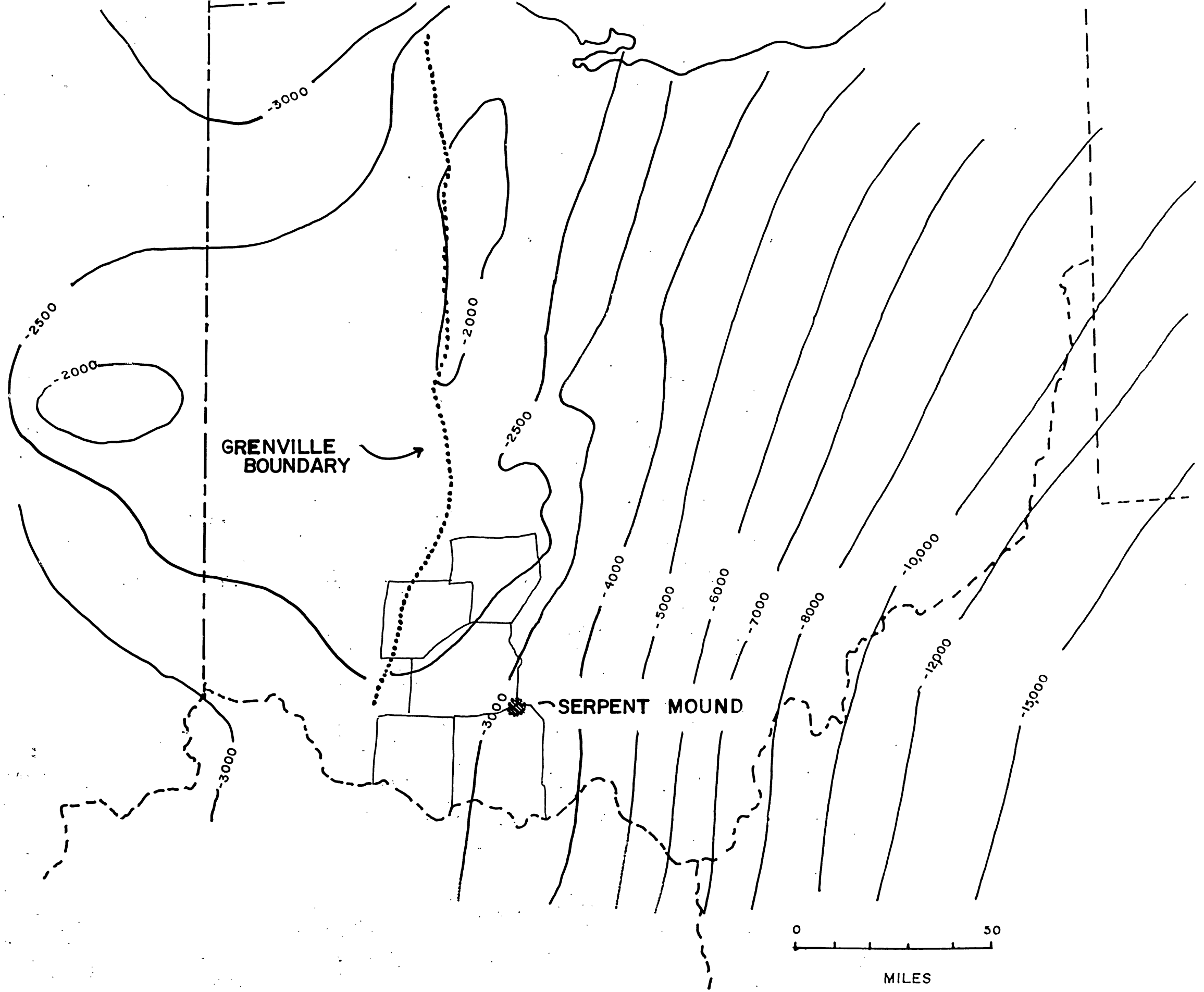

ELEVATION OF THE PRECAMBRIAN SURFACE **FIGURE 23**

Local geophysical studies of the Serpent Mound structure were conducted by Sappenfield (1950) and Zahn (1969). There is a close relationship between Zahn's gravity map and Sappenfield's magnetic map (Figure 24). Both show the axis of their anomalies striking in a northwest direction. Sappenfield's axial trend strikes N25W while Zahn's axis is N50W. Both Zahn and Sappenfield found no relationship between their maps and the surface structure. It is interesting to note that the axis of both anomalies coinside with the two greatest fault direction frequency classes in Figure 18.

Zahn (1969) made several other attempts to fit his map to that of Bucher's (Figure 2). By the least squares method, he made a second degree surface map (Figure 25) and then by subtracting Boulger anomalies, he derived a second degree residual map (Figure 26). Considering this to be noisy, he removed the sixth degree residuals from the second degree surface (Figure 27). He concluded that there was no relationship between the structure and the gravity data.

The regional gradient over the structure, as explained by Zahn (1969), could be accounted for in terms of a horizonal cylinder with a radius of 8 miles and at a depth of 5.7 miles. He felt that something at this depth probably could not produce anything as small as the Serpent Mound disturbance and that the astroblem hypothesis could account for the absence of a relationship between

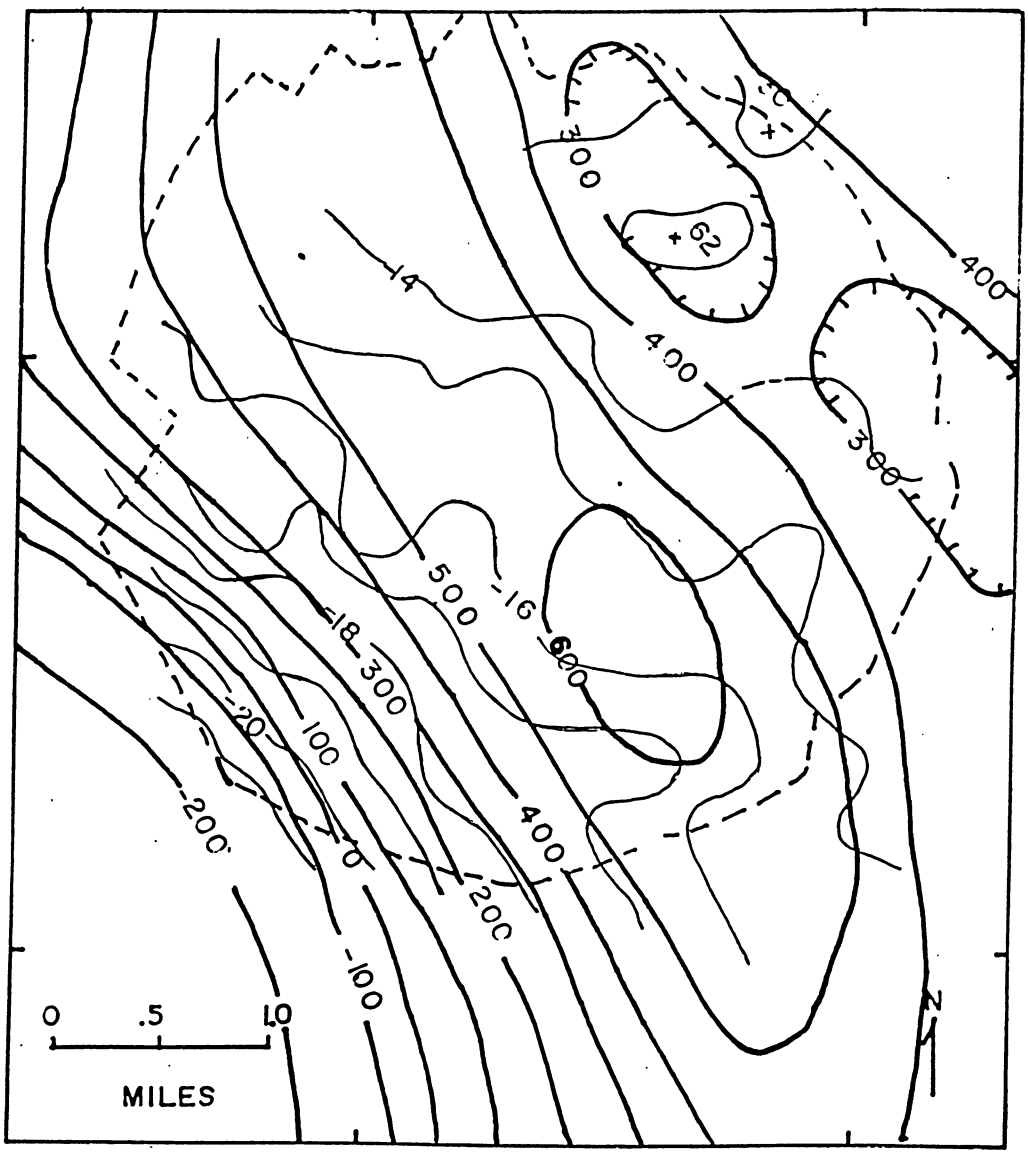

FIGURE 24

Gravity and Magnetic Anomalies Map of the Serpent Mound Cryptoexplosion Structure

Gravity Anomaly Interval - 1 milligal
Magnetic Anomaly Interval - 1 gamma

(after Sappenfield, 1950 and Zahn, 1969)

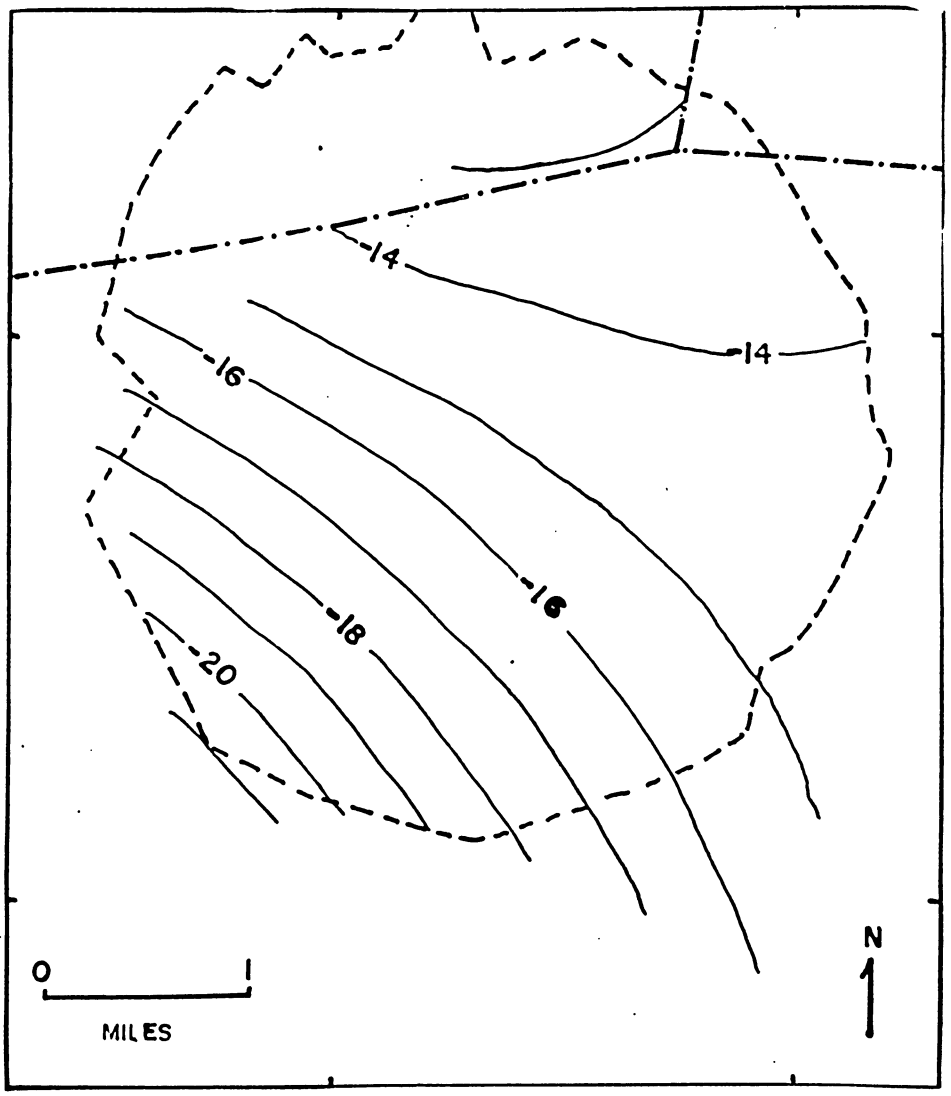

FIGURE 25

Second Degree Gravity Trend Surface Map of the Serpent Mound Cryptoexplosion Structure, Adams Co. Ohio

(after Zahn, 1969)

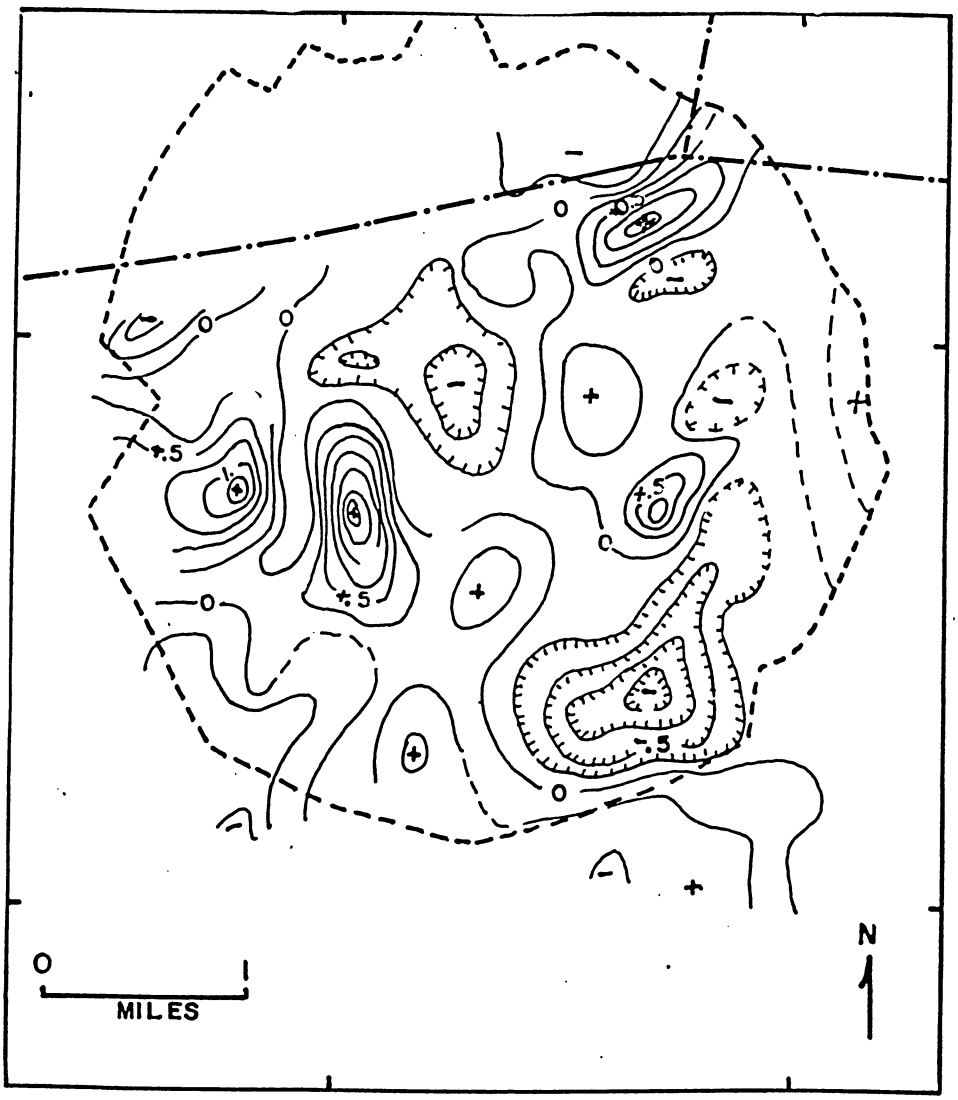

FIGURE 26

Second Degree Gravity Residual Map of the Serpent Mound Cryptoexplosion Structure

(after Zahn,1969)

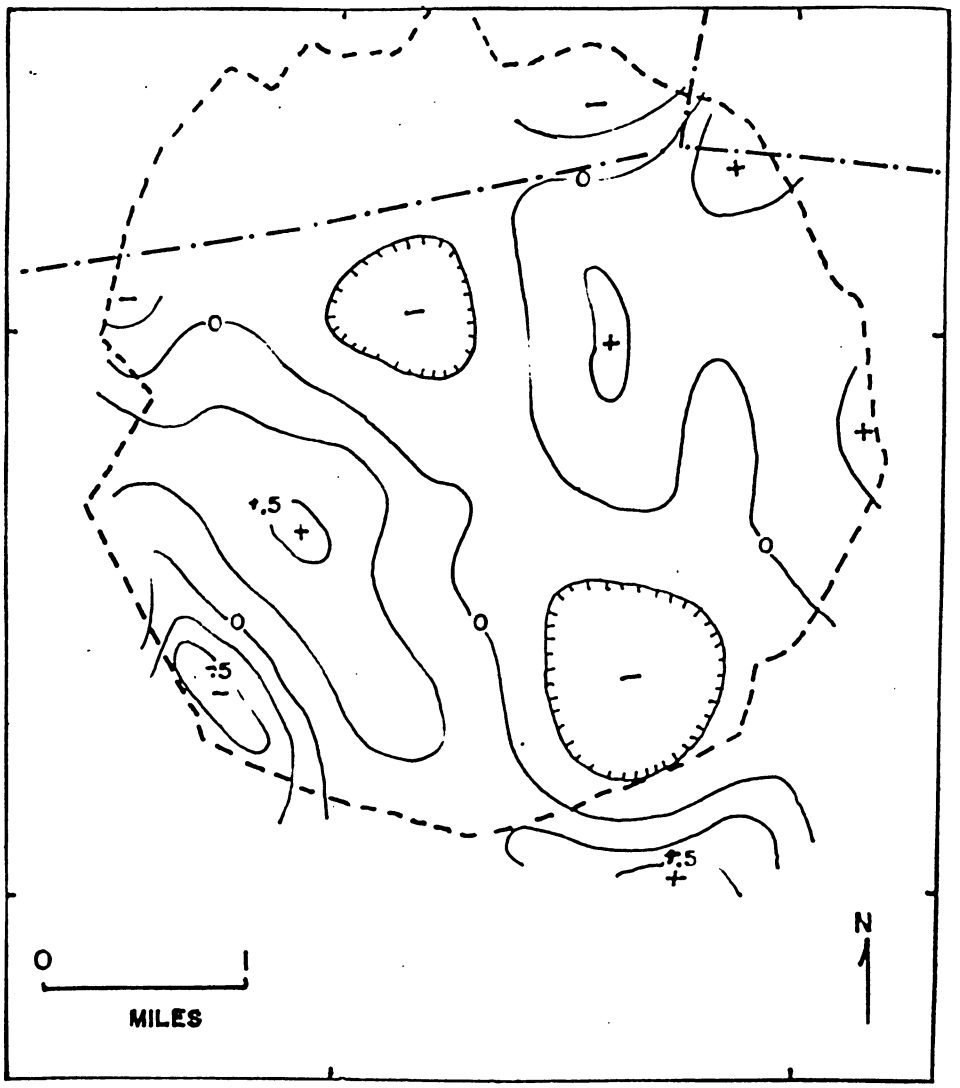

FIGURE 27

(Second Degree Residual) minus (Sixth Degree Residual) Map of the Serpent Mound Cryptoexplosion Structure, Ohio

(after Zahn, 1969)

the anomaly maps and the surface expression by postulating that most of the broken rock had been removed by erosion.

Figure 26 and 27 were transferred to photographs of the geologic map of this study (Figure 28 and 29). Both figures (28 and 29) do show a symmetry about N30°W direction (part of Figure 18's greatest fault direction frequency class).

The second degree surface minus the sixth degree residual map (Figure 29) shows that there is a relationship between the gravity and the geology mapped by this study. A bilateral symmetry about the N 30°W direction is especially noticable. The major negative areas line up in this direction through the central area. On either side are positive areas that have negative patches toward the border.

The positive and negative gravity areas outline various structures within the cryptoexplosion structure. The structures discussed on Plate I are given numerical reference on the Index Map in Appendix IV. The northwest negative gravity contours outline an area enclosed by the northwest radial anticline (Appendix IV, Location 2) the prominent dome (Location 28) west of this, and the faulted dome (Location 29) northeast of this. Figure 28 better shows the effect of the west dome (Location 29). The southeast negative gravity contours lie on the southeast basin (Location 18). The fit of the gravity contours

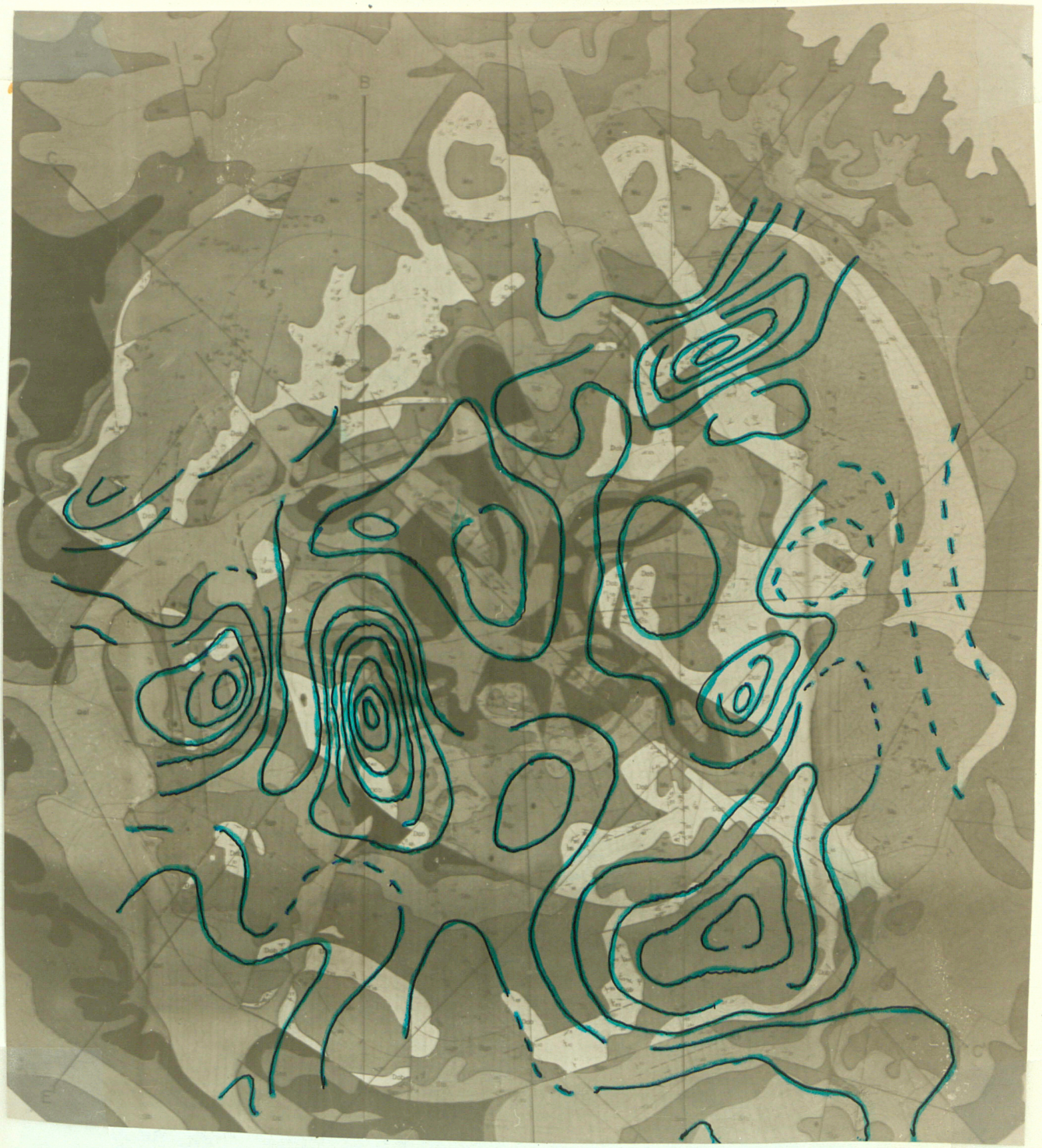

FIGURE 28 Second Degree Gravity Residual Map (figure 26) Superimposed on this Studies' Geologic Map (Plate I) of the Serpent Mound Cryptoexplosion Structure, Ohio

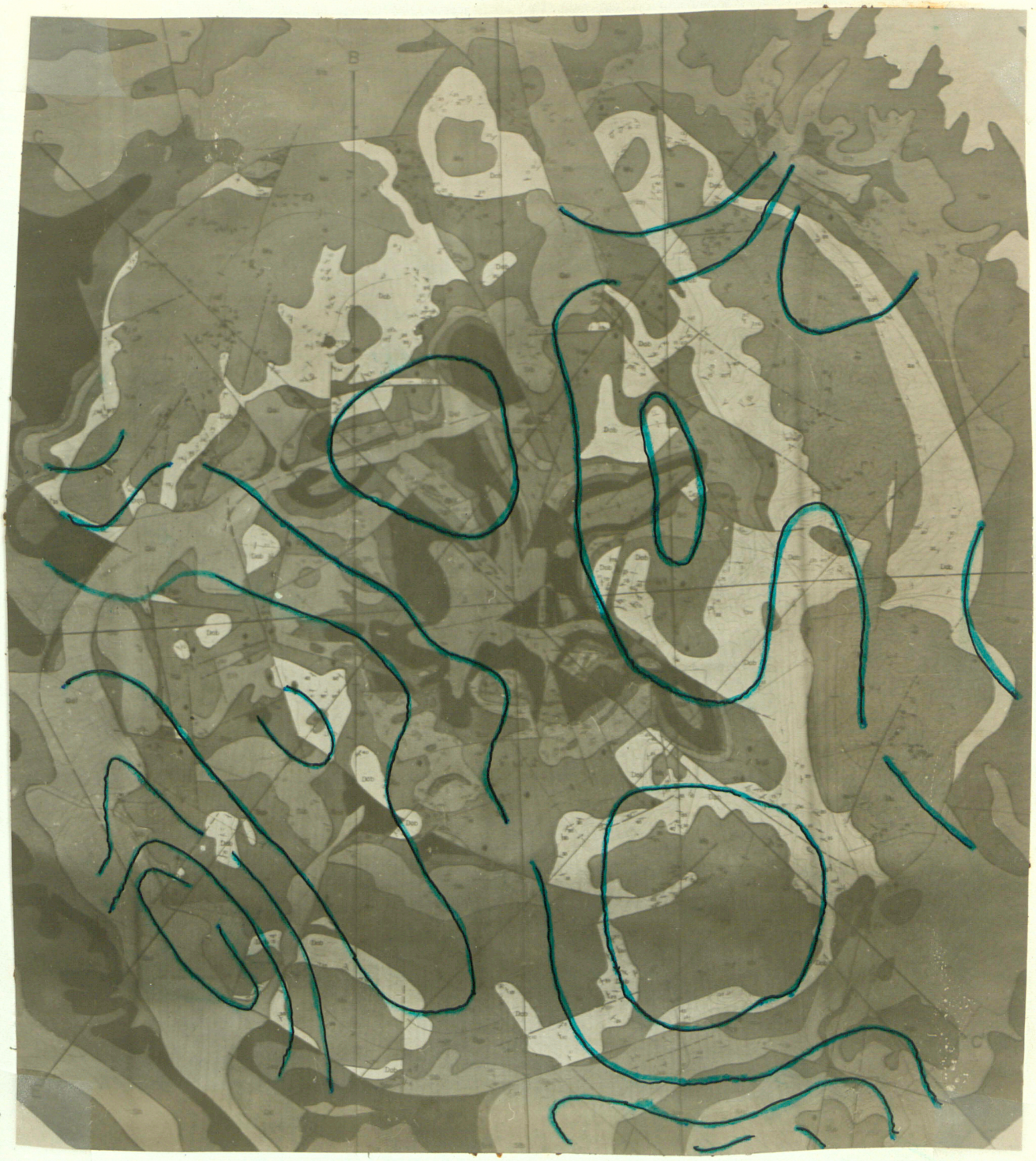

FIGURE 29

(Second Degree Residual) Minus (Sixth Degree Residual) Gravity Map Superimposed on this Studies Geologic Map of the Serpent Mound Cryptoexplosion Structure, Ohio

to the structure is remarkable here, especially on Figure 29. The southwest positive gravity contours appear to be centered almost over the middle ring fault (Location 38) where its displacement is greatest (Figure 28). One is centered on a horst block (Location 48) while the other is centered on a small anticline east of the fault located east of 38). The horst block (location 43) is an area adjacent to where shatter cones were found (Plate I). The southwest negative contours of Figure 29 are centered over the western border (located south of 21) of the southwest part of the ring graben.

The gravity contours of Figure 29 do not show much on the northeast side. There does appear to be a positive area near the northeast anticlinal boundary (Location 35) but Zahn's data is incomplete. Figure 28 does reveal a little more. There is a small anticline east of the central hub (Location 44) between two radial anticlines (Locations 6 and 7) that is expressed as a small gravity high while east of this, a more tightly folded anticline, (Location 16) is a negative area on the gravity map. Almost centered on a dome of the southeast radial anticline (Location 7) is a positive gravity area.

The southern part of the ring graben that is near its normal position (Location 25) is expressed as a positive gravity high.

Not enough is known about the gravity of the northern

part of the structure. The northwest syncline (Location 19) of the ring graben appears to be a negative gravity area similar to the southeast basin (Location 18) but unfortunately Zahn's data are incomplete. On the northeast side the incomplete data show a small negative area.

The gravity study by Zahn (1969) when applied to the geologic map of this study does show a relatable pattern. Unfortunately why one area of uplift will be negative, just as one of the depression, cannot be explained. Deep drilling would be necessary to determine if the degree of brecciation or other factors are the cause. Unfortunately none has been done so any explanation would only be speculation.

The gravity relationship between Serpent Mound and so-called "proven" meteorite craters are dissimilar. Meteorite craters such as Grosse Bluff (Milton et al., 1972), Brent crater (Millman, 1951) Holleford crater (Beals et al., (1956), and Deep Bay (Innes, 1961) all show concentric gravity contours with only a center of symmetry located in the central area. As shown, Serpent Mound is quite different with a bilateral symmetry.

Zahn (1969) had stated that for the Serpent Mound structure to be of an internal origin, the gravity should have some relationship to the geology indicating continuation of the structure at depth. This relationship shown, combined with the dissimilar relationship with meteor

craters, throws doubt upon an astroblem hypothesis.

Besides lying in an area of two geophysical anomalies, the cryptoexplosion structure lies at the intersection of two structures. Galbraith (1968) has shown that the cryptoexplosion structure lies near the east side of a monocline. This monocline has been extended to the south by Jacobs (1971) where it bifidates (Figure 30). Galbraith (1968) has proposed that it be extended to the north to connect with the fault found geophysically by Rudman (1965). Both Galbraith (1968) and Jacobs (1971) have suggested that this is possibly the northern extension of the West Hickman fault zone.

Galbraith (1968) also mapped a series of faults southeast of the cryptoexplosion structure. These strike to the northwest averaging N 30°W. Bowman et al., (1961) described a series of faults forming a graben at the Plum Run stone quarry which strike in the direction of the cryptoexplosion structure. The Plum Run quarry is S 25°E of the cryptoexplosion structure (Figure 30). Because of poor exposures, no definite connection has been found. Bucher (1933) mapped several northwest trending faults on the northwest side of the cryptoexplosion structure. These cannot be traced any farther to the northwest because of glacial cover. The cryptoexplosion structure, therefore, appears to lie on a fault system with strikes NW-SE and if extended could possibly join the faults at the Plum Run quarry.

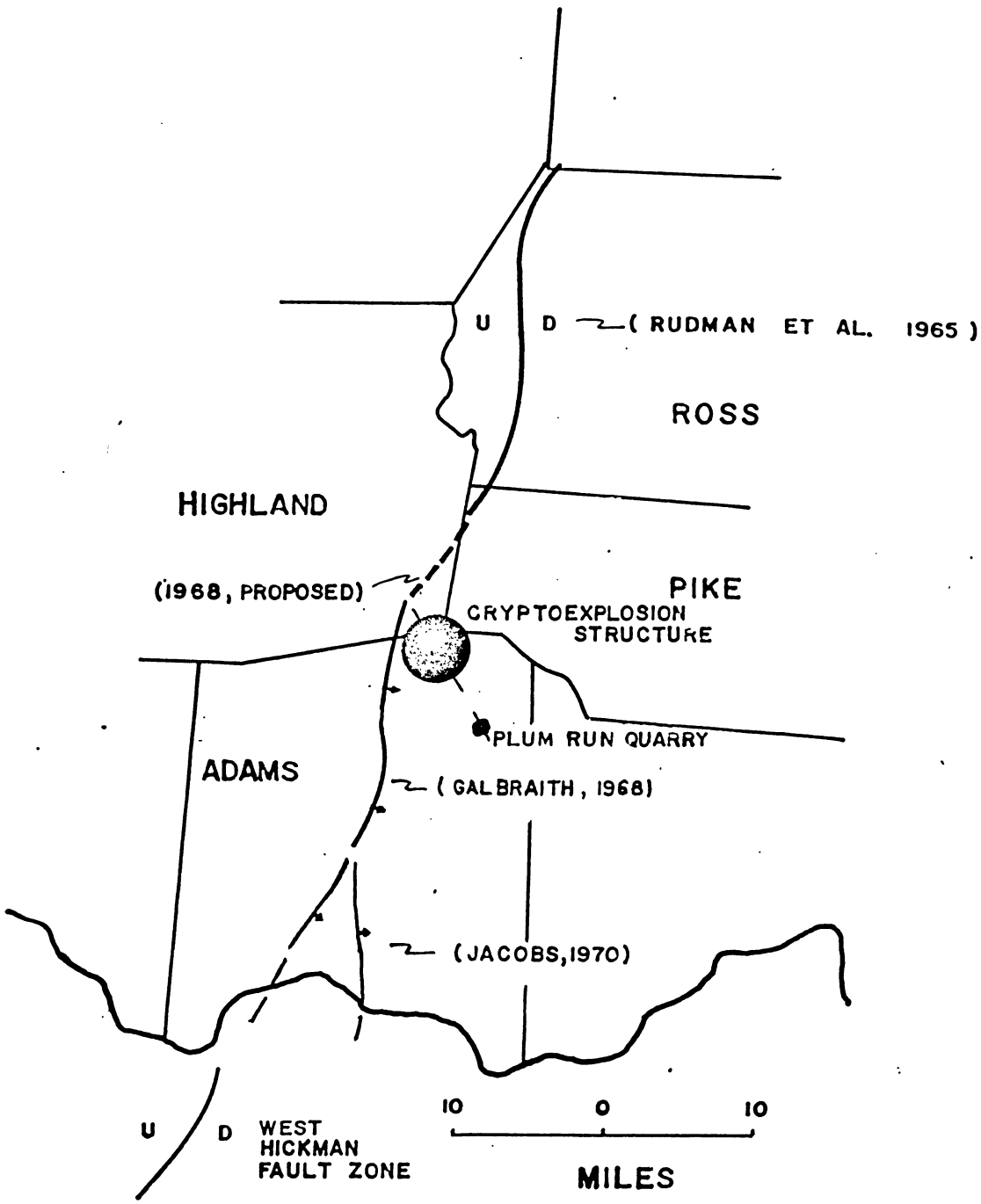

FIGURE 30

RELATIONSHIP BETWEEN SERPENT MOUND CRYPTOEXPLOSION STRUCTURE AND THE NORTH - NORTH EAST STRUCTURE

It is not unusual, however, to see a cryptoexplosion structure lying at the intersection of two structures. As summarized by Koucky (1972) most cryptoexplosion structures do, in fact, lie at the intersection of two structures.

It is beyond the scope of this study to make a detailed analysis of the mechanics that could form the observed structure. Mechanics involving meteorites have been discussed (Shoemaker, 1959) as well as possible mechanisms that would liberate gas at depth (Morev, 1922) and Burnham, 1969). The lack of detailed information involving explosions at depth has resulted in limited explanations of the mechanics that would produce a cryptovolcanic structure. Several aspects of the Serpent Mound Cryptoexplosion Structure can be shown to have some analogies that might suggest the mechanics involved.

The shape of the central uplift of the Decatorville Cryptoexplosion Structure, as described by Offield (1970), can be likened to the same forms that are obtained when a piece of cloth is pulled through a small hole. The mechanism of pulling material through a small hole causes the original surface to be compressed. This compression results in a series of radiating folds from a central point. The same pattern is seen in the central uplift of the Serpent Mound Cryptoexplosion Structure. The central radiating anticlines appear to be the result of rapidly forcing

a great volume of material upward through a small area. Original relatively flat lying material underwent compression and as anticlines formed, younger materials dropped down (relative to the rising anticlines). This was caught either as a synclinal structure with a fault along its axis (on the west and north sides at the center) or as a graben where more material was caught in synclinal part of the radiating folds. Drag folds and shear folds formed on the limbs of the radiating folds in response to the compression by a process of extension along the limbs (Figure 19). That is, compression of the original material, resulted in shear folding that produced the radiating folds. This shearing also caused faulting along the axial planes of the folds.

Grabens appear to represent areas that have been subjected to lateral, as well as vertical, forces. As the central uplift moved up and to the southeast or east, the material that would normally be shear folded into a syncline, began to fold with a concentric pattern from the central area (Figure 16). The folding was a combination of shear folding and flexture slip folding. Underthrusting was important to the rotation in the limbs. The shearing that normally produced the radiating syncline was counteracted by the lateral component of the uplifted force. This shearing was concentrated in a small area on

the limbs of the radiating anticlines. The net result was radiating anticlines separated by grabens. The main radial shearing is concentrated in the faults between the grabens and the radiating anticlines. The shearing resulting from the lateral component is concentrated in the folds and faults within the grabens.

The north and west sides of the central area were not subjected to the lateral component so only faulted synclines developed.

The synclinal ring graben resulted from collapse and drag during the formation of the central area. On the east side(Appendix IV, Location 16), a general damping of the lateral force from the central area resulted in several asymmetrical folds.

The predominance of the northwest fault direction frequency is probably evidence of a precryptoexplosion structure northwest fault system. As the cryptoexplosion structure formed,previous weakness zones of northwest faults became important zones of movement.

In general terms, the cryptoexplosion structure appears to be the result of primarily upward vertical movement (initially or rebound) with an eastward component, on a preexisting fault zone, and complimentary collapse on the edges. The structures of the central area indicate rapid deformation.

The ultimate cause for the formation of cryptoexplosion structures has been attributed to meteorites and gas explosions. It would be useless to discuss the differences explained in the literature because every phenomena within these structures has been attributed to both causes. The literature is very confusing on this point. There is no doubt that meteorites have penetrated the earth and formed craters, but just because no igneous material is present, a gas explosion cannot be ruled out. No one can deny the role of igneous processes in shaping the earth as we see it today. Each structure must be evaluated in terms of the phenomena associated with it. It is this approach that will be followed in suggesting an origin for the Serpent Mound Cryptoexplosion Structure.

Two possible energy sources are available for producing such a structure: a meteorite shock wave striking the ground and an explosion of gas at depth. The energy required for a meteorite to produce a crater the size of Serpent Mound can be computed from an equation derived by Innes (1961):

$$E = 5.08 \times 10^{11} D^3 \sigma \text{ ergs}$$

E = energy in ergs

D = diameter in feet

σ = density of the country rocks

The mechanical energy necessary was calculated to be 8.0065×10^{24} ergs (for calculations, see Appendix II).

A gas explosion would not necessarily require the same amount of energy as a meteorite to produce the same size structure. It was shown earlier that the structure formed on a previously existing fault zone. This weakness would permit less energy to form the same size structure. Nevertheless the energy released by a gas explosion should be comparable to that of a meteorite impact.

Burnham (1969), using experimental determinations of the Pressure - Volume - Temperature - Composition of the system $NaAlSi_3O_8$-H_2O, provided a basis for calculating the thermodynamic behavior of water in a felsic melt. This is based on the first law of thermodynamics and the principle of resurgent boiling. Resurgent boiling is an adiabatic process; so from the first law the mechanical energy is equal to the work done by the system.

$$E = -P. dV$$

Burnham (1969) has shown that there is an expansion of volume during resurgent boiling, and this can be calculated. Knowing the pressure, the composition of the melt can be obtained (Burnham, 1969a, Figure 22, Page 38) and total mechanical energy can be calculated (Burnham, 1969).

This process of explosion due to resurgent boiling has been used to explain the fracturing associated with porphyry copper deposits (Burnham, 1971). In some porphyry copper deposits, a breccia pipe forms with the fracturing,

which could be the means of escape for the steam.

This process could also account for several periods of fracturing. The amount of energy released would depend on how much crystalization had taken place before resurgent boiling.

Burnham (1969) has shown that the mechanical energy released during resurgent boiling is in the range of 10^{24} to 10^{25} ergs per Km of magma. The energy is roughly equivalent to the mechanical energy released in a major volcanic eruption. He has also shown that 10^{24} to 10^{25} ergs of thermal energy can be released at the same time.

Suppose that in a melt only one-third of the melt were crystallized at the time of resurgent boiling. If 9×10^{24} ergs were available in the whole system, only 3×10^{24} ergs could be released. If at a later time one-half of the remaining melt crystallized before resurgent boiling, one-half of the remaining energy could be released (3.0×10^{24} ergs). This mechanism can supply the energy for several equally violent explosions.

This mechanism can easily give a comparable amount of energy for the formation of the cryptoexplosion structure as compared to that needed in a meteorite impact for a similar structure. A preexisting northwest fault system combined with this amount of energy could easily result in the Serpent Mound disturbance.

A gas explosion hypothesis does not necessarily require the release of steam. Other types of gas release from igneous rocks, such as CO_2 release from mantle rock when they crystallize in the crust, are possible. This has been postulated for Kimberlite pipes. The uplift and collapse of the outer margins is a well known feature of Kimberlite pipes. It has also been pointed out (Snyder and Gerdeman, 1965) that Missouri's cryptoexplosion structures lie in line with alkali ultramafic intrusions and appear to be related.

The relationship between the monocline and the cryptoexplosion structure is unclear. It cannot be determined if the monocline existed before the cryptoexplosion structure or if it followed. Any trace of the monoclines effect has either been wiped out or was so minor that it did not noticably effect the cryptoexplosion structure. Only the greater deformation on the west side of the ring graben could possibly be associated with the monocline. If, however, the monocline existed before the cryptoexplosion structure, this would require less energy from a gas explosion.

To account for the structure in terms of a meteorite impact hypothesis, a sequence of events similar to the following would have to occur.

1. Faulting in a northwest-southeast direction.
2. Accidental impact on the fault zone from a high angle to the east.

3. Mineralization along faults.
4. Second meteorite hitting same area (this would be necessary to explain the brecciation of the sphalerite and straining of the calcite).
5. Final mineralization.

The age of the monocline is uncertain and cannot be placed in sequence, but if it predates the cryptoexplosion structure, then the site of a meteor crater is even more unusual.

A gas explosion hypothesis must account for the same sequence of events. Once again the monocline is impossible to place in the sequence.

1. Faulting in a northwest-southeast direction.
2. Crystallization of a melt at depth causes resurgent boiling and rapid release of steam.
3. Mineralization of faults.
4. Further recrystallization of melt causes second rapid release of steam by resurgent boiling.
5. Final mineralization.

Any model for the origin of the Serpent Mound Cryptoexplosion Structure must account for all the phenomena. Both the gas explosion and meteorite impact hypothesis can account for the general features: a central uplift and a ring graben. Both can easily generate the needed energy.

The asymetrical central area is more easily explained by a high angle meteorite striking the ground and causing

asymmetrical rebound. To explain this, a gas explosion would require a mechanism to divert the main force from vertical. Perhaps steam penetrating through vertical joints in eastward dipping sediments would be sufficient (Figure 31a). As it was pointed out earlier, the sediments do indeed dip to the east. Perhaps a westward dipping basement fault might cause an asymmetrical es-

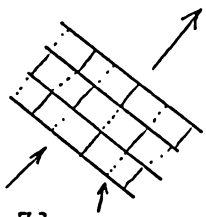

31a

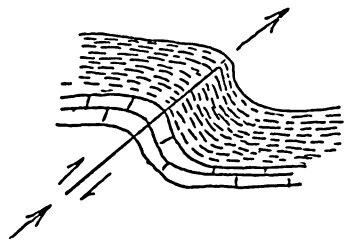

31b

Figure 31 Possible methods of an asymmetrical escape of gas

cape of gas (Figure 31b). Figure 31b could be the mechanism if the monocline predated the cryptoexplosion structure.

A gas explosion, however, more easily explains the second deformation seen in the mineralization. It is hard to visualize a second meteorite striking an area previously struck. It is not difficult however, to visualize a second explosive resurgent boiling by the method previously described.

Circumstantial evidence probably fits a gas explosion hypothesis better than a meteorite hypothesis. The geophysical evidence, although not conclusive, more closely fits the geology mapped by this study than geophysical

pattern from socalled "proved" meteorites thus tending to indicate continuation of the structure at depth. The association of two prominent geophysical anomalies and two structural anomalies could be more easily explained with the gas hypothesis.

Combining all the information available, the Serpent Mound disturbance fits more closely to a gas explosion hypothesis than meteorite impact hypothesis.

Zinc mineralization has been found at several other cryptoexplosion structures: Jepta Knob (Reidel and Koucky, 1970, unpublished research), Decatorville (Offield, 1971), Hicksdome (Snyder, 1968) and others.

Snyder (1968) has defined Mississippi Valley type deposits (Figure 32) as typically strataform in character within a single or few formations. The host rocks are shallow water marine carbonates, on the rim of a sedimentary basin or on a high within the basin, associated with unconformities. The ore bodies are contained in stratigraphic traps, in organic reefs and associated sediments, and in breccia of several types: 1. submarine slide, 2. solution collapse, 3. dissolution, or 4. fault origin. The ore minerals are simple sulfides of Zn, Pb, and Cu with or without Ba, Co, Ni, Cd, Ga and Ag. The lead is J type and associated silica was probably derived from the host rock. Fluid inclusions suggest ore metals were brought in by saline solutions at temperatures between 70° and 150°C.

(1) Ore occurrence in host rock
- A. In shallow water carbonates.
- B. On rim of basin or over high in basin.
- C. Unconformities above, below, or within the host.
- D. At or near the limestone-dolomite interface.
- E. At any depth.

(2) Structural pattern of districts
- A. Ore does not occur on major faults.
- B. Ground prepared by minor faults and fractures.
- C. Ground prepared by subsidence and dissolution.
- D. Filled fissure vein systems usually associated with stratiform deposits.

(3) Types of ore-bearing structures
- A. Stratigraphic traps.
- B. Reefs and associated structures.
- C. Breccias.
  1. Submarine slide.
  2. Solution collapse.
  3. Pseudobreccia formed by dissolution.
  4. Fault breccias.
- D. Fissures.
- E. Size of ore bodies directly related to size of entrapping structures in host.

(4) Mineralogical characteristics
- A. Elements present
  1. Zn, Pb, and Cu always present.
  2. Ba, Co, Ni, Cd, Ge, Ag usually present. Fluorite may be present.
- B. Lead is J-type with considerable range in Pb 206/204 ratio.
- C. Sulfur probably of biogenic origin.
- D. Paragenetic studies are difficult to interpret because of change of solutions with time.
- E. Fluid inclusions are mainly connate water.
- F. Temperatures of formation range from 70° to 150°C.
- G. Silica occurring with the ore is roughly proportional to the abundance of silica in the host.

Figure 32 Characteristics of a typical Mississippi Valley type deposit(after Snyder,1968)

The main mineralization at the Serpent Mound Cryptoexplosion Structure occurs in the Greenfield, Peebles, and Tymochtee dolomites which are shallow marine carbonates occuring on the rim of a sedimentary basin.

There are several unconformities in the stratigraphic units present in the area. The most noticable unconformity occurs at the contact between the Silurian Tymochtee dolomite and the Devonian Ohio black shale. The main mineralization is the carbonates below this.

Even though the cryptoexplosion structure lies at the intersection of a monocline and northwest trending fault system, mineralization is minor along these structures (Jacobs, 1971 and Galbraith, 1968). The major mineralization occurs on the faults of the cryptoexplosion structure. This is similar to most Mississippi Valley type deposits where major structures are not mineralized and only associated smaller structures are mineralized (Snyder, 1968).

The host rock was prepared for mineralization by faults and fractures of the cryptoexplosion structure. The main ore-bearing structures are fault breccias with some solution collapse breccias, and minor veins.

The mineralogy of the area is similar to Mississippi Valley type deposits except no lead or copper is present. Barite has been found near Locust Grove (sample in mineralogy collection at University of Cincinnati) but none has been found within the cryptoexplosion structure. Of the trace elements only cadmium is abundant amounting to 25%

in some sphalerites.

Therefore mineralization at the Serpent Mound Cryptoexplosion Structure fits the description of a typical Mississippi Valley type deposit, and can be classed as such.

If the structure was formed by a gas explosion, then perhaps this deep-seated body can be called upon as a source for the metals. It is certain that the host rocks cannot be the contributing agent since zinc is absent. Only the "lag" layer at the base of the Ohio black shale has any sphalerite present.

Even though most of the sphalerite cannot be explained as to a source, the final unfractured minor sphalerite (Photo 57) could possibly be explained by a model of Barne's (1967a) low temperature ore transport in solutions.

Barnes has summarized (1967) that previous ideas of sulfide ore transport are ineffective and that he favors a metallic complex for the transport of zinc. The two ligands: chloride and bisulfide, appear to be the most important complexes from a chemical point of view (Barnes, 1967a).

Barnes and Kullerud (1967) have calculated the stability of predominant sulfur species in aqueous solutions with respect to PO_2, S, pH, temperature and Pt (Figure 33).

In a sulfur-metal system, two sulfur complexes can

form with zinc: one by complexing Zn with H_2S or other minor species and one by the reaction:

$$ZnS_{(s)} + H_2S_{(g)} + HS^- = Zn(HS)_3^-$$

$Zn(HS)_3^-$ is the most important complex. It is independent of temperature up to 200°c and has a high solubility. Increasing the chloride content from practically zero causes a decrease in the solubility of sphalerite. No important complexes have been found to exist that contain both HS^- and Cl^-.

Two important zinc complexes exist; $ZnCl_2$ and $Zn(HS)_3^-$. The chloride complex predominates in solutions low in total sulfur whereas the bisulfide complex predominates in solutions high in total sulfur. Figure 34 shows that near neutrality, ore transport can occur in either low or high total (H_2S + HS^-) concentrated solutions.

As a potential source for the final generation of sphalerite, consider the basal 2 inches described as a "lag" deposit in the Ohio black shale. Sphalerite and other sulfides are found here (especially marcasite and pyrite with fish bones and teeth).

Ground water is quite plentiful in the area as seen by the numerous springs throughout the area. The springs were described by Locke (1836) noting "although we travelled on that level which should have presented us with the Cliff limestone, yet we were surprised with its total disappearance as we approached the spring, and in its

place was found the sandstone in large upturned and broken masses. The spring has every property of an excellent sulphuretted water (Page 266). This study has found many of these springs throughout the area. The springs are usually at the contact between the Ohio black shale and the Tymochtee dolomite. The water smells of H_2S and a white sulfur skum is found on the surface (Photo 59). The sulfur was apparently derived from the iron sulfides in the "lag" layer and from the breakdown of pyrite and marcasite in the lower shale.

It can probably be reasonably assumed that the S/Cl^- ratio is very high and that the pH is near 8.0 since the water will tend to equilibrate with the carbonate.

According to Figure 33, the dominant aqueous species of sulfur near pH 8 and 25°c should be HS^- and $SO_4^=$ and perhaps solid S. The log PO_2 atm. of the stream is not certain but should be near the point where free sulfur and HS^- approach equal activities because of the H_2S odor and the sulfur skum. Away from the atmosphere, however, the PO_2 should be much less so that the ground water will probably contain more HS^- than $SO_4^=$.

A zinc complex could form by the following reaction:

$$ZnS_{(s)} + 3HS^-_{(ag.)} = Zn(HS)_3^-$$

The zinc for the complex could be derived from the same basal "lag" layer that sulfur was derived.

Normal circulation of groundwater can move the complex.

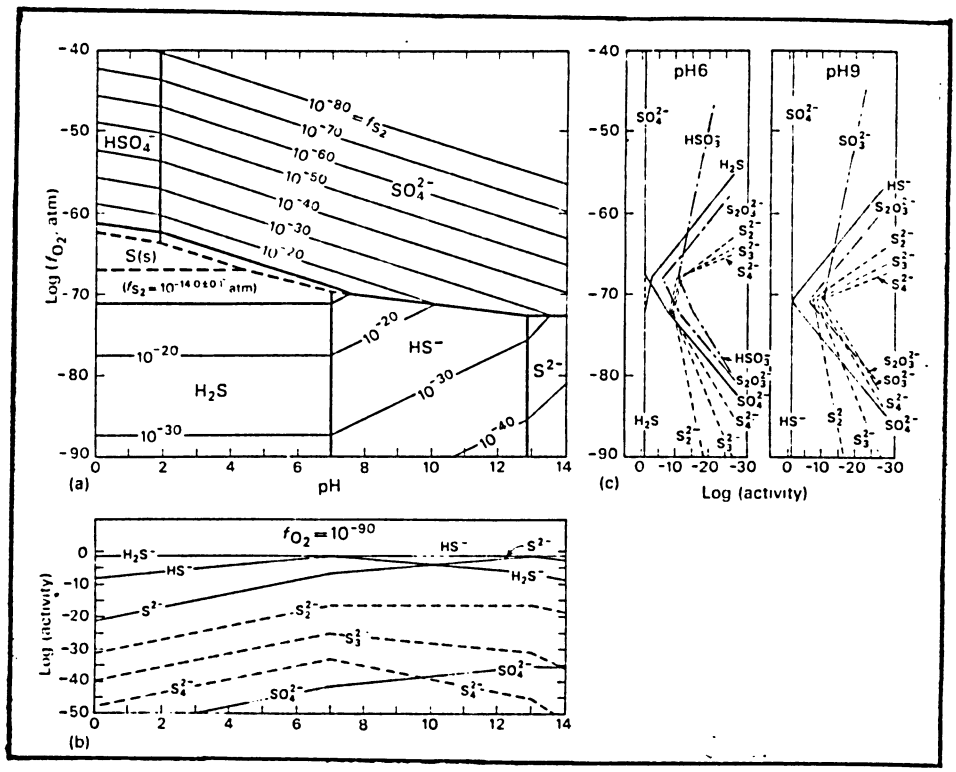

Figure 33 Stabilities of aqueous, sulfur-containing species at S=0.1, 25°C.

a) f_{S2} is shown by the light, solid contours. Changes in the fields of predominance (heavy lines) on S to 0.001 are indicated by the heavy dashed lines.

b) Variation with pH in activities of predominant and minor species under reducing conditions at $f_{O2} = 10^{-90}$ atm.

c) Variation in activities of predominant and minor species with oxidation state at pH6 and at pH9 (after Barnes and Kullerud, 1961)

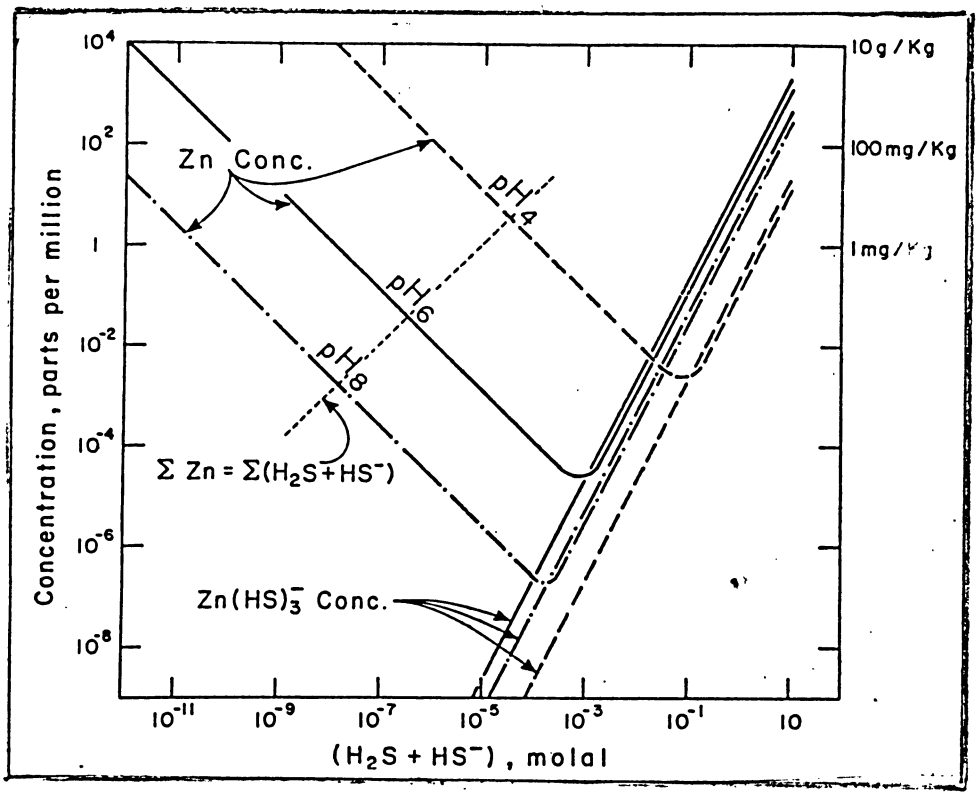

Figure 34 Total zinc concentration and concentration of zinc bisulfide complex in a solution in equilbrium with sphalerite at 100°C. An ionic strenght of 1.0 and a chloride ion activity of 1.0 are assumed. A dotted line, where the mole ratio in solution

$$\frac{(Zn)}{(H_2S + HS^-)} = 1.0$$

separates the sulfide-deficient compositional region, where the metal concentration exceeds total sulfide concentration(upper left),from the sulfide region.

(after Barnes,1967)

PHOTO 59
Sulfur spring in the Serpend Mound
Cryptoexplosion Structure
(located north of 18)

Because of the high permeability of the dolomite and the porous spaces in the breccia, groundwater can easily move through the host rock.

Deposition could occur because of dilution with more groundwater as the complex rich water moves away from the "lag" or as the complex comes in contact with asphalt material in the host rock. In any case transport of the complex would not have to be any more than 150' (the thickness of the dolomite in which the unfractured sphalerite occurs).

This mechanism easily accounts for some sphalerite deposition but since it requires ground water, the depth of burial at the time of sphalerite formation cannot be too great. It could be possible to account for the minor unfractured sphalerite, which is late, by this method but it cannot explain the multicolored sphalerite. The sphalerite from the base of the Ohio black shale is a deep red variety and has no cadmium or mercury. This is very different from most of the sphalerite in the Serpent Mound Cryptoexplosion Structure. The late sphalerite would have an unchanging source and a uniform color could be expected with respect to time. If the process described is responsible for at least the final generation of sphalerite, then sphalerite deposition is now occurring in the Serpent Mound Structure.

The amount of sphalerite in the Greenfield Peebles Tymochtee dolomites is not economical but it is unknown

what more favorable horizons might contain. The Knox formation (middle Ordivician) is an important host rock throughout Tennessee and Kentucky and every core taken from this horizon in the area near Adams County, Ohio has been mineralized (S. Jackson, Cominco Am., personal communication). If this is a gas explosion, as evidence seems to indicate, then brecciation at depth might be expected and the chances of finding mineralization in the Knox formation in this area should be excellent.

CONCLUSIONS

The main goal of this study was mapping in detail the structure of the Serpent Mound Cryptoexplosion Structure and to study the associated mineralization.

Detailed mapping has shown structures caused by a force directed upward and to the east or southeast. Most of the folds formed by a combination of shear folding and rotation of the limbs. The central uplifted area consists of seven radiating anticlines. Grabens formed between the anticlines on the east and south sides in response to lateral forces. Faults formed between the anticlines on the north and west sides where there were no lateral forces acting on them.

Regional geophysical evidence indicates the structure lies in an area where there is a positive magnetic anomaly and a positive gravity anomaly. On a local scale, the gravity and magnetic trends have the same axis as the greatest fault frequency class found in the cryptoexplosion structure. Local residual gravity maps match the mapped surface geology better than others have found from the gravity patterns of so-called meteorite impact craters.

The cryptoexplosion structure is located at the intersection of a NW-SE fault system which existed before the structure formed and a monocline which cannot be dated in relation to the structure.

Paragenesis of the mineralization indicates at least two deformations occured within the structure.

Both a meteorite and a gas explosion resulting from resurgent boiling in a magma can easily supply the needed energy for the formation of a crater this size.

It is concluded from the available evidence that the gas explosion hypothesis fits the Serpent Mound Cryptoexplosion Structure more easily than a meteorite impact hypothesis.

Mineralization is common but nowhere economical on the surface within the cryptoexplosion structure. The mineralization is typically Mississippi Valley type. There are two generations of sphalerite before final deformation and one after. The first generation shows lamellae of multicolored sphalerite but cannot yet be explained by trace elements. The most favorable host rock for zinc mineralization is not exposed and thus the real economic potential of the area cannot be determined.

No source can be given for most of the sphalerite. It is possible that the final generation is the result of deposition now in progress by surface water transporting Zn bisulfide complexes from a "lag" layer at the base of the Ohio black shale.

Several deep core holes in the structure could yield valuable information about the continuation of the structure at depth, the mineralization of the Knox, and the origin of the gravity and magnetic anomalies.

APPENDIX I

METHOD OF ANALYZING THE DRILL CORE FROM THE SERPENT MOUND STRUCTURE

The core was given a preliminary analysis to see if a detailed analysis would be of value. The core from Ca 110 and Ca 111 was sampled every four feet except for the Greenfield Peebles dolomites which was sampled every 2 ft. The core was then sawed into discs paralled to the bedding. The discs were analyzed using tungsten radiation and a LiF 200 crystal in a General Electric XRD-5 fluorescence X-ray unit. The standards used were pelletized standards normally used for analyzing of iron and zinc in sphalerite. Since the core pellets were not of uniform density as were the standard pellets, control core pellets were analyzed several times using several positions including reverse sides. No significant differences in readings were found so it was assumed this method would give a reliable preliminary examination.

The samples are normally plotted on a graph as number of counts vs. concentration, with known standards as the basis for the graph line. These samples were not plotted since the number of counts was well below the number of counts of the lowest standards. The cores were considered to be below the detection limit for these elements and no further analysis was needed.

APPENDIX II

CALCULATION OF MECHANICAL ENERGY OF THE METEORITE

An estimate of the energy involved in the deformation of the Serpent Mound Cryptoexplosion Structure by a meteorite impact can be made based on a formula by Innes (1961):

$$E = 5.08 \times 10^{11} D^3 \sigma$$

E = energy in ergs

D = diameter in feet

σ = the country rock density

Using: A) D = 4.5 miles

$D^3 = 1.34 \times 10^{13}$ ft.^{3}

B) $\sigma = 2.5$ gm/cm^3 - Based on the density assumed by Zahn, 1969)

$E = 8{,}0065 \times 10^{24}$ ergs

The total energy (including that which goes into heating, crushing, fracturings and elastic effect) needed to form a crater the size of Serpent Mound by meteorite impact is 8.0065×10^{24} ergs.

APPENDIX III

Presented in this Appendix is a structure contour map (Plate III). It is an incomplete map and there are mistakes on it. Work is underway at the present time to complete it. As pointed out, the Crab Orchard shale thins and thickens so an accurate map is difficult to make.

This is presented only for determination of the stratigraphic throw of areas and for no other reason.

APPENDIX IV

INDEX MAP FOR PLATE I

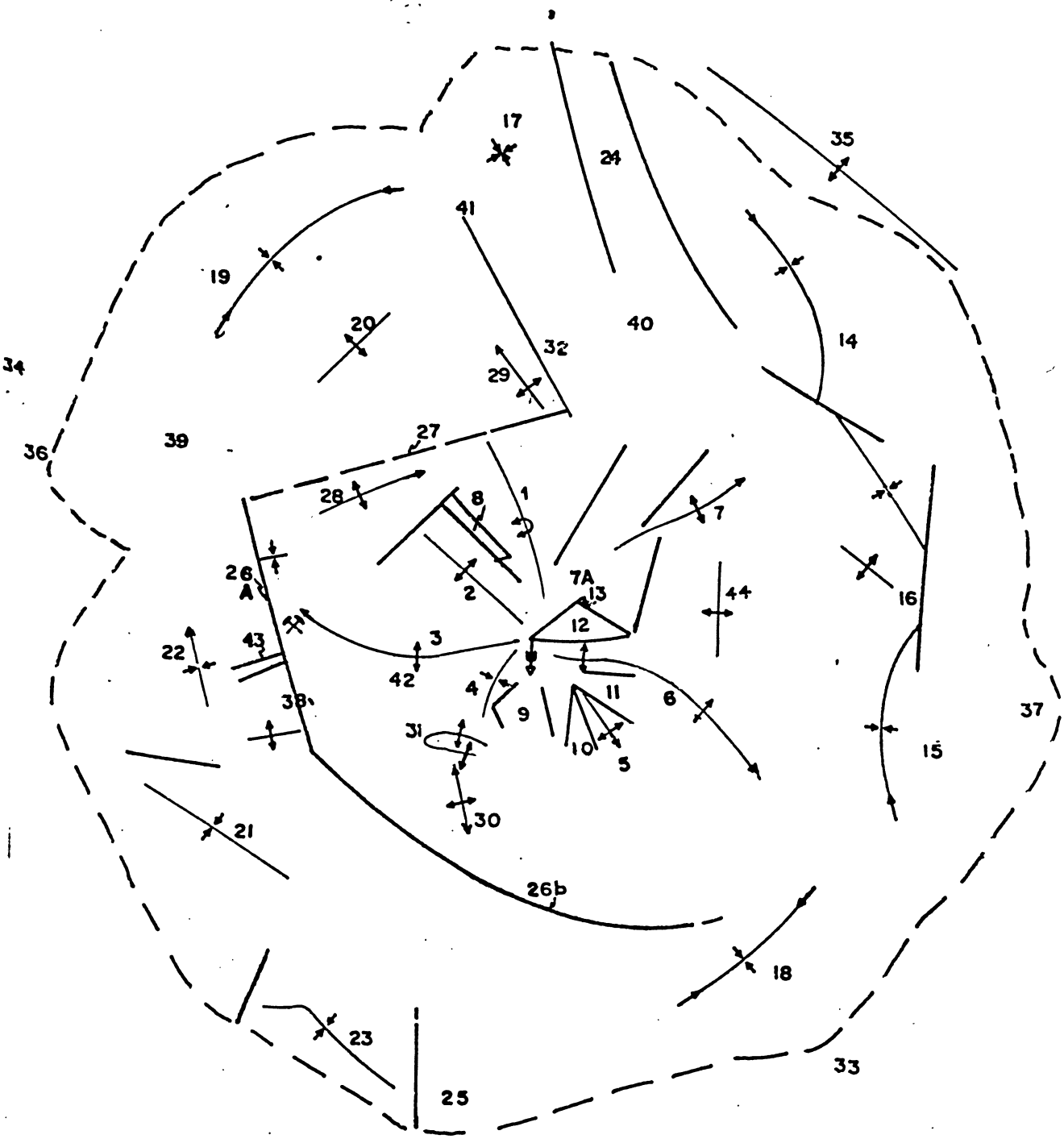

INDEX MAP FOR PLATE ONE

APPENDIX V

CATACLASTIC NOMENCLATURE USED IN THIS STUDY

The nomenclature used in this study is from U.S.G.S. Professional Paper 687 by Higgins (1971). It is the most recent classification and that which the U.S.G.S. plans to adopt. The classification is presented in Figure 35. Below are defined several terms used in this study.

1. FLUXION STRUCTURE: Cataclastically produced directed penetrative texture or structure commonly involving a family or set of S-surfaces; cataclastic foliation.

2. MICROBRECCIA: An intensively fractured but unground fragments have not rolled) cohesive breccia in which the grains and fragments are without form orientation.
(Fragments larger than 0.2 mm make up more than 30% of the rock).

3. MYLONITE: a coherent microscopic pressure-breccia with fluxion structure and with porphyroclasts larger than 0.2 mm. These prophyroclasts make up about 10 to 50% of the rock.

4. PROTOMYLONITE: A coherent crush breccia composed of megascopically visible fragments which are lenticular and are separated by megascopic gliding surfaces filled with finely ground material. The fragments make up more than 50% of the rock.

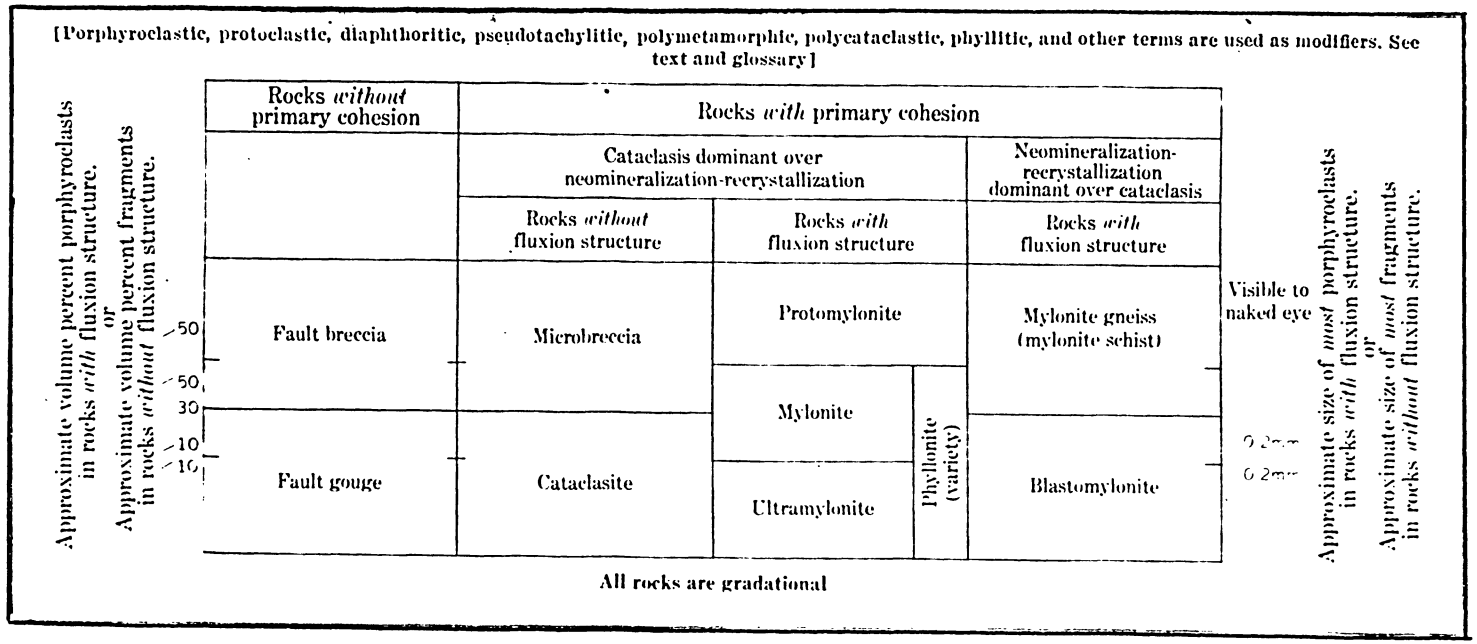

Figure 35 Classification of cataclastic rocks (after Higgins,1971)

REFERENCES

1. Barnes, H. L. and Czamanski, G. K. 1967, Solubilities and Transport of Ore Minerals: Chapter 8 in Geochemistry of Hydrothermal Ore Deposits Edit. by H. L. Barnes; Holt, Rinehart & Winston, New York.

2. Barnes, H. L., 1967a, Sphalerite Solubility in Ore Solutions of the Illinois-Wisconsin District: Symposium on Origin of Strataform Lead-Zinc-Barite-Fluorite Deposits, Economic Geology Monograph #3 326-332.

3. Beals, C. S., Innes, M. J., and Rottenberg, J. A. 1956, The Search for Fossil Meteorite Craters: Current Sci. (India), 29 (6 and 7, June and July, 205-218 and 249-262.

4. Boon and Albritton, 1936, Meteorite Craters and Their Possible Relationships to Cryptovolcanic Structures: Field and Lab., Vol. 5, P. 1-9.

5. Bowman, et al., 1961, G.S.A. Field Trip #8 Examination of Ordovician Through Devonian Stratigraphy and the Serpent Mound Cheotic Structure Area: G.S.A. Guidebook for Field Trips Cincinnati Meeting P. 259.

6. Bucher, W. H. 1921, Cryptovolcanic Structure in Ohio of the Type of the Steinheim Basin: G.S.A. Bulletin, Vol. 32, 74-75.

7. Bucher, W. H. 1933, Uber Eine Typische Kryptovulkanische Störung im Südlichan Ohio; Geol. Rundchau, Vol. 23a (Salomon-Calvi Festschr), PP 65-80, 1933.

8. Bucher, W. H., 1936, Cryptovolcanic Structures in the United States: Internat. Geol. Cong., 16th United States Repts. Vol. 2 PP 1060-1064.

9. Burnham, C. W., Holloway, J. R., and Davis, N. F. 1969, Thermodynamic Properties of Water to 1000°c and 10,000 Bars: The Geology Society of America Special Paper #132.

10. Burnham, C. W., and Davis, N. F., 1969, Energy Relations in Water-Bearing Magmas: Abstract Geology Society of America Annual Meeting, Atlantic City, New Jersey.

11. Burnham, C. W., and Davis, N. F. 1971, The role of H_2O in Sillicate Melts I, P-V-T relations in the System $NaAlSi_3O_8$-H_2O to 10 kilobars and 1000 c: American Journal of Science, Vol. 270 #1 P 54-79.

12. Cohen, A. J., Bunch, T. E. and Reid, A. M. 1961. Cossite Discoveries Establish Cryptovolcanic as Fossil Meteorite Crater: Science V. 134 P 1624-1625.

13. Dietz, R. S., 1947, Meteorite Impact Suggested by the Orientation of Shatter Cones at the Kentland, Indiana Disturbance: Science Vol. 105 P 42-43.

14. Farrer, J. A., 1971, The Correlation of the Physical Parameters and Trace Element Mineralogy of Mid-continent Sphalerites: Unpub. Senior Thesis, University of Cincinnati.

15. Freeburg, J., 1966, Terrestrial Impact Structures, A Bibliography: U.S.G.S. Bul. 1220, 91 P.

16. Galbraith, R. M., 1966, Lithologic Characteristics of the Brassfield Limestone in the Area of the Cryptovolcanic Structure of Adams Co., Ohio: (Unpub. Senior Thesis), University of Cincinnati.

17. Galbraith, R. M. 1968, Peripheral Deformation of the Serpent Mound Cryptoexplosion Structure in Adams County, Ohio: (Unpub. Masters Thesis), University of Cincinnati.

18. Goni, J. and Remond, G., 1969, Localization and Distribution of Impurities in Blende Cathodoluminescence: Mineralogical Magazine, Vol. 37, Number 286, June.

19. Heishanen, W. A. and Uotila, U. A., 1956, Gravity Survey of the State of Ohio: Ohio Div. Geol. Survey Rept. Inv. No. 30, 34 PP.

20. Heyl, A. V. and Brock, M., 1962, Zinc Occurance in the Serpent Mound Structure of Southern Ohio: U.S.G.S. Prof. Paper 450 D, PP 95-97.

21. Higgins, M. W., 1971, Cataclastic Rocks: U.S.G.S. Prof. Paper 687.

22. Innes, M. J. S., 1961, The Use of Gravity Methods to Study the Underground Structure and Impact Energy of Meteorite Craters: J. of Geophysical Res., V 66, #7 P 2225-2239.

23. Jacobs, A. J., 1971, The Geology of Southern Adams County, Ohio: Unpublished Senior Thesis) University of Cincinnati.

24. Jenks, W. F., 1965, Proposal for Investigation of the Origin of Serpent Mound, Ohio Cryptoexplosion (Astrobleme?) Structure: University of Cincinnati (Unpub.).

25. Jolly, J. J. and Heyl, A. V., 1968, Mercury and Other Trace Elements in Sphalerite and Wallrocks from Central Kentucky, Tennessee and Appalachian Zinc Districts: A Geological Survey Bul. 1252-F, 29 P.

26. Koucky, F. L., 1972, A Summary of Recent Studies of Cryptoexplosion Structures as Related to Mid Continent Structure: NAGT Guidebook to the Cincinnati Meeting.

27. Locke, J., 1836, Second Annual Report to the Ohio Geological Survey, P 266.

28. Malcolm, D. S., 1952, Ore Deposits and Structures of the Gratz District: (Unpub. Master Thesis), University of Cincinnati.

29. Millman, P. B., Liberity, B. A., Clark, J. F., Willmore, P. L., and Innes, M. J. S., 1960, The Brent Crater: Publs. Dominion Observatory, P 24.

30. Milton, et al., 1972, Gosses Bluff Impact Structure, Australia: Science Vol 175, No. 4027 PP1199-1207.

31. Morev, G. W., 1922, The Development of Pressure in Magma as Result of Crystallization: Wash. Acad. Sci. Journal, V 12, P 219-230.

32. Offield, T., 1970, Decaturville Structure, Missouri: Abst. at G.S.A. Annual Meeting, Milwaukee, Wis.

33. Peck, J. H., 1966, Upper Ordovician Formation in the Maysville Area Kentucky: Geol. Sur. Bul. 1244-B.

34. Reidel, S. P., 1970, A Geochemical Survey of the Western Portion of the Serpent Mound Cryptoexplosion Structure: (Unpublished Senior Thesis), University of Cincinnati.

35. Rudman, A. J., Summerson, C. H., and Hinze, W. J. 1965, Geology of Basement in Midwestern United States: A.A.P.G. Bul. Vol. 49 #7 PP 894-904.

36. Sappenfield, L. W., 1950. A magnetic Survey of the Adams County Cryptovolcanic Structure: (Unpub. Masters Thesis) University of Cincinnati.

37. Shoemaker, E. M., 1960, Penetration Mechanics of High Velocity Meteorites, Illustrated by Meteor Crater, Ariz.: 21st Intern. Geology Congress, Copenhagen Proc. Sec. 18, P 418-434.

38. Snyder, F. and Gerdemann, P. E., 1965, Explosive Igneous Activity Along an Illinois-Missouri-Kansas Axis: Amer. Jour. Science Vol. 263 PP 465-493.

39. Snyder, F., 1968, Geology and Mineral Deposits, Mid continent United States: Ore Deposits of the United States, Graten-Sales Vol. A.I.M.E.

40 Stryker, J. R., 1971, A Geological and Geochemical Survey of the Area South of Sinking Springs, Highland County, Ohio: (Unpub. Senior Thesis), University of Cincinnati.

41. Van Wie, Wm., 1971 The Petrology of the Floyds Knob Glauconite: Unpublished Master Thesis), University of Cincinnati.

42. Wachter, J., 1971, A Geochemical Study on the Southeast Border of the Serpent Mound Cryptoexplosion Structure: Unpublished Senior Thesis), University of Cincinnati.

43. Zahn, J. C., 1965, A Gravity Survey of the Serpent Mound Area in Southern Ohio: (Unpub. Master Thesis) Ohio State University, Columbus.

44. Zahn, J. C., et al., 1969, Gravity Survey of the Serpent Mound Area, Southern Ohio: Ohio Journal of Science, Vol. 67 #6 P 359-371.

45. Zietz, I., Stockard, H., and Kirby, J., 1968, Trancontinental Geophysical Survey: U.S.G.S. Miscellaneous Geology Investigation, Maps I -535, A, B, C.

46. Zietzm I., 1969, Aeromagnetic Investigations of the Earth's Crust in the United States: Am. Geophysical Union Geophysical Monograph 13, The Earth's Crust and Upper Mantle, Pembroke, J. Hart Editor.

Plate 1

GEOLOGIC MAP OF THE SERPENT MOUND CRYPTOEXPLOSION STRUCTURE

EXPLANATION

RECENT	Qal	ALLUVIUM
LOWER MISSISSIPPIAN	Ms	CUYAHOGA SHALES AND SANDSTONES
		SUNBURY BLACK SHALE
		BEREA SANDSTONE
		BEDFORD SHALE
DEVONIAN	Dob	OHIO BLACK SHALE
MIDDLE SILURIAN	Sgp	TYMOCHTEE DOLOMITE
		GREENFIELD DOLOMITE
		PEEBLES DOLOMITE
	Slb	LILLEY DOLOMITE
		BISHER DOLOMITE
LOWER SILURIAN	Sco	CRAB ORCHARD SHALE
	Sbr	BRASSFIELD LIMESTONE
UPPER ORDOVICIAN	O	UNDIFFERENTIATED

SYMBOLS

- BEDDING PLANE ATTITUDE
- BEDDING PLANE ATTITUDES OF OVERTURNED BEDS
- JOINT ATTITUDES
- FAULTS, DASHED WHERE INFERRED
- CONTACTS, DASHED WHERE INFERRED
- ANTICLINE (PLUNGING)
- SYNCLINE (PLUNGING)
- MINOR ANTICLINE (PLUNGING)
- MINOR SYNCLINE (PLUNGING)
- OVERTURNED ANTICLINE
- OVERTURNED SYNCLINE
- DRILL HOLE
- ZINC LOCATION

SPECIAL

- BRECCIA LOCATION
- SHATTER CONE LOCATION

SCALE
1 : 7385

0 1000 2000 3000 4000
FEET

MAGNETIC NORTH | TRUE NORTH

APPROXIMATE MEAN DECLINATION, 1961

PLATE 1

S.P. REIDEL 1972
INCLUDING REIDEL 1970, GALBRAITH 1968, WACHTER 1971, AND STRYKER 1971

Plate 3

STRUCTURE CONTOUR MAP OF THE SERPENT MOUND CRYPTOEXPLOSION STRUCTURE, SOUTHWESTERN OHIO

STRUCTURE CONTOUR INTERVAL 25 FEET CONTOURS DRAWN ON THE TOP OF THE BRASSFIELD LIMESTONE

ABOVE NORMAL POSITION BELOW NORMAL POSITION

PLATE 3

S.REIDEL 1972

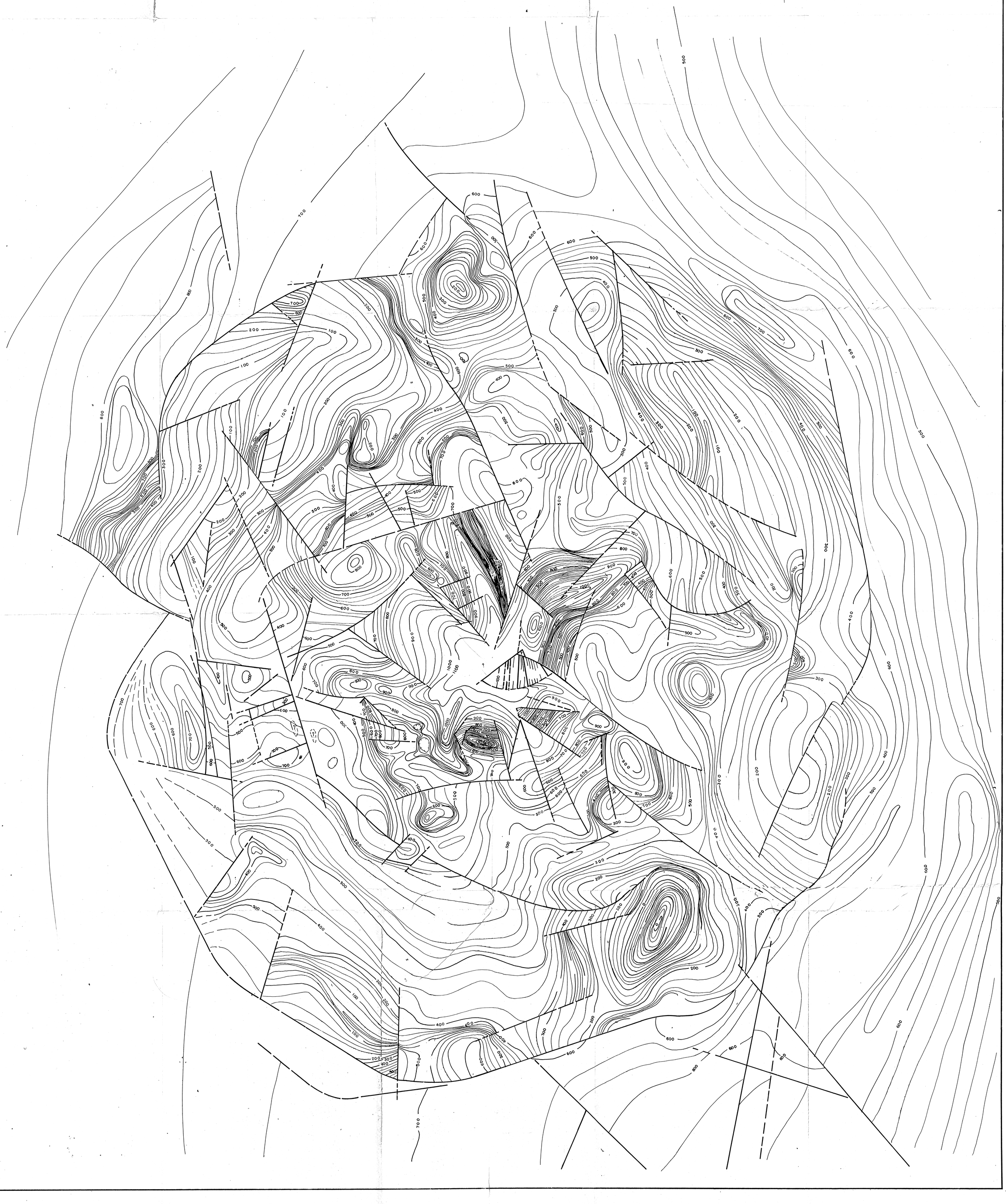

Plate 2

CROSS SECTIONS OF THE SERPENT MOUND CRYPTOEXPLOSION STRUCTURE, OHIO

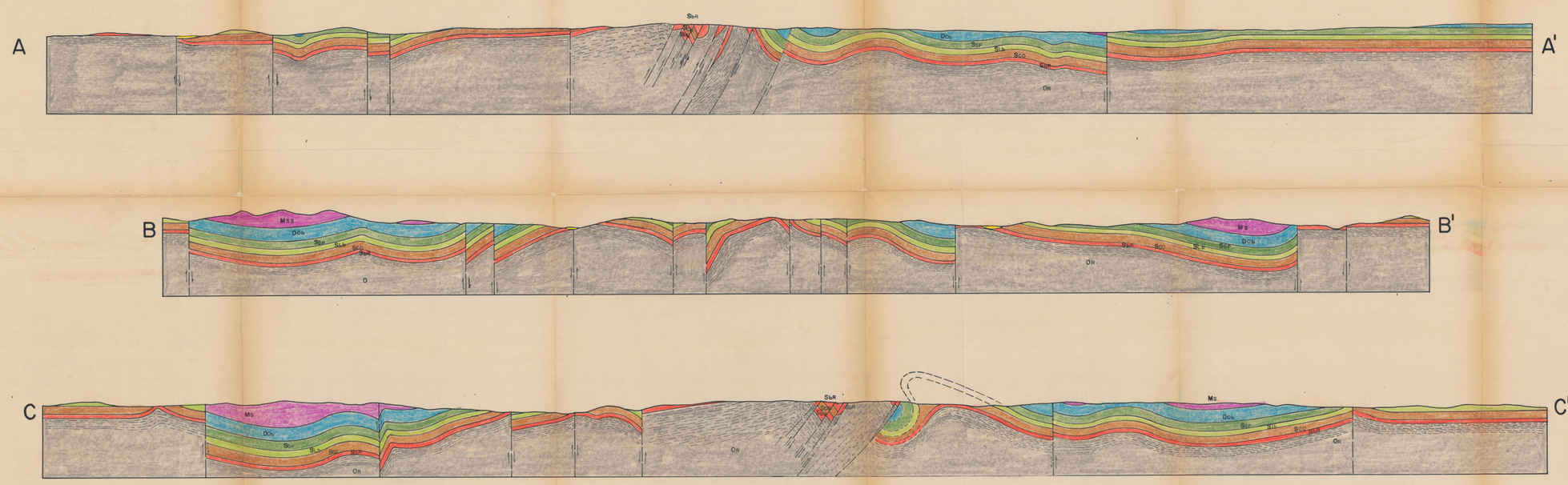

PLATE 2

S. REIDEL 1972

SCALE

HORIZONAL AND VERTICAL
IN FEET

0 1000 2000 3000 4000

500

1000